Microstructures in low-hysteresis shape memory alloys: analysis and computation

Barbara Zwicknagl

Abstract

For certain martensitic phase transformations, one observes a close relation between the width of the thermal hysteresis and the compatibility of two phases. This observation forms the basis of a theory of hysteresis that assigns an important role to the microstructures in the transition layer and their energetics (Zhang, James, Müller, Acta mat. 57(15):43324352, 2009). We study microstructures for almost compatible phases in the context of nonlinear elasticity. Using a scalar valued ansatz we show that one expects a transition from uniform to branched patterns for various typical models of the surface energy. We subsequently consider needle-type transition layers and study quantitative differences between hard and soft austenite, and between twins of different martensitic variants.

1 Introduction

The present work aims at a mathematical corroboration of microstructures of low hysteresis shape memory alloys and their energetics in the context of nonlinear elasticity. It has been conjectured and confirmed experimentally that there is a universal relation between the width of the thermal hysteresis accompanying cyclic martensitic phase transformations and the compatibility of the martensitic variants and the highly symmetric austenite structure [22, 40, 56, 55, 49, 38]. Geometric compatibility between the austenite and martensite phases is measured by the deviation of the middle eigenvalue λ_2 of the transformation stretch matrix from one. The compatibility condition $\lambda_2 = 1$ is the condition that there can be a stress-free planar interface separating pure austenite from a uniform variant of martensite, while for $\lambda_2 \neq 1$ a macroscopically stress-free interface between austenite and martensite is often achieved by a fine scale mixture of multiple martensitic variants [54, 6, 9]. The theory predicts that low hysteresis comes along with special microstructures. The latter were investigated using transmission electron microscopy [26, 27, 28, 25, 29].
The mathematical analysis proceeds from nonlinear elasticity theory [6, 7, 34]. The central goal is to determine the microstructures in the transition layers and their energetics. The theoretical studies performed so far support the experimental findings. This includes the analytical investigation of simplified transition layers [56], numerical phase-field simulations in the context of geometrically linearized elasticity [44] and the study of almost compatible twinned wedges [4].
The focus of the present work lies on two aspects. First, we aim at a qualitative understanding of the energy in the transition layers in terms of the material parameters and the compatibility of the phases, and second, we consider more quantitatively needle-type microstructures.
The text is organized as follows. In Section 2 we briefly recall the standard continuum model within the

framework of continuum mechanics. In Section 3 we focus on quantitative properties of the energies of austenite/martensite interfaces for almost compatible phases. The energy of the transition layer consists of an elastic part, which we model in the context of geometrically non-linear elasticity, and a regularizing interfacial energy contribution. We restrict our studies to the case that the martensite phase is not harder than the austenite phase. Depending on the material parameters, there are several scaling regimes of the minimal energy corresponding to different microstructures. The latter include uniform structures and branched patterns. We employ a scalar-valued ansatz, which reduces the energy functional to a generalization of the classical Kohn-Müller model [41, 42]. This allows us to build on techniques from [41, 42, 20] to rigorously analyze the simplified problem while the behavior of the model problems turns out to be qualitatively different from the one of the Kohn-Müller model. We compare different typical choices of surface energy terms involving second order derivatives. The qualitative overall-behavior of the minimal energies in the physically relevant parameter regime depends only slightly on the specific choice.
From Section 4 on, we deal with more quantitative properties of the energies. Throughout the text we consider the alloy $Ti_{50}Ni_{39}Pd_{11}$ as example, which was found to have λ_2 almost equal to one [56]. In Section 4 we recall its crystallographic properties as far as they are employed later to simplify the analysis. Of particular concern are symmetries between the various twin systems involving different martensitic variants.
Sections 5 and 6 deal with a hierarchy of needle-type non-branching transition layers as they are often observed in experiments, see, e.g., [19]. Section 5 addresses a conjecture raised in [56] concerning the effect of different twin systems on the energy stored in the layers. Studies of a simplified layer structure led to the observation that there is a variation of about two orders of magnitude which could explain why specific combinations of variants are more likely to be observed than others [56, Sec. 6]. We reconsider the model introduced in [56] and use the symmetries derived in Section 4 to show that the ansatz in [56] is too restrictive. A slight modification of the model reduces the effect significantly. If one allows for quite general needle-type layer structures the dependence on the twin system is reduced even further, see Section 6.
In Section 6 we additionally study the influence of different boundary conditions at the austenite/martensite interface on the values of the energies. For periodic, non-branching transition layers we compare the optimal shapes of the layers for hard and soft boundary conditions. The two types of boundary conditions correspond to the relation between the elastic moduli of martensite and austenite. Hard boundary conditions model a very rigid austenite phase, where the elastic modulus of austenite is much larger than the one of martensite, while for soft boundary conditions the two moduli are similar. We study a model introduced in [56, Sec. 8], and consider the energy minimization problem in the variational limit of compatible phases. We show that allowing for soft boundary conditions does not yield more general needle-shapes of the minority phase. In particular, by studying extensions of functions of fractional Sobolev-regularity, we show that in both cases needles are pinched at the interface, that is, the minority phase vanishes at the interface. The limiting problems are solved approximately. We employ semi-analytically a Fourier-type ansatz, and numerically we implement a finite element discretization. We compare the results for these two very different approximations to obtain reliable quantitative insights into the energetics of the transition layers. The values of the energies are found to be only moderately reduced by relaxing austenite, and to depend only weakly on the twin systems. The optimal structures of the needles, however, vary greatly from twin system to twin system.

2 Notation and continuum model of nonlinear elasticity

Martensitic phase transformations have been studied within the framework of continuum mechanics. Throughout the text, we use the continuum model of nonlinear elasticity described in [6, 7, 9, 50, 51, 5]. A homogeneous crystalline body in its stress-free reference configuration is identified with the domain $\Omega \subset \mathbb{R}^3$ that it occupies. At fixed temperature a deformation $\boldsymbol{u} : \Omega \to \mathbb{R}^3$ requires elastic energy

$$\int_\Omega \phi\left(\nabla \boldsymbol{u}\right) \ ,$$

where the stored-energy density $\phi : \mathbb{R}^{3\times 3} \to \mathbb{R}$ is assumed to depend only on the deformation gradient $\nabla \boldsymbol{u}$, and to be frame indifferent, that is, $\phi\left(\boldsymbol{RM}\right) = \phi\left(\boldsymbol{M}\right)$ for all $\boldsymbol{M} \in \mathbb{R}^{3\times 3}$ and all $\boldsymbol{R} \in SO\left(3\right)$. For a matrix $\boldsymbol{M} \in \mathbb{R}^{3\times 3}$ the set $SO\left(3\right)\boldsymbol{M}$ is called energy well.

We consider a basic framework of martensitic transformations. At high temperatures $\theta > \theta_c$ the free energy density ϕ has a unique minimizing energy well, $SO\left(3\right)$. At low temperatures $\theta < \theta_c$, the energy density ϕ has several minimizing wells $SO\left(3\right)\boldsymbol{U}_i$, $i = 1, \ldots, N$, and a local minimum at the austenite well $SO\left(3\right)$. The positive-definite, symmetric, and symmetry-related deformation matrices $\boldsymbol{U}_i$ describe the N variants of martensite.

At temperatures close to θ_c, one often observes complex phase mixtures. To allow for such mixtures, we generally assume that any two martensitic variants satisfy the crystallographic equations of martensite, i.e., for any two variants $\boldsymbol{U}_i$ and $\boldsymbol{U}_j$ there are $\boldsymbol{A} \in SO\left(3\right)\boldsymbol{U}_i$ and $\boldsymbol{B} \in SO\left(3\right)\boldsymbol{U}_j$, vectors $\boldsymbol{a}$, $\boldsymbol{n}$, $\boldsymbol{b}$ and $\boldsymbol{m} \in \mathbb{R}^3$, and $\lambda \in [0, 1]$ such that

$$\boldsymbol{B} - \boldsymbol{A} = \boldsymbol{a} \otimes \boldsymbol{n} \quad \text{and} \quad \lambda \boldsymbol{B} + \left(1 - \lambda\right)\boldsymbol{A} - \boldsymbol{I} = \boldsymbol{b} \otimes \boldsymbol{m} \ . \tag{1}$$

These equations ensure that there are continuous functions with piecewise constant gradients $\boldsymbol{A}$ and $\boldsymbol{B}$, respectively, separated by twin planes with normal $\boldsymbol{n}$. Further there can be macroscopically stress-free austenite-twinned martensite interfaces with habit plane normal $\boldsymbol{m}$, where λ corresponds to the volume fraction of the $\boldsymbol{B}$-variant in the martensite part, see Fig. 1. If the ordered eigenvalues of the transformation stretch matrices are denoted by $0 \leq \lambda_1 \leq \lambda_2 \leq \lambda_3$, then the volume fraction $\lambda \ll 1$ of the minority phase is related to the middle eigenvalue λ_2 via [56, Eq. (35)]

$$\lambda \approx \frac{1}{2} - \frac{1}{2}\sqrt{1 - \frac{4\left|\lambda_2 - 1\right|}{\left|a_2 n_2\right|}} \ . \tag{2}$$

During the last years there has been a growing interest in materials with λ_2 close to 1. If $\lambda_2 = 1$ there can be an exact interface between austenite and one variant of martensite, i.e., Eq. (1) holds with $\lambda = 0$, see [54, 6]. Here, we always deal with the case $\lambda \sim \left|\lambda_2 - 1\right| \ll 1$ being small.

We focus on planar martensite/austenite interfaces where the martensite part consists of a heterogeneous phase mixture of two variants $\boldsymbol{A} \in SO\left(3\right)\boldsymbol{U}_i$ and $\boldsymbol{B} \in SO\left(3\right)\boldsymbol{U}_j$, $i \neq j$ satisfying the crystallographic equations of martensite (1). Fig. 1 shows schematically the transition layer. In view of Eq. (6) the transition layer is described in terms of the natural, in general non-orthogonal coordinates

$$\boldsymbol{x} = x_1 \boldsymbol{n}^\perp + x_2 \boldsymbol{m}^\perp + x_3 \boldsymbol{e} \ , \tag{3}$$

where $\boldsymbol{n}^\perp$ and $\boldsymbol{m}^\perp$ lie in the plane spanned by $\boldsymbol{m}$ and $\boldsymbol{n}$ and satisfy

$$\boldsymbol{n}^\perp \cdot \boldsymbol{n} = 0 = \boldsymbol{m}^\perp \cdot \boldsymbol{m} \quad , \quad \left|\boldsymbol{n}^\perp\right| = 1 = \left|\boldsymbol{m}^\perp\right| \quad \text{and} \quad \boldsymbol{n}^\perp \cdot \boldsymbol{m} = \boldsymbol{m}^\perp \cdot \boldsymbol{n} > 0 \ . \tag{4}$$

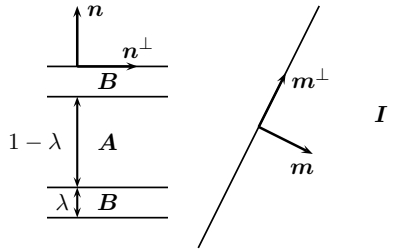

Figure 1: Schematic sketch of the interface (planar projection)

Further, we choose $\boldsymbol{e}$ perpendicular to both, $\boldsymbol{m}$ and $\boldsymbol{n}$ such that

$$|\boldsymbol{e}| = 1 \,, \quad \text{and} \quad \boldsymbol{e} \cdot (\boldsymbol{m} \times \boldsymbol{n}) > 0 \,. \tag{5}$$

In particular,

$$\boldsymbol{A}\boldsymbol{e} = \boldsymbol{B}\boldsymbol{e} = \boldsymbol{I}\boldsymbol{e} = \boldsymbol{e} \,. \tag{6}$$

We put the origin at the martensite/austenite interface. We measure the length ℓ of the martensite part in direction $-\boldsymbol{m}$, the height h in direction $\boldsymbol{n}$ and the width w in direction $\boldsymbol{e}$. We note that this notation differs from the ones used in [56] by geometric factors $\boldsymbol{m} \cdot \boldsymbol{n}^\perp$ reflecting the possible non-orthogonality of the coordinate system given in Eq. (3). The martensite part hence occupies the domain

$$\Omega^{(M)} \;:=\; \left\{ x_1\boldsymbol{n}^\perp + x_2\boldsymbol{m}^\perp + x_3\boldsymbol{e} \quad : \quad -\frac{\ell}{\boldsymbol{m}\cdot\boldsymbol{n}^\perp} \le x_1 \le 0 \,,\; 0 \le x_2 \le \frac{h}{\boldsymbol{m}\cdot\boldsymbol{n}^\perp} \,,\; 0 \le x_3 \le w \right\} \,,$$

while the austenite part is

$$\Omega^{(A)} \;:=\; \left\{ x_1\boldsymbol{n}^\perp + x_2\boldsymbol{m}^\perp + x_3\boldsymbol{e} \quad : \quad 0 \le x_1 \le \frac{L}{\boldsymbol{m}\cdot\boldsymbol{n}^\perp} \,,\; 0 \le x_2 \le \frac{h}{\boldsymbol{m}\cdot\boldsymbol{n}^\perp} \,,\; 0 \le x_3 \le w \right\} \,.$$

Without loss of generality we set $w = h = 1$. The elastic energy contribution of a deformation $\boldsymbol{y} : \Omega^{(M)} \cup \Omega^{(A)} \to \mathbb{R}^3$ is given by

$$\mu \int_{\Omega^{(M)}} \phi\left(\nabla \boldsymbol{y}\right) d\boldsymbol{x} + \beta \int_{\Omega^{(A)}} \phi\left(\nabla \boldsymbol{y}\right) d\boldsymbol{x} \tag{7}$$

with elastic moduli μ and β of martensite and austenite, respectively.
Several models have been suggested for the interfacial energy. Popular examples use the second derivatives of the deformation (see [9] for a detailed discussion). The surface energy is then given by

$$\kappa \int_{\Omega^{(M)}\cup\Omega^{(A)}} \left|\nabla^2 \boldsymbol{y}\right|^2 d\boldsymbol{x} \quad \text{or} \quad \kappa \int_{\Omega^{(M)}\cup\Omega^{(A)}} \left|\nabla^2 \boldsymbol{y}\right| d\boldsymbol{x} \,, \tag{8}$$

where κ denotes a typical interfacial energy per unit area. The total energy is given as the sum of the elastic and the interfacial energy given in Eqs. (7) and (8).

3 Ansatz and generalizations of the Kohn-Müller model

In this section, we focus on the scaling behavior of the minimal energy with respect to the length ℓ of the martensite part, the volume fraction of the minority phase λ, the interfacial energy constant κ and the elastic moduli μ and β. The austenite part is assumed to be infinitely long, i.e., $L = \infty$. Upper bounds for the scaling behavior can be obtained by analyzing suitable test functions. For many similar variational problems one observes a transition between a laminar regime and a branching regime where the laminar patterns refine close to the interface [41, 42, 20, 17, 18]. We can construct test functions building on constructions from [42] where a scalar-valued model problem is considered. The crystallographic equations (1) can be rewritten as

$$\boldsymbol{B} = \boldsymbol{I} + \boldsymbol{b} \otimes \boldsymbol{m} + (1-\lambda)\, \boldsymbol{a} \otimes \boldsymbol{n} \quad \text{and} \quad \boldsymbol{A} = \boldsymbol{I} + \boldsymbol{b} \otimes \boldsymbol{m} - \lambda \boldsymbol{a} \otimes \boldsymbol{n}\,. \tag{9}$$

Motivated by Eqs. (9) and (6) we make a simple ansatz for the deformation

$$\boldsymbol{y}(\boldsymbol{x}) = \begin{cases} (\boldsymbol{I} + \boldsymbol{b} \otimes \boldsymbol{m})\, \boldsymbol{x} - s(x,y) \left(\boldsymbol{n} \cdot \boldsymbol{m}^{\perp}\right) \boldsymbol{a}, & x < 0 \\ \boldsymbol{x} - s(x,y) \left(\boldsymbol{n} \cdot \boldsymbol{m}^{\perp}\right) \boldsymbol{a}\,, & x > 0 \end{cases} \tag{10}$$

with some scalar-valued function $s \in W^{1,2}\left(\Omega^{(M)} \cup \Omega^{(A)}\right)$ that depends only on x and y, where $x = x_1 = \frac{1}{\boldsymbol{n}^{\perp} \cdot \boldsymbol{m}} \boldsymbol{x} \cdot \boldsymbol{m}$ and $y = x_2 = \frac{1}{\boldsymbol{n}^{\perp} \cdot \boldsymbol{m}} \boldsymbol{x} \cdot \boldsymbol{n}$. The deformation gradient is

$$\nabla \boldsymbol{y}(\boldsymbol{x}) = \begin{cases} \boldsymbol{I} + \boldsymbol{b} \otimes \boldsymbol{m} - \left(s_x \boldsymbol{a} \otimes \boldsymbol{m} + s_y \boldsymbol{a} \otimes \boldsymbol{n}\right)\,, & x < 0 \\ \boldsymbol{I} - \left(s_x \boldsymbol{a} \otimes \boldsymbol{m} + s_y \boldsymbol{a} \otimes \boldsymbol{n}\right), & x > 0 \end{cases},$$

where we denote by s_z the partial derivative with respect to the variable z. We assume that the Helmholtz free energy density grows quadratically away from the energy wells. Here and in the following we use the notation $\lesssim, \sim, \gtrsim$ if a relation holds up to constants that may depend only on the crystallographic parameters. The elastic energy contribution from the martensite part is estimated above by (recall that we assume that the angle between $\boldsymbol{m}$ and $\boldsymbol{n}$ is non-degenerate)

$$\begin{aligned} & \mu \int_{\Omega^{(M)}} \operatorname{dist}^2 \left(\boldsymbol{I} + \boldsymbol{b} \otimes \boldsymbol{m} - \left(s_x \boldsymbol{a} \otimes \boldsymbol{m} + s_y \boldsymbol{a} \otimes \boldsymbol{n}\right), SO(3)\, \boldsymbol{A} \cup SO(3)\, \boldsymbol{B}\right) d\boldsymbol{x} \\ \leq\ & \mu \int_{\Omega^{(M)}} \operatorname{dist}^2 \left(\boldsymbol{I} + \boldsymbol{b} \otimes \boldsymbol{m} - \left(s_x \boldsymbol{a} \otimes \boldsymbol{m} + s_y \boldsymbol{a} \otimes \boldsymbol{n}\right), \{\boldsymbol{A}, \boldsymbol{B}\}\right) d\boldsymbol{x} \\ \lesssim\ & \mu \int_{\Omega^{(M)}} \left(s_x^2 + \min\left\{|s_y + 1 - \lambda|^2\,,\ |s_y - \lambda|^2\right\}\right) d\boldsymbol{x}\,, \end{aligned}$$

and similarly for the austenite part

$$\beta \int_{\Omega^{(A)}} \operatorname{dist}^2 \left(\boldsymbol{I} - \left(s_x \boldsymbol{a} \otimes \boldsymbol{m} + s_y \boldsymbol{a} \otimes \boldsymbol{n}\right), SO(3)\right) d\boldsymbol{x} \lesssim \beta \int_{\Omega^{(A)}} \left(s_x^2 + s_y^2\right) d\boldsymbol{x}\,.$$

Thus the elastic energy is bounded above in terms of the scalar-valued ansatz function s, and by the choice of the ansatz (10), the interfacial energy of $\boldsymbol{y}$ is also determined by s. For the remainder of this section, we disregard any dependencies on the crystallographic parameters.

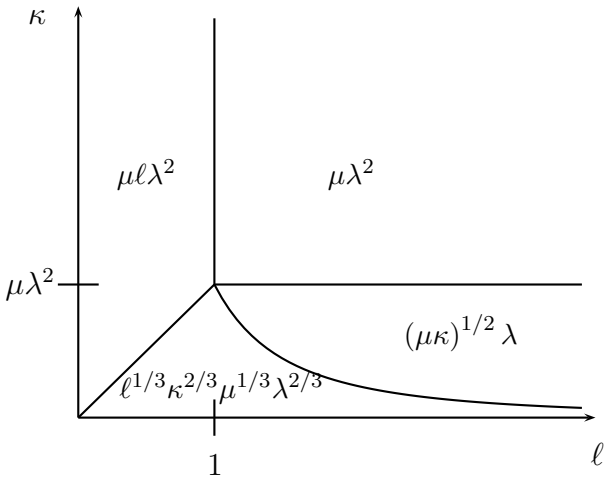

(a) Same scaling regimes for original Kohn-Müller model J_1, and simplified Kohn-Müller functional J_2 with relaxed constraint on the order parameter

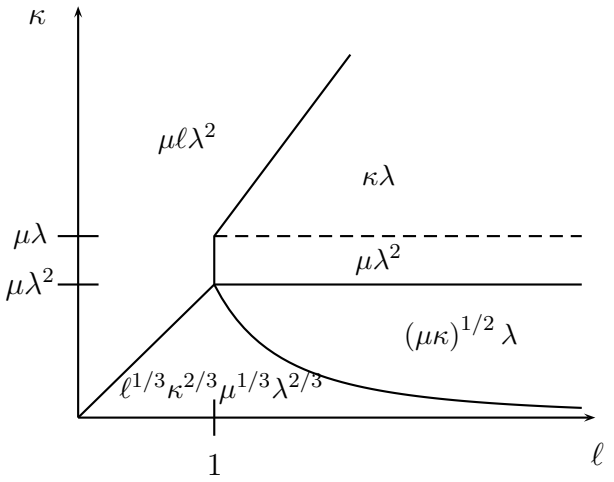

(b) Energy functional J_3: Full anisotropic TV regularization

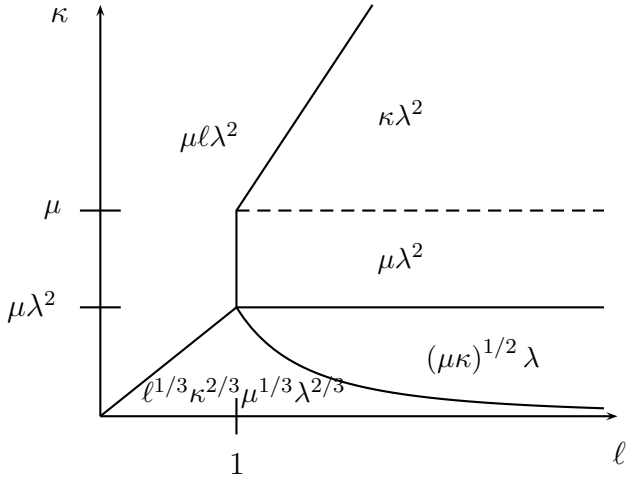

(c) Energy functional J_4: Full $W^{2,2}$-regularization

Figure 2: Comparison of minimal energy scaling regimes for various surface energy terms under the assumption $\beta \gtrsim \mu$

In [41, 42] it is discussed that an appropriate choice for the interfacial energy should involve a term $|s_{yy}|$ in the martensite part. The probably best studied model of this kind is introduced in [42] and reads

$$J(s) := \beta [s_0]^2_{H^{1/2}(0,1)} + \int_{-\ell}^0 \int_0^1 \mu s_x^2 + \kappa |s_{yy}| \, dydx \,, \tag{11}$$

where admissible $s \in W^{1,2}((-\ell,0)\times(0,1))$ satisfy $s_y \in BV((-\ell,0)\times(0,1))$, $s_y \in \{\lambda, -1+\lambda\}$ almost everywhere, and $s_0(\cdot) := s(0,\cdot)$ in the sense of trace. Here, the elastic energy of the austenite part is estimated in terms of the trace norm on the interface (see, e.g., [20]). A discussion of fractional order Sobolev norms is postponed to Section 6.3. The surface energy in (11) is given in terms of the BV-seminorm of $u_y(x,\cdot) : (0,1) \to \mathbb{R}$ which is defined by (see [3])

$$\int_0^1 |u_{yy}| \, dy := \sup \left\{ \int_0^1 u_y(x,y) \, \phi'(y) \, dy \ : \ \phi \in \mathcal{C}_0^1(0,1) \right\} .$$

The behavior of the minimal energy of J from (11) for equal volume fractions is studied in [20]. Usually the elastic moduli μ and β of martensite and austenite, respectively, are expected to be of the same order, i.e., $\mu \sim \beta$. Sometimes one observes softening in the martensite, i.e., $\beta \gtrsim \mu$. The qualitative behavior for $\mu \sim \beta$ of the minimal energies of the model (11) has been found to differ greatly from the behavior for $\beta \gg \mu$, see [42, 20]. We show that this phenomenon is only due to the strong constraint on the order parameter s_y. If this constraint is relaxed, then the qualitative behavior of the minimal energies is equal for all $\beta \gtrsim \mu$.
The functional J arises as simplification of a functional initially suggested in [41], which essentially reads

$$J_1(s) := \beta [s_0]^2_{H^{1/2}(0,1)} + \int_{-\ell}^0 \int_0^1 \mu \operatorname{dist}^2(\nabla s, K) + \frac{\kappa^2}{\mu} |s_{yy}|^2 \, dydx \,, \tag{12}$$

and which is to be minimized among all $s \in W^{1,2}((-\ell,0)\times(0,1))$ with $s_y \in W^{1,2}((-\ell,0)\times(0,1))$. Here and in the following we use the short-hand notation

$$K := \left\{ \begin{pmatrix} 0 \\ -1+\lambda \end{pmatrix}, \begin{pmatrix} 0 \\ \lambda \end{pmatrix} \right\} .$$

The surface energy term is weighted by κ^2/μ in order to assign the parameters κ and μ the same physical meanings as in the functional J. The functional J_1 is addressed in Theorem 3.3.
We consider several variants of the above models and discuss in particular the influence of the choice of the surface energy term. The essential qualitative difference between (12) and (11) lies in the set of admissible functions. First, constant functions, which correspond to pure austenite, are not admissible in the simplification (11). To overcome this issue, we relax the constraint and study the functional (see Theorem 3.1)

$$J_2(s) := \beta [s_0]^2_{H^{1/2}(0,1)} + \int_{-\ell}^0 \int_0^1 \mu \operatorname{dist}^2(\nabla s, K) + \kappa |s_{yy}| \, dydx \,, \tag{13}$$

where $s \in W^{1,2}((-\ell,0)\times(0,1))$ with $s_y \in BV((-\ell,0)\times(0,1))$. As remarked in [42] it suffices to add a term in s_{yy} to regularize the problem. In Theorem 3.2, however, we show that the scaling behavior is slightly different if one considers the full anisotropic total variation (TV) regularization

$$J_3(s) \ := \ \mu \int_{-\ell}^0 \int_0^1 \operatorname{dist}^2(\nabla s, K) \, dydx + \beta \int_0^\infty \int_0^1 |\nabla s|^2 + \kappa \int_{-\ell}^\infty \int_0^1 (|s_{xx}| + |s_{xy}| + |s_{yy}|) \, dydx \,.$$

(a) Branching: $J_2(s) \sim \mu^{1/3}\kappa^{2/3}\ell^{1/3}\lambda^{2/3}$ (b) Truncated branching: $J_2(s) \sim (\mu\kappa)^{1/2}\lambda$

Figure 3: Branched patterns. White regions correspond to $s_y = \lambda$, black regions to $s_y = -1 + \lambda$.

The functional J_3 is to be minimized among all $s \in W^{1,2}((-\ell,\infty)\times(0,1))$ that additionally satisfy s_x, $s_y \in BV((-\ell,\infty)\times(0,1))$. The main difference between the functionals J_3 and J_2 is that for the functional J_3 an austenite / martensite interface always requires interfacial energy. In the functional (14) we assume the same surface energy per unit area constant κ in the austenite part as in the martensite part. This choice is only for the ease of notation and can easily be generalized.
Finally another difference between (11) and the original model (12) is the smoothness assumption on admissible functions. Roughly speaking, in the original model (12) surface energy always comes along with elastic energy. To complete the picture, in Theorem 3.4 we finally consider the fully regularized functional

$$J_4(s) := \mu\int_{-\ell}^{0}\int_0^1 \operatorname{dist}^2(\nabla s, K)\,dydx + \beta\int_0^\infty\int_0^1 |\nabla s|^2\,dydx + \frac{\kappa^2}{\mu}\left(\int_{-\ell}^{\infty}\int_0^1 \left|D^2 s\right|^2\right)dydx\,, \tag{14}$$

which is minimized among all $s \in W^{2,2}((-\ell,\infty)\times(0,1))$.

Anisotropic BV-regularization

To start with, we consider the functional J_2 as defined in Eq. (13), and prove upper and lower bounds for its minimal energy in detail since for all the remaining functionals similar techniques can be applied.

Theorem 3.1 *There are constants C_1 and $C_2 > 0$ such that for all $0 < \mu \lesssim \beta$, κ, $\ell > 0$ and all $0 \le \lambda \le \frac{1}{2}$,*

$$C_1 \min J_2(s) \le \min\left\{\mu^{1/3}\kappa^{2/3}\ell^{1/3}\lambda^{2/3}\,,\ (\mu\kappa)^{1/2}\lambda\,,\ \mu\lambda^2\,,\ \mu\ell\lambda^2\right\} \le C_2 \min J_2(s)\ .$$

Proof: We set $E := \min J_2(s)$. The claim can be split into the following statements:

1. If $\ell \le 1$ and $\kappa \le \mu\ell\lambda^2$, or if $\ell > 1$ and $\kappa \le \frac{\mu\lambda^2}{\ell^2}$, then $E \sim \mu^{1/3}\kappa^{2/3}\ell^{1/3}\lambda^{2/3}$.
2. If $\ell \le 1$ and $\kappa > \mu\ell\lambda^2$, then $E \sim \mu\ell\lambda^2$.
3. If $\ell > 1$ and $\frac{\mu\lambda^2}{\ell^2} \le \kappa \le \mu\lambda^2$, then $E \sim (\mu\kappa)^{1/2}\lambda$.
4. If $\ell > 1$ and $\kappa \ge \mu\lambda^2$, then $E \sim \mu\lambda^2$.

We prove the upper bound first.

1. **Branching**: The construction given in [42, Lemma 2.3] carries over to the case of unequal volume fractions, see. Fig. 3(a). The interval $(-\ell, 0)$ is subdivided geometrically into intervals (x_i, x_{i+1}) with $x_i = -\theta^i \ell$ for $i \in \mathbb{N}$ and some $\frac{1}{4} < \theta < \frac{1}{2}$. To define the test function s on the interval (x_0, x_1) one chooses the function $v_\lambda : [0,1] \times \left[0, \frac{1}{2}\right] \to \mathbb{R}$ given by

$$v_\lambda(x,y) = \begin{cases} (-1+\lambda)\, y & \text{if} \quad 0 < y < \frac{\lambda}{4} + \frac{\lambda}{4} x \\ -\frac{\lambda}{4} x - \frac{\lambda}{4} + \lambda y & \text{if} \quad \frac{\lambda}{4} + \frac{\lambda}{4} x \le y \le \frac{1}{2} - \frac{\lambda}{4} + \frac{\lambda}{4} x \\ \frac{1}{2} - \frac{\lambda}{2} + (-1+\lambda)\, y & \text{if} \quad \frac{1}{2} - \frac{\lambda}{4} + \frac{\lambda}{4} x \le y \le \frac{1}{2} \end{cases}, \tag{15}$$

and extends it anti-periodically in direction y. For $N \in \mathbb{N}$ one sets

$$s(x,y) = \frac{1}{N} v_\lambda\left(\frac{x - x_1}{x_0 - x_1}, Ny\right). \tag{16}$$

Then by construction $s_y \in \{\lambda, -1+\lambda\}$ a.e., $s(x, y+1) = s(x,y)$, and $s(x_1, y) = \frac{1}{2} s(x_0, 2y)$. If $\ell \le 1$ and $\kappa \le \mu \ell \lambda^2$, or if $\ell > 1$ and $\kappa \le \frac{\mu \lambda^2}{\ell^2}$ we may choose $N \sim \frac{\mu^{1/3} \lambda^{2/3}}{\ell^{2/3} (1-\theta)^{2/3} \kappa^{1/3}}$ which yields

$$\int_{x_0}^{x_1} \int_0^1 \mu s_x^2 + \kappa \left| s_{yy} \right| dy dx \sim \frac{\mu}{N^2} \frac{\lambda^2}{\ell (1-\theta)} + N \kappa \ell (1-\theta) \sim \mu^{1/3} \ell^{1/3} (1-\theta)^{1/3} \kappa^{2/3} \lambda^{2/3}.$$

As worked out in [42], the test function s is extended to the remaining intervals via

$$s(x,y) = 2^{-i} s\left(\theta^{-i} x, 2^i y\right) \quad \text{if} \quad x \in [x_i, x_{i+1}]. \tag{17}$$

Then $s_y \in \{\lambda, -1+\lambda\}$ a.e., $s(0,y) = 0$ and $J_2(s) \lesssim \mu^{1/3} \kappa^{2/3} \ell^{1/3} \lambda^{2/3}$.

2. **Constant functions**: $s(x,y) = 0$. This corresponds to pure austenite. Here $J_2(s) = \mu \ell \lambda^2$.

3. **Truncated branching**: We construct a test function s as sketched in Fig. 3(b) on the infinite strip. As the energy is an increasing function in the length ℓ this yields an upper bound. We use the Kohn-Müller branching construction (see above) on $(\overline{x}, 0) \times (0,1)$ with $\overline{x} \sim \left(\frac{\mu}{\kappa}\right)^{1/2} \lambda$. The total energy contribution of the function s on $(\overline{x}, 0) \times (0,1)$ is

$$J_2(s)\big|_{(\overline{x},0)\times(0,1)} \sim \mu^{1/3} \left(\left(\frac{\mu}{\kappa}\right)^{1/2} \lambda\right)^{1/3} \kappa^{2/3} \lambda^{2/3} = (\mu\kappa)^{1/2} \lambda.$$

Note that the construction can be done in such a way that

$$s(\overline{x}, y) = \begin{cases} (-1+\lambda)\, y, & 0 \le y \le \frac{\lambda}{2} \\ -\frac{\lambda}{2} + \lambda y, & \frac{\lambda}{2} \le y \le 1 - \frac{\lambda}{2} \\ 1 - \lambda + (-1+\lambda)\, y, & 1 - \frac{\lambda}{2} \le y \le 1 \end{cases}.$$

We introduce an interpolation region on $(\overline{x} - \delta, \overline{x}) \times (0,1)$, i.e., we set

$$s(x,y) = \begin{cases} (-1+\lambda)\, y, & 0 \le y \le \frac{\lambda}{2\delta}(x - \overline{x}) + \frac{\lambda}{2} \\ \lambda y - \frac{\lambda}{2\delta}(x - \overline{x}) - \frac{\lambda}{2}, & \frac{\lambda}{2\delta}(x - \overline{x}) + \frac{\lambda}{2} \le y \le \frac{\lambda}{2\delta}(\overline{x} - x) + 1 - \frac{\lambda}{2} \\ (-1+\lambda)\, y + \frac{\lambda}{\delta}(\overline{x} - x) - \lambda + 1, & \frac{\lambda}{2\delta}(\overline{x} - x) + 1 - \frac{\lambda}{2} \le y \le 1 \end{cases}.$$

Then the energy contribution from the interpolation region consists of elastic and surface energy and is for $\delta \sim \left(\frac{\mu}{\kappa}\right)^{1/2} \lambda$ estimated by

$$\kappa\delta + \delta\mu\frac{\lambda^2}{\delta^2} \sim (\mu\kappa)^{1/2}\,\lambda\,.$$

By construction $s\,(\overline{x}-\delta, y) = \lambda y$, so that we can extend s constantly in x via

$$s\,(x,y) = s\,(\overline{x}-\delta, y) = \lambda y \quad \text{for all } -\infty < x < \overline{x}-\delta\,.$$

Hence the total energy of this test function is estimated by $J_2\,(s) \lesssim (\mu\kappa)^{1/2}\,\lambda$.

4. **Linear interpolation**: $s\,(x,y) = -\lambda xy$ for $-1 \le x \le 0$, and $s\,(x,y) = \lambda y$ for $x \le -1$. This function possesses only elastic energy,

$$J_2\,(s) = \mu\int_0^1\int_0^1 \lambda^2 y^2 + \lambda^2\,(x-1)^2\,dydx \sim \mu\lambda^2\,.$$

To prove the lower bound we employ techniques from the proof of [20, Theorem 1] adapted to our situation. Since $\beta \gtrsim \mu$ we can bound the energy below by setting $\beta = \mu$. Further, the energy is increasing as function of ℓ. Hence to bound the energy below we may use any restriction of the energy to smaller domains $\left(-\tilde{\ell}, 0\right) \times (0,1)$ for $0 \le \tilde{\ell} \le \ell$, i.e.,

$$J_2\,(s) \ge \mu\,[s_0]^2_{H^{1/2}(0,1)} + \int_{-\tilde{\ell}}^0\int_0^1 \mu\,\mathrm{dist}^2\,(\nabla s, K) + \kappa\,|s_{yy}|\,dydx\,.$$

For all $0 \le \tilde{\ell} \le \ell$ and all $0 < t \le 1$ there is an interval $I = [y, y+t] \subset [0,1]$ such that

$$E_I := \mu\,[s_0]^2_{H^{1/2}(I)} + \int_{-\tilde{\ell}}^0\int_I \mu\,\mathrm{dist}^2\,(\nabla s, K) + \kappa\,|s_{yy}| \le 2tJ_2\,(s)\ .$$

By a Fubini-based argument there is a set $M \subset \left(-\tilde{\ell}, 0\right)$ with positive measure such that for all $x \in M$

$$\int_{\{x\}\times I} \mathrm{dist}^2\,(\nabla s, K)\,dy \lesssim \tilde{\ell}^{-1}\int_{\Omega_t} \mathrm{dist}^2\,(\nabla s, K)\,dydx \quad \text{and} \quad \int_{\{x\}\times I} |s_{yy}|\,dy \lesssim \tilde{\ell}^{-1}\int_{\Omega_t} |s_{yy}|\,dydx\,, \tag{18}$$

where $\Omega_t := \left(-\tilde{\ell}, 0\right) \times I$. One of the following three subsets of M has positive measure:

$$\begin{aligned}
M_1 &:= \{x \in M\ :\ |s_y\,(x,y) - \lambda| \le |s_y\,(x,y) - (-1+\lambda)| \text{ for a.e. } y \in I\}\,,\\
M_2 &:= \{x \in M\ :\ |s_y\,(x,y) - \lambda| \ge |s_y\,(x,y) - (-1+\lambda)| \text{ for a.e. } y \in I\}\,,\\
M_3 &:= \{x \in M\ :\ \exists Y_1, Y_2 \subset I \text{ with positive measure s.t.}\\
&\qquad |s_y - \lambda| \le |s_y - (-1+\lambda)| \text{ for all } y \in Y_1, \text{ and } |s_y - \lambda| \ge |s_y - (-1+\lambda)| \text{ for all } y \in Y_2\}\,.
\end{aligned} \tag{19}$$

We consider the three possibilities separately. Assume that M_1 has positive measure and fix $x \in M_1$. Then by definition of M_1 we have with Eq. (18)

$$\int_{\{x\}\times I} \left|\nabla s - \begin{pmatrix} 0 \\ \lambda \end{pmatrix}\right| = \int_{\{x\}\times I} \operatorname{dist}\left(\nabla s, K\right) \leq t^{\frac{1}{2}} \left(\int_{\{x\}\times I} \operatorname{dist}^2\left(\nabla s, K\right)\right)^{\frac{1}{2}} \lesssim \left(\frac{t}{\mu\tilde{\ell}} E_I\right)^{\frac{1}{2}} .$$

By Poincaré's inequality there is a constant $\bar{s} \in \mathbb{R}$ such that

$$\int_{\{x\}\times I} \left|s\left(x,y\right) - \lambda y + \bar{s}\right| dy \lesssim t \int_{\{x\}\times I} \left|\nabla s - \begin{pmatrix} 0 \\ \lambda \end{pmatrix}\right| \lesssim \left(\frac{t^3}{\mu\tilde{\ell}} E_I\right)^{\frac{1}{2}} . \tag{20}$$

For almost every $x \in M_1$ (cf. [20, p. 473])

$$\left\|s_0\left(y\right) - s\left(x,y\right)\right\|_{L^1(I)} \leq \left\|\partial_x s\right\|_{L^1\left(\left(-\tilde{\ell},0\right)\times I\right)} \leq \left(\frac{\tilde{\ell} t}{\mu}\right)^{1/2} E_I^{1/2} . \tag{21}$$

Combining Eqs. (21) and (20) we find

$$\left\|s_0\left(y\right) - \lambda y - \bar{s}\left(x\right)\right\|_{L^1(I)} \leq \left\|s_0\left(\cdot\right) - s\left(x,\cdot\right)\right\|_{L^1(I)} + \left\|s\left(x,y\right) - \lambda y + \bar{s}\right\|_{L^1(I)} \lesssim \left(\frac{\tilde{\ell} t}{\mu} E_I\right)^{\frac{1}{2}} + \left(\frac{t^3}{\mu\tilde{\ell}} E_I\right)^{\frac{1}{2}} .$$

We use the following result [20, Lemma 1]: There is a universal constant $c > 0$ such that for any $t > 0$, any $s : (0,t) \to \mathbb{R}$, and any $\bar{s} \in \mathbb{R}$,

$$\left\|s\left(y\right) - y - \bar{s}\right\|_{L^1(0,t)} + \left[s\left(y\right)\right]^2_{H^{1/2}(0,t)} \geq c t^2 .$$

We multiply this uniform bound with λ^2 and substitute $\tilde{s} = \lambda s$, and $\hat{s} = \lambda \bar{s}$. This yields the following rescaled version: There is a universal constant $c > 0$ (from the above cited [20, Lemma 1]) such that for any $t > 0$, and $\lambda > 0$, any $s : (0,t) \to \mathbb{R}$, and any $\bar{s} \in \mathbb{R}$,

$$\lambda \left\|\tilde{s}\left(y\right) - \lambda y - \hat{s}\right\|_{L^1(0,t)} + \left[\tilde{s}\left(y\right)\right]^2_{H^{1/2}(0,t)} \geq c\lambda^2 t^2 . \tag{22}$$

This finally yields

$$\lambda^2 t^2 \lesssim \lambda \left(\frac{\tilde{\ell} t}{\mu} E_I\right)^{\frac{1}{2}} + \lambda \left(\frac{t^3}{\mu\tilde{\ell}} E_I\right)^{\frac{1}{2}} + \frac{1}{\mu} E_I , \tag{23}$$

and in particular

$$J_2\left(s\right) \gtrsim \min\left\{\frac{\mu\lambda^2 t^2}{\tilde{\ell}}, \quad \mu\tilde{\ell}\lambda^2, \quad \mu t\lambda^2\right\} . \tag{24}$$

If M_2 has positive measure we can proceed analogously and obtain the greater lower bound (recall $\lambda \leq 1-\lambda$)

$$J_2\left(s\right) \gtrsim \min\left\{\frac{\mu\left(1-\lambda\right)^2 t^2}{\tilde{\ell}}, \quad \mu\tilde{\ell}\left(1-\lambda\right)^2, \quad \mu t\left(1-\lambda\right)^2\right\} .$$

Suppose now that M_3 has positive measure and fix $x \in M_3$. Then there are two possibilities. Suppose first that there is a set $Y_M \subset I$ with $|Y_M| > 0$ such that $\operatorname{dist}(\nabla s(x,y), K) \leq \frac{1}{4}$ for all $y \in Y_M$. In the following we assume that $|s_y(x,y) - \lambda| \leq \frac{1}{4}$, the other cases being equivalent. By definition of M_3 and $|\lambda - (-1+\lambda)| = 1$ we have

$$|s_y(x,y) - s_y(x,y_2)| \geq \frac{1}{4}$$

for all $y \in Y_M$ and $y_2 \in Y_2$. Hence

$$\frac{1}{4} \leq \int_{\{x\}\times I} |s_{yy}|\, dy \lesssim \frac{1}{\tilde{\ell}} \int_{\Omega_t} |s_{yy}|\, dy \lesssim \frac{1}{\tilde{\ell}\kappa} E_I \,,$$

and therefore

$$J_2(s) \gtrsim \frac{\tilde{\ell}\kappa}{t} \,.$$

Otherwise, we have $\operatorname{dist}(\nabla s(x,y), K) > \frac{1}{4}$ for almost every $y \in I$. Then

$$\frac{t}{16} \leq \int_{\{x\}\times I} \operatorname{dist}^2(\nabla s, K)\, dy \lesssim \frac{1}{\mu\tilde{\ell}} E_I \,,$$

which implies

$$J_2(s) \gtrsim \mu\tilde{\ell} \geq \mu\tilde{\ell}\lambda^2 \,.$$

Putting things together, we obtain that for all $0 \leq \tilde{\ell} \leq \ell$ and all $0 \leq t \leq 1$,

$$J_2(s) \gtrsim \min\left\{ \frac{\mu\lambda^2 t^2}{\tilde{\ell}}, \quad \mu\tilde{\ell}\lambda^2, \quad \mu\lambda^2 t, \quad \frac{\tilde{\ell}\kappa}{t} \right\} . \tag{25}$$

We consider the regimes identified at the beginning of the proof separately.

1. If $\ell \leq 1$ and $\kappa \leq \mu\ell\lambda^2$, or if $\ell > 1$ and $\kappa \leq \frac{\mu\lambda^2}{\ell^2}$ we choose $\tilde{\ell} = \ell$ and $t = \mu^{-1/3}\ell^{2/3}\kappa^{1/3}\lambda^{-2/3} \leq 1$, which yields $J_2(s) \gtrsim \mu^{1/3}\kappa^{2/3}\ell^{1/3}\lambda^{2/3}$.
2. If $\ell \leq 1$ and $\kappa \geq \mu\ell\lambda^2$ we choose $\tilde{\ell} = t = \ell < 1$ and find $J_2(s) \gtrsim \mu\ell\lambda^2$.
3. If $\ell > 1$ and $\frac{\mu\lambda^2}{\ell^2} \leq \kappa \leq \mu\lambda^2$ we choose $\tilde{\ell} = \mu^{1/2}\kappa^{-1/2}\lambda$ and $t = 1$ which gives $J_2(s) \gtrsim (\mu\kappa)^{1/2}\lambda$.
4. If $\ell > 1$ and $\kappa \geq \mu\lambda^2$ we choose $\tilde{\ell} = t = 1$ which yields $J_2(s) \gtrsim \mu\lambda^2$.

□

We now address the functional J_3 as defined in Eq. (14) with the full anisotropic TV seminorm regularization.

Theorem 3.2 *There are constants C_1 and $C_2 > 0$ such that for all $0 < \mu \lesssim \beta$, κ, $\ell > 0$ and all $0 \leq \lambda \leq \frac{1}{2}$,*

$$\begin{aligned} C_1 \min J_3(s) &\leq \min\left\{ \mu\ell\lambda^2 \,,\, \max\left\{ \kappa\lambda,\, \min\left\{ \mu\lambda^2 \,, \mu^{1/3}\kappa^{2/3}\ell^{1/3}\lambda^{2/3} \,,\, (\mu\kappa)^{1/2}\lambda \right\} \right\} \right\} \\ &= \min\left\{ \mu\ell\lambda^2, \max\left\{\kappa\lambda, \mu\lambda^2\right\} \,,\, \mu^{1/3}\kappa^{2/3}\ell^{1/3}\lambda^{2/3} \,,\, (\mu\kappa)^{1/2}\lambda \right\} \leq C_2 \min J_3(s) \,. \end{aligned}$$

Proof: To prove the lower bound we observe that by trace theorem for all admissible functions s we have $J_3(s) \gtrsim J_2(s)$. Hence Theorem 3.1 implies that

$$\min J_3 \gtrsim \min\left\{\mu\ell\lambda^2\,,\ \mu^{1/3}\kappa^{2/3}\ell^{1/3}\lambda^{2/3}\,,\ (\mu\kappa)^{1/2}\lambda\,,\ \mu\lambda^2\,,\ \mu\ell\lambda^2\right\}\,.$$

Therefore it suffices to show that $J_3(s) \gtrsim \min\left\{\mu\ell\lambda^2\,,\ \kappa\lambda\right\}$ for all admissible s. Fix a constant $c_0 \ll 1$, and consider an arbitrary admissible function s with $J_3(s) \le c_0\mu\ell\lambda^2$. We show that then $J_3(s) \ge C\kappa\lambda$ for a constant $C > 0$ that depends only on c_0. Again by a Fubini-based argument there is a set $M \subset (-\ell, 0)$ with $|M| > 0$ such that for all $x^\star \in M$

$$\int_0^1 \operatorname{dist}^2\left(\nabla s\left(x^\star, y\right), K\right) dy \le c_0\lambda^2\,.$$

In particular, if we choose $c_0 \ll 1$ small, there is a $c_1 > 0$ that depends only on $c_0 \ll 1$ such that for $x^\star \in M$

$$\int_0^1 \left|s_y\left(x^\star, y\right)\right| dy \ge c_1\lambda\,.$$

This implies

$$\int_{-\ell}^0\int_0^1 |s_{yx}|\,dydx \;\;\ge\;\; \int_0^1 \left|\int_{x^\star}^0 s_{yx}dx\right| dy \ge \int_0^1 \left|s_y\left(x^\star, y\right)\right| dy - \int_0^1 \left|s_y(0,y)\right| dy\,.$$

Finally we have (see [45, Theorem 15.15])

$$\int_0^\infty\int_0^1 \left(|s_{xx}| + |s_{xy}| + |s_{yy}|\right) dydx \gtrsim \int_0^1 \left|\mathrm{Tr}_{x=0}\left(s_x\right)\right| + \left|\mathrm{Tr}_{x=0}\left(s_y\right)\right| dy\,, \tag{26}$$

where $\mathrm{Tr}_{x=0}(u)$ denotes the trace of u at the interface $\{x = 0\}$. Thus,

$$J_3(s) \gtrsim \kappa\left(\int_{-\ell}^0\int_0^1 \left|s_{yx}(x,y)\right| dydx + \int_0^1 \left|\nabla s(0,y)\right| dy\right) \gtrsim \kappa\lambda\,,$$

which concludes the proof.
For the upper bound one uses the same type of functions as in the proof of Theorem 3.1, extended constantly by 0 to the austenite part $\{x > 0\}$.

1. **Finite branching:** In case of full regularization, the branching constructions are not infinitely fine but stop at some refinement level I. We use a variant of the construction from [42, Lemma 2.3] that is described in detail in [15]. We briefly recall it to keep track of the additional parameter λ and the slightly different regularization term. As above, one chooses $\theta \in \left(\frac{1}{4}, \frac{1}{2}\right)$ and $N,\ I \in \mathbb{N}$ such that $N \sim \mu^{1/3}\lambda^{2/3}\kappa^{-1/3}\ell^{-2/3}$, and $\theta^I \sim \kappa^{2/3}\mu^{-2/3}\ell^{-2/3}\lambda^{-1/3}$. In the relevant regime $\kappa \lesssim \mu\lambda^2\min\left\{\ell, \frac{1}{\ell^2}\right\}$ we have $1 \lesssim I \lesssim \mu^{1/3}\ell^{1/3}\kappa^{-1/3}\lambda^{-1/3}$. The branching construction from [41] is carried out on $\left(-\ell, -\ell\theta^I\right)\times(0,1)$. On the remaining part we interpolate linearly between $s\left(-\ell\theta^I, y\right)$

and $s(0,y)=0$. The energy contribution from the branching construction is estimated above by

$$\begin{aligned}
&\sum_{i=0}^{I-1}\left\{\mu\int_{-\ell\theta^{i}}^{-\ell\theta^{i+1}}\int_0^1 \operatorname{dist}^2(\nabla s,K)\,dydx+\kappa\int_{-\ell\theta^{i}}^{-\ell\theta^{i+1}}\int_0^1 |s_{yy}|+|s_{xx}|+|s_{xy}|\,dydx\right\}\\
\lesssim\ &\sum_{i=0}^{I-1}\left\{\frac{\mu\lambda^2}{(4\theta)^i\,\ell N^2}+\kappa\,(2\theta)^i\,\ell N+\frac{\kappa\lambda}{(2\theta)^i\,N\ell}+\kappa\lambda\right\}\\
\lesssim\ &\frac{\mu\lambda^2}{\ell N^2}+\kappa\ell N+\frac{\kappa\lambda}{\theta^I N\ell}+\kappa\lambda I\sim\mu^{1/3}\ell^{1/3}\kappa^{2/3}\lambda^{2/3}\,.
\end{aligned}$$

The interpolation layer yields the additional contributions to the elastic energy

$$\begin{aligned}
&\mu\int_{-\ell\theta^{i}}^{0}\int_0^1 s_x^2dydx\lesssim\frac{\mu\lambda^2}{(4\theta)^I\,N^2\ell}\quad\text{and}\\
&\mu\int_{-\ell\theta^{I}}^{0}\int_0^1 \operatorname{dist}^2(s_y,\{\lambda,-1+\lambda\})\,dydx\lesssim\mu 2^I N\left\{\int_0^{\frac{\lambda}{2^IN}}\int_0^{\ell\theta^I}1dydx+\int_0^{\frac{1-\lambda}{2^IN}}\int_0^{\ell\theta^I}\lambda dydx\right\}\\
\sim\ &\mu\lambda\ell\theta^I\lesssim\mu^{1/3}\ell^{1/3}\kappa^{2/3}\lambda^{2/3}\,.
\end{aligned}$$

Analogously to the estimates for the branching construction, the additional contribution from the regularization terms can be bounded by $\sim\ \mu^{1/3}\ell^{1/3}\kappa^{2/3}\lambda^{2/3}+\kappa\lambda\lesssim\mu^{1/3}\ell^{1/3}\kappa^{2/3}\lambda^{2/3}$. For the austenite part we have $s_x=s_y=0$, and hence there is an additional contribution to the surface energy at the interface,

$$\sim\frac{\kappa\lambda}{N\ell\,(2\theta)^I}\lesssim\mu^{1/3}\ell^{1/3}\kappa^{2/3}\lambda^{2/3}\,.$$

2. **Constant functions:** For $s=0$, we have $J_3(s)=\mu\ell\lambda^2$.

3. **Truncated finite branching:** As above, for large ℓ, the finite branching construction is carried out on $(\bar{x},0)\times(0,1)$ with $\bar{x}\sim\left(\frac{\mu}{\kappa}\right)^{1/2}\lambda$. On the remaining part we use the interpolation described in the proof of Theorem 3.1. By the above computations, for this test function, $J_3(s)\lesssim(\mu\kappa)^{1/2}\,\lambda+\kappa\lambda$. In the relevant regime $\kappa\lesssim\mu\lambda^2$ one has $\kappa\lambda\lesssim(\kappa\mu)^{1/2}\,\lambda$.

4. **Linear interpolation:** For the function

$$s(x,y)=\begin{cases}0\,, & 0\le x\\ -\lambda xy\,, & -1\le x\le 0\\ \lambda y\,, & -1\le x\end{cases}$$

we have $J_3(s)\lesssim\mu\lambda^2+\kappa\lambda\lesssim\max\left\{\mu\lambda^2\,,\ \kappa\lambda\right\}$.

□

Quadratic regularization

We consider the scaling regimes of the energy functionals J_1 and J_4 given in Eqs. (12) and (14), respectively. We notice that the scaling regimes for J_1 equal the ones for J_2, cf. Theorem 3.1.

Theorem 3.3 *There are constants C_1, $C_2 > 0$ such that for all $0 < \mu \lesssim \beta$, all κ, $\ell > 0$, and all $\lambda \leq \frac{1}{2}$,*

$$C_1 \min J_1(s) \leq \min\left\{\mu\ell\lambda^2\,,\ \mu^{1/3}\kappa^{2/3}\ell^{1/3}\lambda^{2/3}\,,\ \mu^{1/2}\kappa^{1/2}\lambda\,,\ \mu\lambda^2\right\} \leq C_2 \min J_1\,.$$

Proof: To prove the lower bound we proceed along the lines of the proof of Theorem 3.1. For all $0 \leq \tilde{\ell} \leq \ell$ and all $0 < t \leq 1$ there is an interval $I = [y, y+t] \subset [0,1]$ such that

$$E_I := \mu\,[s_0]^2_{H^{1/2}(I)} + \int_{-\tilde{\ell}}^{0}\int_I \mu\,\mathrm{dist}^2\left(\nabla s, K\right) + \frac{\kappa^2}{\mu}\,|s_{yy}|^2\,dydx \leq 2tJ_1(s)\ .$$

By a Fubini-based argument, there is a set $M \subset \left(-\tilde{\ell}, 0\right)$ with positive measure such that for all $x \in M$

$$\int_{\{x\}\times I}\mathrm{dist}^2\left(\nabla s, K\right)dy \lesssim \tilde{\ell}^{-1}\int_{\Omega_t}\mathrm{dist}^2\left(\nabla s, K\right)dydx \quad\text{and}\quad \int_{\{x\}\times I}|s_{yy}|^2 \lesssim \tilde{\ell}^{-1}\int_{\Omega_t}|s_{yy}|^2\,dydx\,, \tag{27}$$

where $\Omega_t := \left(-\tilde{\ell}, 0\right)\times I$. Without restriction we may assume that for some fixed $x \in M$, the function $s_y(x,\cdot)$ is continuous on I. We use the definitions of the sets M_i, $i = 1,2,3$ as given in Eq. (19). If M_1 or M_2 has positive measure we proceed word by word as in the proof of Theorem 3.1 above and find

$$J_1(s) \gtrsim \min\left\{\frac{\mu\lambda^2t^2}{\tilde{\ell}}\,,\quad \mu\tilde{\ell}\lambda^2\,,\quad \mu t\lambda^2\right\}.$$

Suppose now that M_3 has positive measure and fix some $x \in M_3$. If $\mathrm{dist}\left(\nabla s(x,y), K\right) > \frac{1}{4}$ for almost every $y \in I$ then it follows as in the proof of Theorem 3.1 that

$$J_1(s) \gtrsim \mu\tilde{\ell} \geq \mu\tilde{\ell}\lambda^2\,.$$

Suppose now that there is $Y_M \subset I$ with positive measure such that $\mathrm{dist}\left(\nabla s(x,y), K\right) \leq \frac{1}{4}$ for all $y \in Y_M$. By definition of M_3 and continuity there is an interval $\mathcal{I} = (y_\ell, y_r)$ such that

$$\mathrm{dist}\left(s_y(x,y), K_y\right) > \frac{1}{4} \text{ for almost all } y \in \mathcal{I}\,,\quad \mathrm{dist}\left(s_y(x,y_\ell), K_y\right) = \frac{1}{4}\quad\text{and}\quad \mathrm{dist}\left(s_y(x,y_r), K_y\right) \geq \frac{3}{8}\,,$$

where $K_y := \{\lambda\,,\ -1+\lambda\}$. Hence

$$\int_{\{x\}\times I}|s_{yy}|^2 \geq \int_{\{x\}\times\mathcal{I}}|s_{yy}|^2 \gtrsim \frac{1}{|\mathcal{I}|}\quad\text{and}\quad \int_{\{x\}\times\mathcal{I}}\mathrm{dist}^2\left(\nabla s, K\right) \gtrsim |\mathcal{I}|\ .$$

Then by Eq. (27), we have

$$E_I \gtrsim \tilde{\ell}\left(\frac{\kappa^2}{\mu\,|\mathcal{I}|} + \mu\,|\mathcal{I}|\right) \geq \kappa\tilde{\ell}\,.$$

Altogether, for all $0 < \tilde{\ell} \leq \ell$ and all $0 < t \leq 1$, the energy is bounded below by

$$J_1(s) \gtrsim \min\left\{\frac{\lambda^2 t^2}{\tilde{\ell}}, \quad \tilde{\ell}\lambda^2, \quad \lambda^2 t, \quad \frac{\tilde{\ell}\kappa}{t}\right\},$$

and we conclude as in the proof of Theorem 3.1.

For the upper bound, we use essentially the same test functions as above: The constant and affine functions as in the less smooth setting have energies bounded above by $\mu\ell\lambda^2$ and $\mu\lambda^2$, respectively. The branching construction from [42] is slightly adapted in order to ensure $s_y \in W^{1,2}((-\ell, 0) \times (0, 1))$. An explicit mollification in y of the branching construction for equal volume fractions can be found in [52]. We do not recall the construction here to keep track of the additional parameters, but refer to the proof of Theorem 3.4 where we consider a function S for which $J_1(S) \leq J_4(S) \lesssim \kappa^{2/3}\lambda^{2/3}\mu^{1/3}\ell^{1/3}$. We note that the truncated branching construction can be smoothed analogously. □

Finally, we consider the fully regularized smoothed functional J_4 as given in Eq. (14).

Theorem 3.4 *There are constants C_1, $C_2 > 0$ such that for all $0 < \mu \lesssim \beta$, all κ, $\ell > 0$ and $0 < \lambda \leq \frac{1}{2}$,*

$$C_1 \min J_4(s) \leq \min\left\{\mu\ell\lambda^2, \max\left\{\kappa\lambda^2, \min\left\{\mu\lambda^2\ ,\ \mu^{1/3}\kappa^{2/3}\ell^{1/3}\lambda^{2/3}\ ,\ (\mu\kappa)^{1/2}\lambda\right\}\right\}\right\} \leq C_2 \min J_4(s)\ .$$

Proof: To show the lower bound we first observe that $J_4(s) \gtrsim J_1(s)$ for all admissible s. Hence Theorem 3.3 implies that for all admissible s,

$$J_4(s) \gtrsim \min\left\{\mu\ell\lambda^2\ ,\ \mu^{1/3}\kappa^{2/3}\ell^{1/3}\lambda^{2/3}\ ,\ (\mu\kappa)^{1/2}\lambda\ ,\ \mu\lambda^2\right\}\ .$$

Therefore it suffices to show that the inequality $J_4(s) \gtrsim \min\left\{\mu\ell\lambda^2\ ,\ \kappa\lambda^2\right\}$ holds for all admissible functions s. We estimate the energy contributions from the austenite part below by trace theorem,

$$\begin{aligned} &\beta\int_0^\infty\int_0^1 |\nabla s|^2\, dydx + \frac{\kappa^2}{\mu}\int_0^\infty\int_0^1 \left|\nabla^2 s\right|^2 dydx \\ \gtrsim\ &\kappa\left(\frac{\mu}{\kappa}\int_0^\infty\int_0^1 |\nabla s|^2\, dydx + \frac{\kappa}{\mu}\int_0^\infty\int_0^1 \left|\nabla^2 s\right|^2 dydx\right) \gtrsim \kappa\,|s_0|^2_{H^1(0,1)} = \kappa\int_0^1 |Ds(0,y)|^2\, dy\ . \end{aligned}$$

We fix some small constant $c_0 \ll 1$. If

$$\int_0^1 |Ds(0,y)|\, dy > c_0\lambda$$

then by the above estimate

$$J_4(s) \geq \kappa\int_0^1 |Ds(0,y)|^2\, dy \gtrsim \kappa\lambda^2\ .$$

Otherwise, for c_0 small enough,

$$\int_0^1 \operatorname{dist}(\nabla s(0,y), K)\, dy > \frac{1}{4}\lambda\ . \tag{28}$$

Suppose now that $J_4(s) < c_0\mu\ell\lambda^2$. Then there is a set $M \subset (-\ell, 0)$ with $|M| > 0$ and

$$\int_0^1 \operatorname{dist}(\nabla s(x,y), K)\, dy \le 2c_0\lambda \quad \text{for all } x \in M .$$

We fix $x_0 \in (-\ell, 0)$ such that

$$\int_0^1 \operatorname{dist}(\nabla s(x_0,y), K)\, dy \le 2c_0\lambda \quad \text{and} \quad \int_0^1 (\nabla s(x,y), K)\, dy > 2c_0\lambda \quad \text{for almost all } x_0 < x < 0 .$$

Notice that $x_0 < 0$ in view of Eq. (28). Then

$$\mu \int_{-\ell}^0 \int_0^1 \operatorname{dist}^2(\nabla s(x,y), K)\, dydx \ge \mu \int_{x_0}^0 \int_0^1 \operatorname{dist}^2(\nabla s(x,y), K)\, dydx \gtrsim \mu |x_0| \lambda^2 . \tag{29}$$

On the other hand-side as in the proof of Theorem 3.2 we have $\int_0^1 |s_y(x_0,y)|\, dy \ge \frac{\lambda}{4}$ and hence

$$\int_{x_0}^0 \int_0^1 \left|D^2 s(x,y)\right| + \int_0^1 |Ds(0,y)|\, dydx \ge \frac{\lambda}{4} .$$

Since $\int_0^1 |Ds(0,y)|\, dy \le c_0\lambda$, this implies for c_0 small enough,

$$\frac{\kappa^2}{\mu} \int_{x_0}^0 \int_0^1 \left|D^2 s(x,y)\right|^2 dydx \gtrsim \frac{\kappa^2\lambda^2}{\mu |x_0|} ,$$

which with Eq. (29) finally yields

$$J_4(s) \gtrsim \frac{\kappa^2\lambda^2}{\mu |x_0|} + \mu\lambda^2 |x_0| \ge \kappa\lambda^2 .$$

For the upper bound we use again the same type of test functions with slight modifications to satisfy the smoothness conditions.

1. **Smoothed linear interpolation:** For $\delta > 0$ we define

$$s(x,y) = \begin{cases} \frac{2\lambda}{\delta^3} yx^3 + \frac{3\lambda}{\delta^2} yx^2 & \text{if } -\delta \le x \le 0 \\ \lambda y & \text{if } x \le -\delta \\ 0 & \text{if } x \ge 0 \end{cases} .$$

Then $v \in W^{2,2}((\min\{-\delta, -\ell\}, \infty) \times (0,1))$, and

$$J_4(s) \lesssim \frac{\mu\lambda^2}{\delta} + \mu\delta\lambda^2 + \frac{\kappa^2\lambda^2}{\mu}\left(\frac{1}{\delta} + \frac{1}{\delta^3}\right) .$$

   (a) If $\mu\lambda^2 \le \kappa \le \mu$ we choose $\delta \sim 1$. Then $J_4(s) \sim \mu\lambda^2 + \frac{\kappa^2}{\mu}\lambda^2 \lesssim \mu\lambda^2$.

   (b) If $\mu \le \kappa$ we choose $\delta \sim \frac{\kappa}{\mu}$. Then $J_4(s) \lesssim \kappa\lambda^2$.

2. **Smoothed finite branching:** We consider the case $\kappa \lesssim \mu\lambda^2 \min\left\{\ell, \ell^{-2}\right\}$. In [21] it is announced that a mollification of the Kohn-Müller construction will appear in [16]. Again we fix some $\theta \in \left(\frac{1}{4}, \frac{1}{2}\right)$, and choose I, $N \in \mathbb{N}$ such that $N \sim \mu^{1/3}\lambda^{2/3}\kappa^{-1/3}\ell^{-2/3}$, and $\theta^I \sim \kappa^{2/3}\mu^{-2/3}\ell^{-2/3}\lambda^{-1/3}$. Further we choose a mollification parameter $\delta \sim \kappa/\mu$. We note that these parameter choices imply that for all $i \leq I$,

$$\delta \lesssim \frac{\lambda}{2^i N}\,, \quad \delta \lesssim \ell\theta^i \quad \text{and} \quad \frac{\lambda}{(2\theta)^i\,\ell N} < \frac{\lambda}{\theta^{I/2}\ell N} \sim \lambda^{1/2} \ll 1\,. \tag{30}$$

Let $s \in W^{1,2}\left((-\ell,\infty)\times(0,1)\right)$ be the finite branching construction defined in the proof of Theorem 3.2, and define a $W^{1,2}$-extension of s to $(-\ell-\delta,\infty)\times(-\delta,1+\delta)$ by extending s constantly in x for $x < -\ell$ or $x = 0$, and antiperiodically in y for $y < 0$ or $y > 1$. We set $S := \mathcal{E}s * \phi_\delta$, where $\phi_\delta : \mathbb{R}^2 \to \mathbb{R}$ is a mollifier, i.e., $\phi_\delta(\boldsymbol{x}) = \frac{1}{\delta}\phi\left(\frac{\boldsymbol{x}}{\delta}\right)$ with $\phi \in \mathcal{C}_0^\infty\left(B_1(0)\right)$ such that $\int_{B_1(0)}\phi(y)\,dy = 1$, $0 \leq \phi \leq 1$ and $\phi(\boldsymbol{x}) = \mu(|\boldsymbol{x}|)$ for some $\mu : [0,\infty) \to \mathbb{R}$.
We collect the energy contributions separately. Since $\mathcal{E}s$ is piecewise affine, the partial derivatives S_x, S_y differ from $\mathcal{E}s_x$, $\mathcal{E}s_y$ only in δ-neighborhoods of the boundaries of the domain $\{y = 0 \text{ or } y = 1\}$ and $\{x = -\ell \text{ or } x = 0\}$, the refinement boundaries $\left\{x = -\ell\theta^i, i \leq I\right\}$, and the twin boundaries where the gradient of $\mathcal{E}s$ jumps. By definition of the convolution, we have a pointwise bound on S_x, i.e.,

$$\mu\int_{-\ell}^{-\ell\theta^I}\int_0^1 S_x^2(x,y)\,dydx \lesssim \sum_{i=0}^{I-1}\frac{\mu\ell\theta^i\lambda^2}{(2\theta)^{2i}\,\ell^2N^2} \lesssim \kappa^{2/3}\lambda^{2/3}\mu^{1/3}\ell^{1/3}\,.$$

For S_y we consider the contribution from the δ-neighborhoods of the twin boundaries and the refinement boundaries separately,

$$\mu\int_{-\ell}^{-\ell\theta^I}\operatorname{dist}^2\left(s_y,\{\lambda,-1+\lambda\}\right)dydx \lesssim \sum_{i=0}^{I-1}\left\{\mu\left(\ell\theta^i\right)\delta\left(2^iN\right) + \mu\delta\lambda\right\} \lesssim \kappa^{2/3}\lambda^{2/3}\mu^{1/3}\ell^{1/3}\,,$$

where the last step follows as for the unsmoothed finite branching construction in the proof of Theorem 3.2. We consider the partial second derivatives separately. Again we expect contributions from the twin boundaries and the refinement boundaries which we estimate above very roughly by

$$\begin{aligned}\frac{\kappa^2}{\mu}\int_{-\ell}^{-\ell\theta^I}\int_0^1 S_{xx}(x,y)\,dydx &\lesssim \sum_{i=0}^{I-1}\frac{\kappa^2}{\mu}\left\{\left(2^iN\right)\left(\ell\theta^i\right)\delta\frac{\lambda^2}{(2\theta)^{2i}\,\ell^2N^2\delta^2} + \delta\frac{\lambda^2}{(2\theta)^{2i}\,\ell^2N^2\delta^2}\right\}\\ \lesssim\ \frac{\kappa\lambda^2}{(2\theta)^I\,\ell N} + \frac{\kappa\lambda^2}{(2\theta)^{2I}\,\ell^2N^2} &\lesssim \frac{\kappa\lambda^2}{\theta^I\ell N} + \kappa \lesssim \kappa^{2/3}\lambda^{2/3}\mu^{1/3}\ell^{1/3}\,.\end{aligned}$$

Next, the estimates (30) imply that the slopes of the twin boundaries for all $i \leq I$ are bounded in absolute value by ~ 1. Hence,

$$\frac{\kappa^2}{\mu}\int_{-\ell}^{-\ell\theta^I}\int_0^1 S_{yy}^2(x,y)\,dydx \lesssim \frac{\kappa^2}{\mu}\sum_{i=0}^{I-1}\left\{\left(2^iN\right)\delta\left(\ell\theta^i\right)\frac{1}{\delta^2} + \frac{\kappa^2}{\mu}\left(2^iN\right)\delta^2\frac{1}{\delta^2}\right\} \lesssim \kappa\ell N + \kappa\lambda I\,,$$

which again is bounded above by $\kappa^{2/3}\lambda^{2/3}\mu^{1/3}\ell^{1/3}$ as spelled out for the finite branching construction. Finally, since s_x and s_y are piecewise constant with the same jump set, by (30),

$$\int_{-\ell}^{-\ell\theta^I}\int_0^1 S_{xy}^2\,(x,y)\,dydx \lesssim \int_{-\ell}^{-\ell\theta^I}\int_0^1 S_{yy}^2\,(x,y)\,dydx\,,$$

which concludes the estimates on $\left(-\ell,-\ell\theta^I\right)\times(0,1)$. In the interpolation layer $-\ell\theta^I \le x \le \delta$ we proceed similarly as on the above treated intervals, and observe additionally (see proof of Theorem 3.2 and recall that $\delta \lesssim \ell\theta^I$)

$$\mu\int_{-\ell\theta^I}^{\delta}\int_0^1 \operatorname{dist}^2\left(S_y,\{\lambda,-1+\lambda\}\right)dydx \lesssim \mu\ell\theta^I\left(\lambda+\lambda^2\right) \lesssim \mu^{1/3}\ell^{1/3}\kappa^{2/3}\lambda^{2/3}\,.$$

3. **Truncated smoothed finite branching:** The truncated branching construction can be mollified analogously.

□

4 An example of a low-hysteresis alloy

We now focus on more quantitative properties of the transition layers. As an example we consider the alloy $Ti_{50}Ni_{39}Pd_{11}$. This alloy undergoes a cubic to orthorhombic transformation. The six variants of martensite are given by the transformation stretch matrices

$$\begin{aligned}
\boldsymbol{U}_1 &= \begin{pmatrix} \frac{\lambda_2+\lambda_3}{2} & \frac{\lambda_2-\lambda_3}{2} & 0 \\ \frac{\lambda_2-\lambda_3}{2} & \frac{\lambda_2+\lambda_3}{2} & 0 \\ 0 & 0 & \lambda_1 \end{pmatrix},\ \boldsymbol{U}_2 = \begin{pmatrix} \frac{\lambda_2+\lambda_3}{2} & \frac{\lambda_3-\lambda_2}{2} & 0 \\ \frac{\lambda_3-\lambda_2}{2} & \frac{\lambda_2+\lambda_3}{2} & 0 \\ 0 & 0 & \lambda_1 \end{pmatrix},\ \boldsymbol{U}_3 = \begin{pmatrix} \frac{\lambda_2+\lambda_3}{2} & 0 & \frac{\lambda_2-\lambda_3}{2} \\ 0 & \lambda_1 & 0 \\ \frac{\lambda_2-\lambda_3}{2} & 0 & \frac{\lambda_2+\lambda_3}{2} \end{pmatrix}, \\
\boldsymbol{U}_4 &= \begin{pmatrix} \frac{\lambda_2+\lambda_3}{2} & 0 & \frac{\lambda_3-\lambda_2}{2} \\ 0 & \lambda_1 & 0 \\ \frac{\lambda_3-\lambda_2}{2} & 0 & \frac{\lambda_2+\lambda_3}{2} \end{pmatrix},\ \boldsymbol{U}_5 = \begin{pmatrix} \lambda_1 & 0 & 0 \\ 0 & \frac{\lambda_2+\lambda_3}{2} & \frac{\lambda_2-\lambda_3}{2} \\ 0 & \frac{\lambda_2-\lambda_3}{2} & \frac{\lambda_2+\lambda_3}{2} \end{pmatrix},\ \boldsymbol{U}_6 = \begin{pmatrix} \lambda_1 & 0 & 0 \\ 0 & \frac{\lambda_2+\lambda_3}{2} & \frac{\lambda_3-\lambda_2}{2} \\ 0 & \frac{\lambda_3-\lambda_2}{2} & \frac{\lambda_2+\lambda_3}{2} \end{pmatrix}
\end{aligned} \tag{31}$$

with ordered eigenvalues $\lambda_1 \le \lambda_2 \le \lambda_3$. The measured eigenvalues are [56, Tab. 1]

$$\lambda_1 = 0.9280, \quad \lambda_2 = 1.0001, \quad \lambda_3 = 1.0674\,,$$

but following [56] we set the middle eigenvalue to $\lambda_2 = 1$. Up to sign, there are two different habit plane normals which we abbreviate by

$$\text{pmm} := (0.5005, -0.5005, -0.7064) \quad \text{and} \quad \text{mpm} := (-0.5005, 0.5005, -0.7064)\,. \tag{32}$$

Throughout the text we refer to the habit plane with normal pmm as *habit plane pmm*, and similarly to the one with normal mpm as *habit plane mpm*.

The six variants can pairwise form twins [9], and all variants are symmetry-related in the sense that for all $1 \le i,j \le 6$ there are rotations $\boldsymbol{R}_{ij} = \boldsymbol{R}_{ij}^T \in SO\,(3)$ such that $\boldsymbol{U}_i = \boldsymbol{R}_{ij}\boldsymbol{U}_j\boldsymbol{R}_{ij}$. As we aim at comparing transition layers for the possible twin systems we make use of these symmetries to restrict the number of different structures.

4.1 Symmetries among the crystallographic parameters for different twin systems

In [56, Sec. 6] it is remarked that for cubic to orthorhombic transformations due to symmetries it suffices to consider twin systems that consist of a fixed variant twinned with all other variants. In [30, Sec. 5.5] symmetry relations between variants are invoked to restrict the discussion of uniqueness of simple laminates to representative twin systems. We spell out the symmetries and their consequences explicitly to apply them in the subsequent sections.
Suppose that the positive definite symmetric matrices $\boldsymbol{V}_i$, $\boldsymbol{V}_\ell$, $\boldsymbol{U}_i$, $\boldsymbol{U}_\ell \in \mathbb{R}^{3\times 3}$, $\boldsymbol{U}_i \notin SO(3)\,\boldsymbol{V}_i$ and $\boldsymbol{U}_\ell \notin SO(3)\,\boldsymbol{V}_\ell$ have the following properties:

- There is a solution

$$\left(\hat{\boldsymbol{R}}_i, \boldsymbol{R}_i, \boldsymbol{a}_i, \boldsymbol{n}_i, \boldsymbol{b}_i, \boldsymbol{m}_i\right) \in SO(3)\times SO(3)\times \mathbb{R}^3 \times S^2 \times \mathbb{R}^3 \times S^2 \tag{33}$$

  of the crystallographic equations

$$\boldsymbol{R}_i\boldsymbol{U}_i - \hat{\boldsymbol{R}}_i\boldsymbol{V}_i = \boldsymbol{a}_i\otimes\boldsymbol{n}_i \quad , \quad \text{and} \quad \lambda\boldsymbol{R}_i\boldsymbol{U}_i + (1-\lambda)\,\hat{\boldsymbol{R}}_i\boldsymbol{V}_i - \boldsymbol{I} = \boldsymbol{b}_i\otimes\boldsymbol{m}_i \tag{34}$$

  where $S^2 := \left\{\boldsymbol{x}\in\mathbb{R}^3 \,:\, |\boldsymbol{x}| = 1\right\}$.

- There is an orthogonal transformation $\boldsymbol{Q}\in O(3)$ such that

$$\boldsymbol{Q}\boldsymbol{V}_i = \boldsymbol{V}_\ell\boldsymbol{Q} \quad , \quad \text{and} \quad \boldsymbol{Q}\boldsymbol{U}_i = \boldsymbol{U}_\ell\boldsymbol{Q}\,. \tag{35}$$

We note that we allow for general orthogonal matrices to simplify the notation later. The two assumptions hold true for mot of the common crystallographic changes. If we define

$$\hat{\boldsymbol{R}}_\ell = \boldsymbol{Q}\hat{\boldsymbol{R}}_i\boldsymbol{Q}^T\,, \quad \boldsymbol{R}_\ell = \boldsymbol{Q}\boldsymbol{R}_i\boldsymbol{Q}^T\,, \quad \boldsymbol{a}_\ell = \boldsymbol{Q}\boldsymbol{a}_i\,, \quad \boldsymbol{n}_\ell = \boldsymbol{Q}\boldsymbol{n}_i\,, \quad \boldsymbol{b}_\ell = \boldsymbol{Q}\boldsymbol{b}_i\,, \quad \boldsymbol{m}_\ell = \boldsymbol{Q}\boldsymbol{m}_i\,. \tag{36}$$

Then

$$\left(\hat{\boldsymbol{R}}_\ell, \boldsymbol{R}_\ell, \boldsymbol{a}_\ell, \boldsymbol{n}_\ell, \boldsymbol{b}_\ell, \boldsymbol{m}_\ell\right) \in SO(3)\times SO(3)\times \mathbb{R}^3 \times S^2 \times \mathbb{R}^3 \times S^2 \tag{37}$$

and

$$\boldsymbol{R}_\ell\boldsymbol{U}_\ell - \hat{\boldsymbol{R}}_\ell\boldsymbol{V}_\ell = \boldsymbol{a}_\ell\otimes\boldsymbol{n}_\ell \quad , \quad \text{and} \quad \lambda\boldsymbol{R}_\ell\boldsymbol{U}_\ell + (1-\lambda)\,\hat{\boldsymbol{R}}_\ell\boldsymbol{V}_\ell - \boldsymbol{I} = \boldsymbol{b}_\ell\otimes\boldsymbol{m}_\ell\,.$$

Proposition 4.1 *Assume that Eqs.* (33)*,* (34) *and* (35) *hold. Suppose further that there is a* $180°$*-rotation* $\boldsymbol{D}_i = \boldsymbol{D}_i^T \in SO(3)$ *about some axis* $\boldsymbol{e}_i \in S^2$ *such that* $\boldsymbol{U}_i = \boldsymbol{D}_i\boldsymbol{V}_i\boldsymbol{D}_i$*. Then* $\boldsymbol{U}_\ell = \boldsymbol{D}_\ell\boldsymbol{V}_\ell\boldsymbol{D}_\ell$ *for the* $180°$*-rotation* $\boldsymbol{D}_\ell = \boldsymbol{D}_\ell^T \in SO(3)$ *about the axis* $\boldsymbol{e}_\ell = \boldsymbol{Q}\boldsymbol{e}_i \in S^2$*. In particular, with the notation introduced above the pair* $(\boldsymbol{a}_\ell, \boldsymbol{n}_\ell)$ *describes a twin of the same crystallographic type as* $(\boldsymbol{a}_i, \boldsymbol{n}_i)$*.*

Proof: The $180°$-rotation is represented by the matrix $\boldsymbol{D}_i = -\boldsymbol{I} + 2\boldsymbol{e}_i\otimes\boldsymbol{e}_i$. By the commutator relations given in Eq. (35) we find

$$\begin{aligned}\boldsymbol{U}_\ell &= \boldsymbol{Q}\boldsymbol{U}_i\boldsymbol{Q}^T = \boldsymbol{Q}\boldsymbol{D}_i\boldsymbol{V}_i\boldsymbol{D}_i\boldsymbol{Q}^T = \boldsymbol{Q}\left(-\boldsymbol{I} + 2\boldsymbol{e}_i\otimes\boldsymbol{e}_i\right)\left(\boldsymbol{Q}^T\boldsymbol{Q}\right)\boldsymbol{V}_i\left(-\boldsymbol{I} + 2\boldsymbol{e}_i\otimes\boldsymbol{e}_i\right)\boldsymbol{Q}^T \\ &= \left(-\boldsymbol{I} + 2\left(\boldsymbol{Q}\boldsymbol{e}_i\right)\otimes\left(\boldsymbol{Q}\boldsymbol{e}_i\right)\right)\boldsymbol{V}_\ell\left(-\boldsymbol{I} + 2\left(\boldsymbol{Q}\boldsymbol{e}_i\right)\otimes\left(\boldsymbol{Q}\boldsymbol{e}_i\right)\right) =: \boldsymbol{D}_\ell\boldsymbol{V}_\ell\boldsymbol{D}_\ell\,,\end{aligned}$$

where $\boldsymbol{D}_\ell = \boldsymbol{D}_\ell^T \in SO\,(3)$ describes a $180°$-rotation about the axis $\boldsymbol{Q}\boldsymbol{e}_i$.
If $(\boldsymbol{a}_i, \boldsymbol{n}_i)$ describes a type I twin then $\boldsymbol{n}_i \in \{\pm\boldsymbol{e}_i\}$ (see [9, Res. 5.2]). This implies $\boldsymbol{n}_\ell \in \{\pm\boldsymbol{Q}\boldsymbol{e}_i\} = \{\pm\boldsymbol{e}_\ell\}$, i.e., $(\boldsymbol{a}_\ell, \boldsymbol{n}_\ell)$ describes also a type I twin. On the other hand, if $(\boldsymbol{a}_i, \boldsymbol{n}_i)$ describes a type II twin then $\boldsymbol{a}_i \in \{\pm\rho\boldsymbol{V}_i\boldsymbol{e}_i\}$ with $\rho = \left|2\left(\boldsymbol{e}_i - \frac{\boldsymbol{V}_i^2\boldsymbol{e}_i}{|\boldsymbol{V}_i\boldsymbol{e}_i|^2}\right)\right|$ (see again [9, Res. 5.2]). Hence, $\boldsymbol{a}_\ell = \boldsymbol{Q}\boldsymbol{a}_i = \pm\rho\boldsymbol{Q}\boldsymbol{V}_i\boldsymbol{e}_i = \pm\rho\boldsymbol{V}_\ell\boldsymbol{e}_\ell$, which implies that $(\boldsymbol{a}_\ell, \boldsymbol{n}_\ell)$ describes a type II twin, as well. Finally, if $(\boldsymbol{a}_i, \boldsymbol{n}_i)$ describes a compound twin, that is, it can be described as both, a type I and a type II twin (corresponding to different rotations $\boldsymbol{D}_i$), then the above arguments show that so does $(\boldsymbol{a}_\ell, \boldsymbol{n}_\ell)$. □
If the orthogonal transformation $\boldsymbol{Q}$ is symmetric, then many more quantities are also related via the orthogonal transformation. We collect them in the following remark as far as they will be needed later.

Remark 4.2 *Under the assumptions* (33)*,* (34) *and* (35)*, suppose* $\boldsymbol{Q} = \boldsymbol{Q}^T$ *and set* $\boldsymbol{A}_i := \hat{\boldsymbol{R}}_i\boldsymbol{V}_i = \boldsymbol{Q}\boldsymbol{A}_\ell\boldsymbol{Q}$*. Then the following relations hold true:*

$$\boldsymbol{A}_\ell^{-T}\boldsymbol{m}_\ell \;=\; \boldsymbol{Q}\left(\boldsymbol{A}_i^{-T}\boldsymbol{m}_i\right)\,, \quad \boldsymbol{A}_\ell^{-T}\boldsymbol{n}_\ell = \boldsymbol{Q}\left(\boldsymbol{A}_i^{-T}\boldsymbol{n}_i\right)\,, \quad \boldsymbol{n}_\ell^\perp = \boldsymbol{Q}\boldsymbol{n}_i^\perp\,, \tag{38}$$

where $\boldsymbol{n}^\perp := -\frac{\boldsymbol{m}\cdot\boldsymbol{n}}{\sqrt{1-(\boldsymbol{m}\cdot\boldsymbol{n})^2}}\,\boldsymbol{n} + \frac{1}{\sqrt{1-(\boldsymbol{m}\cdot\boldsymbol{n})^2}}\,\boldsymbol{m}$*. Due to orthogonality of* $\boldsymbol{Q}$ *scalar products are preserved, i.e.,*

$$\boldsymbol{x}_i \cdot \boldsymbol{y}_i = \boldsymbol{x}_\ell \cdot \boldsymbol{y}_\ell \quad \textit{for all} \quad \boldsymbol{x}, \boldsymbol{y} \in \left\{\boldsymbol{a}, \boldsymbol{n}, \boldsymbol{b}, \boldsymbol{m}, \boldsymbol{A}^{-T}\boldsymbol{m}, \boldsymbol{A}^{-T}\boldsymbol{n}, \boldsymbol{n}^\perp\right\}\,.$$

Example 4.3 *In [30, Sec. 5.5] symmetries between twin systems involving different variants of martensite are listed. As discussed above, these symmetries carry over to solution of the crystallographic equations. It is found that for cubic to orthorhombic transformations there are up to orthogonal transformation only five different structures of interfaces. With the notation introduced in Eq.* (31)*, the five different structures can be represented by a compound twin with variants* $1/2$*, and the two type I and the two type II twins with variants* $1/3$*.*

5 Piecewise affine needle-type microstructures

From now on, we focus on more quantitative properties of the energies of the transition layers. Experimentally, one often observes needle-type structures, where the volume fraction of the minority phase drops to zero close to the interface. We consider a hierarchy of needle-type models and compare the energies for different twin systems and for different types of boundary conditions.
The first more quantitative question addresses the influence of the twin system on the energy. In [56] it has been conjectured that there could be a significant variation of the energies. The conjecture is based on the study of simplified transition layers. We reconsider the model introduced in [56] with a slight modification to make it well-definite in the sense that the energy does not depend on the parametrization of the transition layer. The values of the energy are then found to depend only weakly on the twin system while the optimal structures vary greatly.
Given a solution to the crystallographic equations (1) with a quadruple $S_1 = (\mathbf{a}, \mathbf{n}, \mathbf{b}, \mathbf{m})$, the sets of parameters

$$S_2 = (-\mathbf{a}, -\mathbf{n}, \mathbf{b}, \mathbf{m})\,,\; S_3 = (\mathbf{a}, \mathbf{n}, -\mathbf{b}, -\mathbf{m}) \;\text{ and }\; S_4 = (-\mathbf{a}, -\mathbf{n}, -\mathbf{b}, -\mathbf{m}) \tag{39}$$

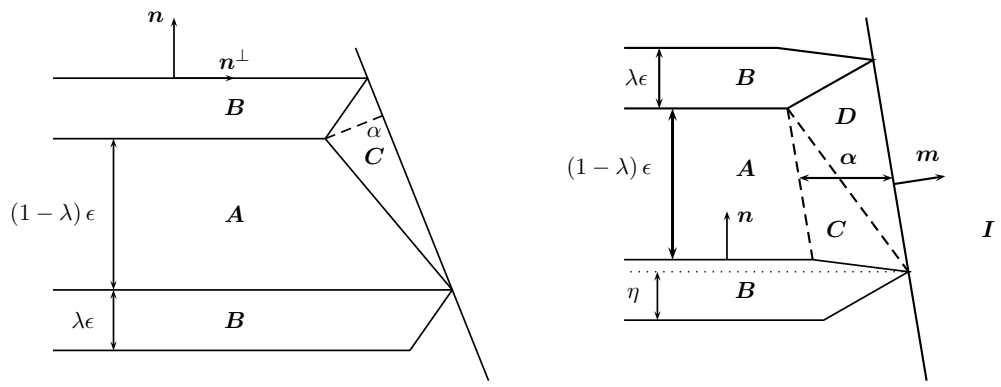

(a) One-parameter transition layer from [56] (b) Two-parameter transition layer

Figure 4: Piecewise affine transition layers

describe the same twin system. This observation corresponds to the fact that the map

$$\mathbb{R}^3 \times \mathbb{R}^3 \to \left\{ \boldsymbol{M} \in \mathbb{R}^{3\times 3} \,:\, \text{rank}\,(\boldsymbol{M}) = 1 \right\} \quad , \quad (\boldsymbol{a}, \boldsymbol{b}) \mapsto \boldsymbol{a} \otimes \boldsymbol{b}$$

is not one-to-one but two-to-one. The minimal energy of a transition layer should not depend on the choice of the quadrupel of parameters from Eq. (39). This invariance requires some symmetry in the set of admissible deformations. We briefly recall the setting studied in [56]. We fix a solution $(\boldsymbol{a}, \boldsymbol{n}, \boldsymbol{b}, \boldsymbol{m})$ of the crystallographic equations. Recall that changing sign of $\boldsymbol{n}$ or $\boldsymbol{m}$ implies a reorientation of $\boldsymbol{m}^\perp$ or $\boldsymbol{n}^\perp$, respectively. The piecewise affine test function introduced in [56, Eq. (14)] is pictured in Fig. 4(a), where the linear interpolation matrix $\boldsymbol{C}$ in a triangle of height $|\alpha|$ is determined by the conditions of crystallographic compatibility,

$$\boldsymbol{C} \;=\; \boldsymbol{A} + \lambda \boldsymbol{a} \otimes \left[\boldsymbol{n} + \frac{\epsilon}{\alpha} (1-\lambda)\, \boldsymbol{m} \right] = \boldsymbol{I} + \boldsymbol{b} \otimes \boldsymbol{m} + \frac{\epsilon}{\alpha} \lambda (1-\lambda)\, \boldsymbol{a} \otimes \boldsymbol{m} \,. \tag{40}$$

We note that the deformation is a special case of the ansatz (10). In contrast to [56], we allow for positive and negative α. The formula for the matrix $\boldsymbol{C}$ depends on the choice of the solution S_i, $i = 1, \ldots, 4$. To estimate the energy of the triangles, a linear elasticity theory is used. We linearize about $\boldsymbol{A}$ and introduce a typical elastic modulus μ. The area of each triangle containing $\boldsymbol{C}$ is $\frac{\epsilon|\alpha|}{2\boldsymbol{m}_\lambda \cdot \boldsymbol{n}_\lambda^\perp}$. Hence the energy of one triangle is (cf. [56, Eq. (20)] but recall that we allow for positive and negative α)

$$\begin{aligned}
\frac{1}{2}E \;&=\; \tilde{E} = \frac{\epsilon\,|\alpha|\,w}{2\boldsymbol{m}\cdot\boldsymbol{n}^\perp} \left(\frac{\mu}{2} \left| \frac{1}{2} \left[\left(\boldsymbol{C}\boldsymbol{A}^{-1} - \boldsymbol{I} \right) + \left(\boldsymbol{C}\boldsymbol{A}^{-1} - \boldsymbol{I} \right)^T \right] \right|^2 \right) \\
&=\; \frac{\epsilon w \mu \lambda^2}{8\boldsymbol{m}\cdot\boldsymbol{n}^\perp} \left\{ |\alpha| \left[\left(\boldsymbol{a} \cdot \left(\boldsymbol{A}^{-T}\boldsymbol{n} \right) \right)^2 + |\boldsymbol{a}|^2 \left| \boldsymbol{A}^{-T}\boldsymbol{n} \right|^2 \right] + \right. \\
&+\; \frac{|\alpha|}{\alpha^2} \epsilon^2 (1-\lambda)^2 \left[\left(\boldsymbol{a} \cdot \left(\boldsymbol{A}^{-T}\boldsymbol{m} \right) \right)^2 + |\boldsymbol{a}|^2 \left| \boldsymbol{A}^{-T}\boldsymbol{m} \right|^2 \right] \\
&+\; \left. \frac{|\alpha|}{\alpha} 2\epsilon (1-\lambda) \left[\left(\boldsymbol{a} \cdot \left(\boldsymbol{A}^{-T}\boldsymbol{n} \right) \right) \left(\boldsymbol{a} \cdot \left(\boldsymbol{A}^{-T}\boldsymbol{m} \right) \right) + |\boldsymbol{a}|^2 \left(\boldsymbol{A}^{-T}\boldsymbol{n} \right) \cdot \left(\boldsymbol{A}^{-T}\boldsymbol{m} \right) \right] \right\} .
\end{aligned} \tag{41}$$

In the remaining sections of this text, we use E as energy in a super-isotropic setting. This definition differs from the one used in [56] by a factor of 2. This factor comes from the choice of the elastic modulus, namely the Young's modulus or the shear modulus. There are two local minima of the energy at

$$\alpha_\pm = \pm\epsilon\,(1-\lambda)\,\sqrt{\frac{\left(\boldsymbol{a}\cdot\left(\boldsymbol{A}^{-T}\boldsymbol{m}\right)\right)^2+|\boldsymbol{a}|^2\left|\boldsymbol{A}^{-T}\boldsymbol{m}\right|^2}{\left(\boldsymbol{a}\cdot\left(\boldsymbol{A}^{-T}\boldsymbol{n}\right)\right)^2+|\boldsymbol{a}|^2\left|\boldsymbol{A}^{-T}\boldsymbol{n}\right|^2}}\,. \tag{42}$$

The positive solution α_+ is the solution obtained in [56, Eq. (21)]. The energy in Eq. (41), however, depends in general crucially on the sign of α. We consider a martensite plate of height h and width w. Then the local minima of the total energy of the triangles are (cf. [56, Eq. (22)]

$$\frac{1}{2}\text{total energy of triangles} = \epsilon w h \mu \lambda^2\,(1-\lambda)\,\xi_\pm\,,$$

where the geometric factors corresponding to $\alpha_\pm$ are

$$\begin{aligned}\xi_\pm \;=\; & \frac{1}{4\boldsymbol{m}\cdot\boldsymbol{n}^\perp}\left(\sqrt{\left(\left(\boldsymbol{a}\cdot\left(\boldsymbol{A}^{-T}\boldsymbol{m}\right)\right)^2+|\boldsymbol{a}|^2\left|\boldsymbol{A}^{-T}\boldsymbol{m}\right|^2\right)\left(\left(\boldsymbol{a}\cdot\left(\boldsymbol{A}^{-T}\boldsymbol{n}\right)\right)^2+|\boldsymbol{a}|^2\left|\boldsymbol{A}^{-T}\boldsymbol{n}\right|^2\right)}\pm\right.\\ \pm\; & \left.\left(\boldsymbol{a}\cdot\left(\boldsymbol{A}^{-T}\boldsymbol{m}\right)\right)\left(\boldsymbol{a}\cdot\left(\boldsymbol{A}^{-T}\boldsymbol{n}\right)\right)\pm|\boldsymbol{a}|^2\left(\boldsymbol{A}^{-T}\boldsymbol{m}\right)\cdot\left(\boldsymbol{A}^{-T}\boldsymbol{n}\right)\right)\,.\end{aligned} \tag{43}$$

Note that if we use another set of parameters S_i, we end up with the same two local minimal values of the energy. To be more precise, denoting with the index $\pm$ the sign of the corresponding α, we find $\xi_\pm$ for S_1 and S_4, and $\xi_\mp$ for S_2 and S_3.

The geometric factors in Eq. (43) involve only scalar products which are preserved under orthogonal transformations. Suppose twin systems consisting of variants i/k and variants j/ℓ, respectively, such that there is a symmetric orthogonal transformation $\boldsymbol{Q}$ with $\boldsymbol{Q}\boldsymbol{U}_i = \boldsymbol{U}_j\boldsymbol{Q}$ and $\boldsymbol{Q}\boldsymbol{U}_k = \boldsymbol{U}_\ell\boldsymbol{Q}$. Then by Remark 4.2, $\boldsymbol{A}_j = \boldsymbol{Q}\boldsymbol{A}_i\boldsymbol{Q}$, $\boldsymbol{B}_j = \boldsymbol{Q}\boldsymbol{B}_i\boldsymbol{Q}$, and $\boldsymbol{C}_j = \boldsymbol{Q}\boldsymbol{C}_i\boldsymbol{Q}$. Hence there is an energy-preserving one-to-one map

$$\boldsymbol{y}_i \mapsto \boldsymbol{y}_j = \boldsymbol{Q}\boldsymbol{y}_i\boldsymbol{Q} \tag{44}$$

between the sets of piecewise affine transition layers involving variants i and ℓ with respect to corresponding sets of crystallographic parameters, and in particular minimizers are mapped to minimizers, and minimal energies coincide.

The geometry of the transition layer varies a lot between the twin systems. We collect the values for $\boldsymbol{m}\cdot\boldsymbol{n}^\perp > 0$ for the representative twin systems in Tab. 1. A vanishing scalar product $\boldsymbol{m}\cdot\boldsymbol{n}^\perp = 0$ corresponds to a degenerate twin system with parallel habit and twin planes, while $\boldsymbol{m}\cdot\boldsymbol{n}^\perp = 1$ corresponds to orthogonal habit and twin planes.

As in all cases $\boldsymbol{m}\cdot\boldsymbol{n} \neq 0$, we can distinguish the local minima by the sign of this scalar product $\boldsymbol{m}\cdot\boldsymbol{n}$. We collect all possible local minimal values for the geometric factors according to Eq. (43) for $Ti_{50}Ni_{39}Pd_{11}$ in Table 1. We collect the four possible values for representative twin systems, i.e., compound twins and the values for the four twin systems involving variants 1 and 3. Then all remaining values can be determined using the symmetries studied in Section 4.1. Up to round-off errors we recover all values from [56, Table 4]. In some cases, however, they do not correspond to the global minima. There is still a remarkable variation in the minimal geometric factors of almost an order of magnitude, and it also varies within a given twin type but the variation is by far not as drastic as claimed in [56]. In the subsequent sections, it is shown that the dependence becomes even weaker if we allow for more flexibility in the transition layers.

Variants	twin type	habit plane	$\boldsymbol{m}\cdot\boldsymbol{n}^\perp$	$\xi\times 10^3$ [56, Tab. 4]	$\xi\times 10^3$	
					$\boldsymbol{m}\cdot\boldsymbol{n}\geq 0$	$\boldsymbol{m}\cdot\boldsymbol{n}<0$
1 and 2	compound	either one	0.87	8.07	7.99	**3.38**
1 and 3	type I	mpm	0.52	48.6	48.3	**3.63**
1 and 3	type II	mpm	1.00	17.6	**17.6**	19.14
1 and 3	type I	pmm	1.00	23.4	22.5	**15.4**
1 and 3	type II	pmm	0.17	162	162.9	**2.07**

Table 1: Geometric factor ξ of the minimal energy for the piecewise affine transition layer from [56]. Bold numbers highlight the minimal value of the energy. Values from [56] were computed using Mathematica, the others using MATLAB.

5.1 Two-parameter ansatz allowing for asymptotic offset

We consider a class of more general piecewise affine transition layers where the interpolation layer allows for two matrices that do not lie on the energy wells, see Fig. 4(b). This model in particular allows for an asymptotic offset η, and we do not require that one of the twin boundaries remains straight up to the interface which allows for symmetric and asymmetric needles. The model will serve as validation for our numerical results in Sec. 6.4.

We proceed as in the previous section along the lines of [56, Sec. 5 and 6], but optimize the geometry with respect to η and α. Here we may assume $\alpha>0$ if we account for the various orientations of the $(\boldsymbol{n},\boldsymbol{m})$-plane, see Eq. (39). Note that reorientation comes along with the change $\eta\to-\lambda-\eta$, where $\eta\epsilon$ denotes the asymptotic offset of the lower needle boundary plane. To measure asymptotic symmetry of the needle, we are hence mainly interested in the deviation of η from $-\frac{\lambda}{2}$. The gradients $\boldsymbol{C}$ and $\boldsymbol{D}$ taking part in the interpolation layer, are determined by the compatibility conditions

$$\boldsymbol{C} \;=\; \boldsymbol{A}+\lambda\boldsymbol{a}\otimes\boldsymbol{n}-\frac{1}{\alpha}(1-\lambda)\,\eta\epsilon\boldsymbol{a}\otimes\boldsymbol{m} \quad\text{and}\quad \boldsymbol{D}=\boldsymbol{A}-\frac{(\eta+\lambda)\,\epsilon}{\alpha}\boldsymbol{a}\otimes\boldsymbol{m}\,. \tag{45}$$

The area of each triangle containing $\boldsymbol{C}$ is $\frac{\epsilon\alpha}{2\boldsymbol{m}\cdot\boldsymbol{n}^\perp}$, and the area of each triangle containing $\boldsymbol{D}$ is $\frac{\epsilon\alpha(1-\lambda)}{2\boldsymbol{m}\cdot\boldsymbol{n}^\perp}$. As in [56, Sec. 6], we estimate the elastic energy of the transition layer in the context of linear elasticity. Since we are only interested in the geometric factor of the energy, we compute the energy only up to a factor depending on the elastic shear modulus and the width of the martensite plate. The geometric factor of the energy of the triangles is

$$\begin{aligned}&\frac{1}{4}\frac{\alpha\epsilon}{2\boldsymbol{m}\cdot\boldsymbol{n}^\perp}\left(\left|\left(\boldsymbol{C}\boldsymbol{A}^{-1}-\boldsymbol{I}\right)+\left(\boldsymbol{C}\boldsymbol{A}^{-1}-\boldsymbol{I}\right)^T\right|^2+(1-\lambda)\left|\left(\boldsymbol{D}\boldsymbol{A}^{-1}-\boldsymbol{I}\right)+\left(\boldsymbol{D}\boldsymbol{A}^{-1}-\boldsymbol{I}\right)^T\right|^2\right)\\ =\;&\frac{1}{4}\frac{\alpha\epsilon}{\boldsymbol{m}\cdot\boldsymbol{n}^\perp}\left((\boldsymbol{a}\cdot\boldsymbol{c}_\lambda)^2+|\boldsymbol{a}|^2\,|\boldsymbol{c}_\lambda|^2\right)+\frac{1}{4}\frac{\epsilon\alpha}{\boldsymbol{m}\cdot\boldsymbol{n}^\perp}(1-\lambda)\left((\boldsymbol{a}\cdot\boldsymbol{d}_\lambda)^2+|\boldsymbol{a}|^2\,|\boldsymbol{d}_\lambda|^2\right)\,,\end{aligned} \tag{46}$$

where $\boldsymbol{c}_\lambda=\lambda\boldsymbol{A}^{-T}\boldsymbol{n}-\frac{1}{\alpha}(1-\lambda)\,\eta\epsilon\boldsymbol{A}^{-T}\boldsymbol{m}$, and $\boldsymbol{d}_\lambda=-\frac{\eta+\lambda}{\alpha}\epsilon\boldsymbol{A}^{-T}\boldsymbol{m}$. We optimize the energy with respect to the height of the trapezoid $\alpha>0$ and the offset η. We keep only the leading order term of the energy. We put $\hat\eta=\frac{\eta}{\lambda}$, divide the energy by λ^2 and evaluate at $\lambda=0$. Then with

$$\boldsymbol{c}_0=\boldsymbol{A}^{-T}\boldsymbol{n}-\frac{1}{\alpha}\hat\eta\epsilon\boldsymbol{A}^{-T}\boldsymbol{m} \quad\text{and}\quad \boldsymbol{d}_0=-\frac{\hat\eta+1}{\alpha}\epsilon\boldsymbol{A}^{-T}\boldsymbol{m}$$

Variants	Twin type	Habit plane	$\boldsymbol{m}\cdot\boldsymbol{n}>0$				$\boldsymbol{m}\cdot\boldsymbol{n}<0$			
			$\hat{\eta}_+$	E_+	$\hat{\eta}_-$	E_-	$\hat{\eta}_+$	E_+	$\hat{\eta}_-$	E_-
1 and 2	compound	either one	-0.35	10.0	-0.65	11.4	-0.35	6.8	-0.65	$\mathbf{5.4}$
1 and 3	type I	pmm	-0.57	31.1	-0.43	30.1	-0.57	$\mathbf{23.0}$	-0.43	24.0
1 and 3	type I	mpm	-0.88	85.7	-0.12	51.5	-0.88	$\mathbf{6.8}$	-0.12	41.0
1 and 3	type II	pmm	-0.98	317.9	-0.02	164.9	-0.98	$\mathbf{4.1}$	-0.02	157.1
1 and 3	type II	mpm	-0.51	$\mathbf{25.2}$	-0.49	25.2	-0.51	26.8	-0.49	26.7

Table 2: Geometric factors of the energy $E_\pm \times 10^3$ and the corresponding offset $\hat{\eta}_\pm$ of the more general piecewise affine transition layer according to Eqs. (48) and (49) for $\epsilon = 1$. Bold numbers highlight the minimal energy. Habit plane normals as defined in Eq. (32).

the geometric factor of the energy of the triangles is

$$\begin{aligned} & \frac{1}{4}\frac{\alpha\epsilon}{\boldsymbol{m}\cdot\boldsymbol{n}^\perp}\left((\boldsymbol{a}\cdot\boldsymbol{c}_0)^2+|\boldsymbol{a}|^2|\boldsymbol{c}_0|^2+(\boldsymbol{a}\cdot\boldsymbol{d}_0)^2+|\boldsymbol{a}|^2|\boldsymbol{d}_0|^2\right) \\ = \; & \frac{1}{4}\frac{\epsilon}{\boldsymbol{m}\cdot\boldsymbol{n}^\perp}\left(\frac{\epsilon^2}{\alpha}\left(2\hat{\eta}^2+2\hat{\eta}+1\right)\left(\left(\boldsymbol{a}\cdot\boldsymbol{A}^{-T}\boldsymbol{m}\right)^2+|\boldsymbol{a}|^2\left|\boldsymbol{A}^{-T}\boldsymbol{m}\right|^2\right)+\right. \\ & \left.+\,\alpha\left(\left(\boldsymbol{a}\cdot\boldsymbol{A}^{-T}\boldsymbol{n}\right)^2+|\boldsymbol{a}|^2\left|\boldsymbol{A}^{-T}\boldsymbol{n}\right|^2\right)-2\hat{\eta}\epsilon\left(\left(\boldsymbol{a}\cdot\boldsymbol{A}^{-T}\boldsymbol{m}\right)\left(\boldsymbol{a}\cdot\boldsymbol{A}^{-T}\boldsymbol{n}\right)+|\boldsymbol{a}|^2\boldsymbol{A}^{-T}\boldsymbol{n}\cdot\boldsymbol{A}^{-T}\boldsymbol{m}\right)\right). \end{aligned} \tag{47}$$

The optimal $\alpha > 0$ is

$$\alpha = \epsilon\sqrt{\frac{\left(2\hat{\eta}^2+2\hat{\eta}+1\right)\left(\left(\boldsymbol{a}\cdot\boldsymbol{A}^{-T}\boldsymbol{m}\right)^2+|\boldsymbol{a}|^2\left|\boldsymbol{A}^{-T}\boldsymbol{m}\right|^2\right)}{\left(\boldsymbol{a}\cdot\boldsymbol{A}^{-T}\boldsymbol{n}\right)^2+|\boldsymbol{a}|^2\left|\boldsymbol{A}^{-T}\boldsymbol{n}\right|^2}}\,. \tag{48}$$

Inserting this α into the energy there are two optimal rescaled offsets $\hat{\eta}$ symmetric around $-\frac{1}{2}$, namely

$$\hat{\eta}_\pm = -\frac{1}{2}\pm\frac{Y}{2\sqrt{2X-Y^2}}\,, \tag{49}$$

with the terms

$$\begin{aligned} X &= \left(\left(\boldsymbol{a}\cdot\boldsymbol{A}^{-T}\boldsymbol{m}\right)^2+|\boldsymbol{a}|^2\left|\boldsymbol{A}^{-T}\boldsymbol{m}\right|^2\right)\left(\left(\boldsymbol{a}\cdot\boldsymbol{A}^{-T}\boldsymbol{n}\right)^2+|\boldsymbol{a}|^2\left|\boldsymbol{A}^{-T}\boldsymbol{n}\right|^2\right)\,, \\ Y &= \left(\boldsymbol{a}\cdot\boldsymbol{A}^{-T}\boldsymbol{m}\right)\left(\boldsymbol{a}\cdot\boldsymbol{A}^{-T}\boldsymbol{n}\right)+|\boldsymbol{a}|^2\boldsymbol{A}^{-T}\boldsymbol{m}\cdot\boldsymbol{A}^{-T}\boldsymbol{n}\,. \end{aligned}$$

The values for the optimal $\hat{\eta}$ and the associated energies for representative twin systems for $\epsilon = 1$ are collected in Tab. 2. We observe again a wide variation of the geometric factors with respect of the choice of the set of parameters. The twin systems leading to offsets $\hat{\eta}$ far away from $-\frac{1}{2}$ are those for which both geometric factors, the ones given in Tab. 2 and the ones from [56] vary strongly with a change of the orientation, cf. Tab. 1.

6 General needle-type periodic non-branching transition layers

We consider a model for periodic non-branching transition layers that was introduced in [56, Sec. 8]. Generalizing the ansatz we allow for relaxation of the austenite, and aim at comparing hard and soft boundary

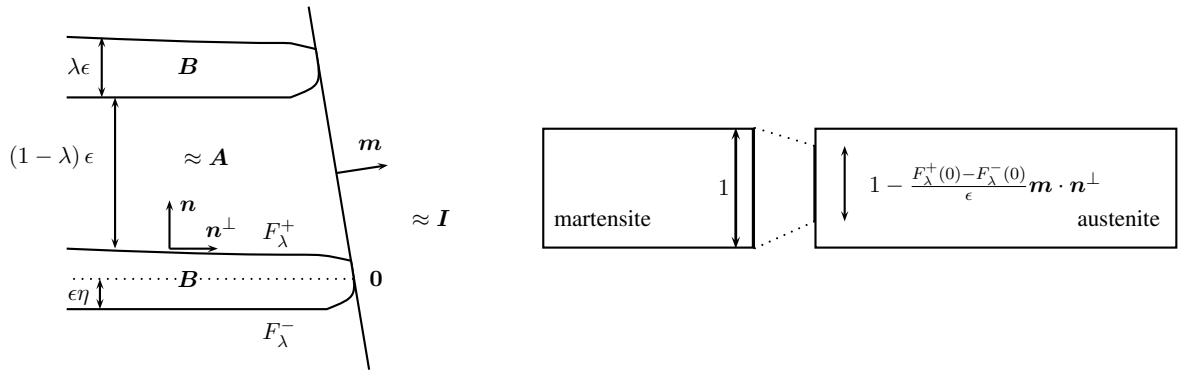

(a) Periodic non-branching transition layer.

(b) Sketch of the reference domain.

Figure 5: Needle-type periodic non-branching transition layers

conditions. For soft boundary conditions we set $\mu = \beta = 1$, and for hard boundary conditions $\mu = 1$ and $\beta = \infty$. We briefly recall the parameters used to describe the transition layer where we essentially follow the paths of [56, Sec. 8] and comment on the differences arising from relaxation of austenite. For the derivation of the model we keep a fixed set of parameters $(\boldsymbol{a}_\lambda, \boldsymbol{n}_\lambda, \boldsymbol{b}_\lambda, \boldsymbol{m}_\lambda)$, and we show later that the minimal energy and the minimizer do not depend on the specific choice of sets of parameters from Eq. (39), see Prop. 6.1.

We assume that there are two compatible variants of martensite represented by matrices $\boldsymbol{A}$ and $\boldsymbol{B}$ that satisfy the crystallographic equations (1) with $\lambda \ll 1$. As sketched in Fig. 5(a) the minority variant $\boldsymbol{B}$ is assumed to occur as thin needles. Essentially following the approach from [56] we use the natural, in general non-orthogonal coordinates given in Eq. (3), where we now place the origin at a middle point of the intersection of the $\boldsymbol{B}_\lambda$-needle with the interface. The twin boundaries are parameterized by Lipschitz functions $F^\pm_\lambda$, i.e., the $\boldsymbol{B}_\lambda$-layer defining the origin is confined by the two surfaces

$$x_2 = F^+_\lambda(x_1), \quad x_2 = F^-_\lambda(x_1), \quad x_1 \le 0 \quad \text{with} \quad F^+_\lambda \ge F^-_\lambda \,. \tag{50}$$

We assume that $F^+ - F^- \le \frac{\xi}{2}$. In terms of the deformation gradients, the transition layer is periodic in x_2-direction. We consider the periodic cell that consists of the $\boldsymbol{A}_\lambda$-layer

$$\mathcal{M}_\lambda := \left\{ \boldsymbol{x} \in \mathbb{R}^3 \,:\, -l < x_1 < 0 \,,\; F^+_\lambda(x_1) < x_2 < F^-_\lambda(x_1) + \xi \,,\; 0 < x_3 < w \right\} \,, \tag{51}$$

the $\boldsymbol{B}_\lambda$-layer

$$\mathcal{B}_\lambda := \left\{ \boldsymbol{x} \in \mathbb{R}^3 \,:\, -l < x_1 < 0 \,,\; F^-_\lambda(x_1) < x_2 < F^+_\lambda(x_1) \,,\; 0 < x_3 < w \right\} \,, \tag{52}$$

and the austenite part

$$\mathcal{A} := \left\{ \boldsymbol{x} \in \mathbb{R}^3 \,:\, 0 < x_1 < \mathcal{L} \,,\; 0 < x_2 < \xi \,,\; 0 < x_3 < w \right\} \,. \tag{53}$$

We formulate the energy minimization problem in terms of the displacement. For a deformation $\boldsymbol{y}_\lambda$, the associated displacement is

$$\boldsymbol{z}_\lambda = \boldsymbol{y}_\lambda - \boldsymbol{I} \,. \tag{54}$$

Outside the transition layer for $x_1 \leq -l$ the twin boundaries are planar. To explicitly describe the needle bending an asymptotic offset parameter η_λ is introduced, that is (see [56, Eq.(47)])

$$\begin{aligned} \boldsymbol{z}_\lambda(\boldsymbol{x}) &= \boldsymbol{y}_\lambda^{(M)}(\boldsymbol{x} - \eta_\lambda \epsilon \boldsymbol{n}\lambda) - \boldsymbol{x} \quad \text{for } x_1 = -l \quad \text{with} \\ F_\lambda^-(-l) &= \eta_\lambda \xi \quad \text{and} \quad F_\lambda^+(-l) = (\eta_\lambda + \lambda)\,\xi \end{aligned} \tag{55}$$

where the deformation $\boldsymbol{y}_\lambda^{(M)}$ describes the martensite laminate and is given by (see [56, Eq. (39)])

$$\begin{aligned} \boldsymbol{y}_\lambda^{(M)}(\boldsymbol{x}) &= (\lambda \boldsymbol{B}_\lambda + (1-\lambda)\,\boldsymbol{A}_\lambda)\,\boldsymbol{x} + \epsilon \boldsymbol{a}_\lambda \int_0^{\frac{1}{\epsilon}\boldsymbol{x}\cdot\boldsymbol{n}_\lambda} \chi_\lambda(s)\,ds \quad \text{with} \\ \chi_\lambda(s) &= \begin{cases} 1-\lambda\,, & 0 \leq s \leq \lambda \\ -\lambda\,, & \lambda \leq s < 1 \end{cases} . \end{aligned} \tag{56}$$

Some studies on needle bending can be found in [11, 46]. Further, following [56, Eq. (49)] we assume constant gradient in the $\boldsymbol{B}_\lambda$-layers,

$$\begin{aligned} \boldsymbol{z}_\lambda(\boldsymbol{x}) &= x_1(\boldsymbol{B}_\lambda - \boldsymbol{I})\,\boldsymbol{n}_\lambda^\perp + x_2(\boldsymbol{B}_\lambda - \boldsymbol{I})\,\boldsymbol{m}_\lambda^\perp - \eta_\lambda \epsilon \boldsymbol{B}_\lambda \boldsymbol{n}_\lambda \\ &\quad \text{for} \quad F_\lambda^-(x_1) < x_2 < F_\lambda^+(x_1)\,, \quad x_1 < 0\,. \end{aligned} \tag{57}$$

If the martensitic variants are not compatible with austenite, that is, if $\lambda_2 \neq 1$, then there cannot be an exact planar interface between one variant of martensite and pure austenite. Hence in the case of hard boundary conditions $\beta \gg \mu$ that is studied in [56] the condition that the gradient in the $\boldsymbol{B}_\lambda$-needle is constant implies that the needles are pinched at the interface, that is $F_\lambda^+(0) = F_\lambda^-(0)$. In case of soft boundary conditions $\beta \sim \mu$, however, there is no such restriction. In the following we set $\mu = \beta = 1$.
By periodicity, Eq. (57) implies boundary conditions for the $\boldsymbol{A}_\lambda$-layer, namely (see [56, Eq.(50)])

$$\begin{aligned} \boldsymbol{z}_\lambda\left(x_1, F_\lambda^+(x_1), x_3\right) &= x_1(\boldsymbol{B}_\lambda - \boldsymbol{I})\,\boldsymbol{n}^\perp + F_\lambda^+(x_1)(\boldsymbol{B}_\lambda - \boldsymbol{I})\,\boldsymbol{m}_\lambda^\perp - \eta_\lambda \epsilon \boldsymbol{B}_\lambda \boldsymbol{n}_\lambda\,, \\ \boldsymbol{z}_\lambda\left(x_1, F_\lambda^-(x_1) + \xi, x_3\right) &= x_1(\boldsymbol{B}_\lambda - \boldsymbol{I})\,\boldsymbol{n}^\perp + F_\lambda^-(x_1)(\boldsymbol{B}_\lambda - \boldsymbol{I})\,\boldsymbol{m}_\lambda^\perp - \eta_\lambda \epsilon \boldsymbol{B}_\lambda \boldsymbol{n}_\lambda \quad \text{for } x_1 < 0\,. \end{aligned}$$

In contrast to [56], we do not assume pure austenite for $x_1 \geq 0$ but only for $x_1 \geq \mathcal{L} := \frac{L}{\boldsymbol{n}^\perp \cdot \boldsymbol{m}}$, that is,

$$\boldsymbol{y}_\lambda(\boldsymbol{x}) = \boldsymbol{y}_\lambda^{(A)}(\boldsymbol{x}) = \boldsymbol{x} - \eta \epsilon \boldsymbol{B}_\lambda \boldsymbol{n}_\lambda\,. \tag{58}$$

Motivated by Eq. (6) we again assume

$$\nabla \boldsymbol{z}_\lambda(\boldsymbol{x})\,\boldsymbol{e} = \boldsymbol{0} \quad \text{for all } \boldsymbol{x} \tag{59}$$

so that $\boldsymbol{z}$ can be considered as a function of x_1 and x_2. Let us summarize the boundary conditions:

$$
\begin{aligned}
&F_\lambda^-(-l) = \eta_\lambda \xi \quad F_\lambda^+(-l) = (\eta_\lambda + \lambda)\,\xi\,, \quad \xi = \frac{\epsilon}{\boldsymbol{m}_\lambda^\perp \cdot \boldsymbol{n}_\lambda} \\
&F_\lambda^+(x_1) \geq F_\lambda^-(x_1) \qquad \text{for} \quad x_1 \leq 0, \\
&\boldsymbol{z}\left(x_1, F_\lambda^+(x_1)\right) = x_1 (\boldsymbol{B}_\lambda - \boldsymbol{I})\,\boldsymbol{n}_\lambda^\perp + F_\lambda^+(x_1)\,(\boldsymbol{B}_\lambda - \boldsymbol{I})\,\boldsymbol{m}_\lambda^\perp - \eta_\lambda \epsilon \boldsymbol{B}_\lambda \boldsymbol{n}_\lambda \quad \text{for} \quad x_1 \leq 0, \\
&\boldsymbol{z}\left(x_1, F_\lambda^-(x_1) + \xi\right) = x_1 (\boldsymbol{B}_\lambda - \boldsymbol{I})\,\boldsymbol{n}_\lambda^\perp + F_\lambda^-(x_1)\,(\boldsymbol{B}_\lambda - \boldsymbol{I})\,\boldsymbol{m}_\lambda^\perp - \eta_\lambda \epsilon \boldsymbol{B}_\lambda \boldsymbol{n}_\lambda \quad \text{for} \quad x_1 \leq 0\,, \\
&\boldsymbol{z}_\lambda(-l, x_2) = -l\,(\boldsymbol{A}_\lambda - \boldsymbol{I})\,\boldsymbol{n}_\lambda^\perp + x_2\,(\boldsymbol{A}_\lambda - \boldsymbol{I})\,\boldsymbol{m}_\lambda^\perp + \epsilon\lambda \boldsymbol{a}_\lambda - \eta_\lambda \epsilon \boldsymbol{A}_\lambda \boldsymbol{n}_\lambda \\
&\quad \text{for } (\eta_\lambda + \lambda)\,\xi < x_2 < (\eta_\lambda + 1)\,\xi, \\
&\boldsymbol{z}_\lambda(0, x_2) = \boldsymbol{z}_\lambda^{(0)}(x_2) \quad \text{for} \quad F_\lambda^+(0) < x_2 < F_\lambda^-(0) + \xi\,, \\
&\boldsymbol{z}_\lambda(0, x_2) = x_2\,(\boldsymbol{B}_\lambda - \boldsymbol{I})\,\boldsymbol{m}_\lambda^\perp - \eta_\lambda \epsilon \boldsymbol{B}_\lambda \boldsymbol{n}_\lambda \text{ for } 0 < x_2 < F_\lambda^+(0)\,, \\
&\boldsymbol{z}_\lambda(0, x_2) = (x_2 - \xi)\,(\boldsymbol{B}_\lambda - \boldsymbol{I})\,\boldsymbol{m}_\lambda^\perp - \eta_\lambda \epsilon \boldsymbol{B}_\lambda \boldsymbol{n}_\lambda \quad \text{for} \quad F_\lambda^-(0) + \xi < x_2 < \xi\,, \\
&\boldsymbol{z}_\lambda(\mathcal{L}, x_2) = \boldsymbol{c}_\lambda^{(A)} = -\eta \epsilon \boldsymbol{B}\boldsymbol{n} \text{ for } 0 < x_2 < \xi\,, \\
&\boldsymbol{z}_\lambda(x_1, 0) = \boldsymbol{z}_\lambda(x_1, \xi)\,, \quad \text{for} \quad x_1 > 0\,.
\end{aligned}
\tag{60}
$$

Formulation on the reference domain: Boundary conditions

To simplify the notation we introduce the function

$$
\tilde{\boldsymbol{z}}_\lambda(x_1, x_2) = \boldsymbol{z}_\lambda(x_1, x_2) + \eta_\lambda \epsilon \boldsymbol{B}_\lambda \boldsymbol{n}_\lambda - \begin{cases} x_1\,(\boldsymbol{A} - \boldsymbol{I})\,\boldsymbol{n}_\lambda^\perp\,, & x_1 \leq 0 \\ 0\,, & x_1 \geq 0 \end{cases}\,. \tag{61}
$$

Following [56, Sec. 8.2], we consider the energy minimization problem on a λ-independent reference domain. For the $\boldsymbol{A}_\lambda$-layer, we follow [56, (56)] but keep track of the constants reflecting the non-orthogonality of the natural coordinate system introduced in Eq. (3). For $\boldsymbol{x} \in \mathbb{R}^3$ we set $\tilde{x}_j := \boldsymbol{x} \cdot \boldsymbol{e}_j$, $j = 1, 2, 3$, where $\{\boldsymbol{e}_1, \boldsymbol{e}_2, \boldsymbol{e}_3\}$ denotes the standard basis in $\mathbb{R}^3$. We consider the transformation

$$
\begin{aligned}
&\left(T_\lambda^{(M)}\right)^{-1} : \left\{\boldsymbol{x} \in \mathbb{R}^3 \ : l \leq \tilde{x}_1 \leq 0\ ,\ 0 \leq \tilde{x}_2 \leq 1\ ,\ 0 \leq \tilde{x}_3 \leq w\right\} \to \mathcal{M}_\lambda\,, \\
&(t_1, t_2, t_3) = t_1 \boldsymbol{e}_1 + t_2 \boldsymbol{e}_2 + t_3 \boldsymbol{e}_3 \mapsto t_1 \boldsymbol{n}^\perp + \left(\left(\xi - \left(F_\lambda^+(t_1) - F_\lambda^-(t_1)\right)\right) t_2 + F_\lambda^+(t_1)\right) \boldsymbol{m}^\perp + t_3 \boldsymbol{e}\,.
\end{aligned}
$$

We refer to the transformed independent variables on the rectangle $\{-l \leq \tilde{x}_1 \leq 0\ ,\ 0 \leq \tilde{x}_2 \leq 1\}$ as (t_1, t_2). For the dependent variables, we make the change

$$
\boldsymbol{u}_\lambda^{(M)}(t_1, t_2) \;=\; \frac{1}{\boldsymbol{m}^\perp \cdot \boldsymbol{n}} \tilde{\boldsymbol{z}}\left(\left(T_\lambda^{(M)}\right)^{-1}(t_1, t_2)\right)\,.
$$

As in [56, Eqs. (59)-(60)], the crystallographic equations yield for $t_1 = x_1 < 0$

$$
\nabla \boldsymbol{y}_\lambda^{(M)}(x_1, x_2) \;=\; \boldsymbol{A}_\lambda + (\boldsymbol{u}_{\lambda,1}(t_1, t_2) - g_\lambda \boldsymbol{u}_{\lambda,2}(t_1, t_2)) \otimes \boldsymbol{m}_\lambda + (\lambda \boldsymbol{a}_\lambda + h_\lambda \boldsymbol{u}_{\lambda,2}(t_1, t_2)) \otimes \boldsymbol{n}_\lambda\,, \tag{62}
$$

where $g_\lambda(t_1,t_2) = \frac{t_2 F_\lambda^{-\prime}(t_1)+(1-t_2)F_\lambda^{+\prime}(t_1)}{\xi-\left(F_\lambda^+(t_1)-F_\lambda^-(t_1)\right)}$, and $h_\lambda(t_1,t_2) = \frac{1}{\xi-\left(F_\lambda^+(t_1)-F_\lambda^-(t_1)\right)}$. The Dirichlet boundary conditions for $\boldsymbol{u}_\lambda^{(M)}$ are

$$\begin{aligned}
\boldsymbol{u}_\lambda^{(M)}(-l,t_2) &= \xi\left((\lambda+\eta_\lambda)-\lambda t_2\right)(1-\lambda)\,\boldsymbol{a}_\lambda \quad , \quad 0<t_2<1 \quad , \\
\boldsymbol{u}_\lambda^{(M)}(t_1,0) &= F_\lambda^+(t_1)(1-\lambda)\,\boldsymbol{a}_\lambda \quad , \quad -l<t_1<0 \quad , \\
\boldsymbol{u}_\lambda^{(M)}(t_1,1) &= F_\lambda^-(t_1)(1-\lambda)\,\boldsymbol{a}_\lambda \quad , \quad -l<t_1<0\,, \\
F_\lambda^+(t_1) &\geq F_\lambda^-(t_1) \quad , \quad -l<t_1<0\,. \qquad (63)
\end{aligned}$$

We note that the boundary conditions of $\boldsymbol{u}_\lambda^{(M)}$ allow to recover the twin boundary curves $F_\lambda^\pm$ from $\boldsymbol{u}_\lambda^{(M)}$ in the sense of traces on the upper and lower boundaries. We use this fact when studying the optimal shapes of the needles. This property, however, strongly relies on the assumption of constant gradient in the $\boldsymbol{B}_\lambda$-layer. Suppose we allow for some relaxation, i.e., we introduce an additional free variable $\boldsymbol{s}_\lambda$ to take part in the minimization and instead of Eq. (57) set

$$\begin{aligned}
\boldsymbol{z}_\lambda(\boldsymbol{x}) &= \boldsymbol{s}_\lambda(x_1,x_2) + x_1(\boldsymbol{B}_\lambda-\boldsymbol{I})\,\boldsymbol{n}_\lambda^\perp + x_2(\boldsymbol{B}_\lambda-\boldsymbol{I})\,\boldsymbol{m}_\lambda^\perp - \eta_\lambda\epsilon\boldsymbol{B}_\lambda\boldsymbol{n}_\lambda \\
&\quad \text{for} \quad F_\lambda^-(x_1)<x_2<F_\lambda^+(x_1)\,, \quad x_1<0\,.
\end{aligned}$$

Then the function $\boldsymbol{s}_\lambda$ enters the boundary conditions for the transformed function $\boldsymbol{u}$ on the reference domain:

$$\begin{aligned}
\boldsymbol{u}_\lambda^{(M)}(t_1,0) &= F_\lambda^+(t_1)(1-\lambda)\,\boldsymbol{a}_\lambda + \frac{1}{\boldsymbol{m}\cdot\boldsymbol{n}^\perp}\boldsymbol{s}_\lambda(x_1,x_2) \quad , \quad -l<t_1<0 \\
\boldsymbol{u}_\lambda^{(M)}(t_1,1) &= F_\lambda^-(t_1)(1-\lambda)\,\boldsymbol{a}_\lambda + \frac{1}{\boldsymbol{m}\cdot\boldsymbol{n}^\perp}\boldsymbol{s}_\lambda(x_1,x_2) \quad , \quad -l<t_1<0\,.
\end{aligned}$$

If $\boldsymbol{s}_\lambda$ depends only on x_1, the width of the needle $F_\lambda^+(x_1)-F_\lambda^-(x_1)$ is still recovered from the boundary data. The offset η_λ, however, is not easily accessible.
We proceed analogously in the austenite part $\mathcal{A}_\lambda$. We apply the transformation

$$\begin{aligned}
T_\lambda^{(A)}\ : \qquad & \mathcal{A}_\lambda \to \left\{\boldsymbol{x}\in\mathbb{R}^3\ :\ 0<\tilde{x}_1<\mathcal{L}\,,\ 0<\tilde{x}_2<1\,,\ 0<\tilde{x}_3<w\right\} \\
& \boldsymbol{x} \mapsto x_1\boldsymbol{e}_1 + \frac{1}{\xi}x_2\boldsymbol{e}_2 + x_3\boldsymbol{e}_3 = \frac{\boldsymbol{x}\cdot\boldsymbol{m}}{\boldsymbol{m}\cdot\boldsymbol{n}^\perp}\boldsymbol{e}_1 + \frac{1}{\xi}\frac{\boldsymbol{x}\cdot\boldsymbol{n}}{\boldsymbol{m}\cdot\boldsymbol{n}^\perp}\boldsymbol{e}_2 + (\boldsymbol{x}\cdot\boldsymbol{e})\,\boldsymbol{e}_3\,,
\end{aligned}$$

and again refer to the transformed variables on the rectangle $(0,\mathcal{L})\times(0,1)$ as (t_1,t_2). For the dependent variables, we make the change

$$\boldsymbol{u}_\lambda(t_1,t_2) = \frac{1}{\boldsymbol{m}\cdot\boldsymbol{n}^\perp}\tilde{\boldsymbol{z}}\left(\left(T_\lambda^{(A)}\right)^{-1}(t_1,t_2)\right)\,,$$

which implies

$$\nabla\boldsymbol{y}_\lambda^{(A)} = \boldsymbol{I} + \boldsymbol{u}_{\lambda,1}\otimes\boldsymbol{m}_\lambda + \frac{1}{\xi}\boldsymbol{u}_{\lambda,2}\otimes\boldsymbol{n}_\lambda\,. \qquad (64)$$

The Dirichlet boundary conditions for $\boldsymbol{u}_\lambda$ in the austenite part are

$$\begin{aligned}
\boldsymbol{u}_\lambda^{(A)}(0,t_2) &= \xi t_2(1-\lambda)\boldsymbol{a}_\lambda \quad , 0<t_2<\frac{F_\lambda^+(0)}{\xi}\,,\\
\boldsymbol{u}_\lambda^{(A)}(0,t_2) &= \xi(t_2-1)(1-\lambda)\boldsymbol{a}_\lambda \quad , \quad \frac{F_\lambda^-(0)}{\xi}+1<t_2<1\,,\\
\boldsymbol{u}_\lambda^{(A)}(t_1,0) &= \boldsymbol{u}_\lambda(t_1,1) \quad , \quad 0<t_1<\mathcal{L}\,,\\
\boldsymbol{u}_\lambda^{(A)}(\mathcal{L},t_2) &= \boldsymbol{0} \quad , \quad 0<t_2<1\,.
\end{aligned} \tag{65}$$

The gluing condition at $t_1=0$ can be reformulated in the sense of traces

$$\boldsymbol{u}_\lambda^{(A)}(0,t_2)=\boldsymbol{u}_\lambda^{(M)}\left(0,\frac{\xi t_2-F_\lambda^+(0)}{\xi+F_\lambda^-(0)-F_\lambda^+(0)}\right) \quad \text{for} \quad \frac{F_\lambda^+(0)}{\xi}<t_2<\frac{F_\lambda^-(0)+\xi}{\xi}\,. \tag{66}$$

The minimization problem

To formulate the minimization problem for the elastic energy on the reference domain we follow the paths of [56, Sec. 8.4]. We study the leading order behavior of minimizing (or almost minimizing) deformations for $\lambda\to 0$, and hence consider sequences of sets of parameters $\{\boldsymbol{A}_\lambda,\boldsymbol{B}_\lambda,\boldsymbol{a}_\lambda,\boldsymbol{n}_\lambda,\boldsymbol{b}_\lambda,\boldsymbol{m}_\lambda\}$ that satisfy the crystallographic equations (1) with $\lambda\ll 1$. The middle eigenvalue of $\boldsymbol{A}_\lambda$ satisfies $\lambda_2=\lambda_2(\lambda)$. We assume that the limit as $\lambda\to 0$ is non-degenerate, i.e., $\boldsymbol{I}\neq\boldsymbol{A}_0$ where the middle eigenvalue of $\boldsymbol{A}_0$ satisfies $\lambda_2=1$. Further $\boldsymbol{n}_0\nparallel\boldsymbol{m}_0$, and $\boldsymbol{a}_0\neq\boldsymbol{0}$, and finally $|\boldsymbol{A}_\lambda-\boldsymbol{A}_0|\leq C\lambda$ as $\lambda\to 0$.
The energy $I(\boldsymbol{u}_\lambda)$ of an admissible function on the reference domain is defined as the elastic energy of the corresponding deformation. Without restriction we may set the width of the specimen to $w=1$. We consider a sequence of free energy densities ϕ_λ such that there is a constant $C>0$ independent of λ such that

$$\phi_\lambda(\nabla\boldsymbol{y}_\lambda(\boldsymbol{x}))\geq C\begin{cases}\operatorname{dist}^2\left(\nabla\boldsymbol{y}_\lambda\boldsymbol{A}_\lambda^{-1},SO(3)\right) & \text{if } x_1<0\\ \operatorname{dist}^2\left(\nabla\boldsymbol{y}_\lambda,SO(3)\right) & \text{if } x_1>0\end{cases}\,. \tag{67}$$

In particular, ϕ depends on λ only via the matrices $\boldsymbol{A}_\lambda$ and $\boldsymbol{B}_\lambda$. We note that this condition can easily be relaxed if we assume that the second derivatives of ϕ_λ are uniformly bounded close to their wells. Motivated by the scaling properties of the piecewise affine test functions we consider the rescaled energy functional

$$\begin{aligned}
&I_\lambda^{c_L}\left(\boldsymbol{u}^{(M)},\boldsymbol{u}^{(A)}\right):=\\
=\;&\begin{cases}\frac{1}{\lambda^2}\left[\int_{-l}^0\int_0^1\phi_\lambda\left(\boldsymbol{A}_\lambda+(\boldsymbol{u}_{,1}(t_1,t_2)-g_\lambda\boldsymbol{u}_{,2}(t_1,t_2))\otimes\boldsymbol{m}_\lambda+(\lambda\boldsymbol{a}_\lambda+h_\lambda\boldsymbol{u}_{,2}(t_1,t_2))\otimes\boldsymbol{n}_\lambda\right)J_\lambda^{(M)}+\right.\\ \left.+\int_0^L\int_0^1\phi_\lambda\left(\boldsymbol{I}+\boldsymbol{u}_{,1}\otimes\boldsymbol{m}_\lambda+\frac{1}{\xi}\boldsymbol{u}_{,2}\otimes\boldsymbol{n}_\lambda\right)J_\lambda^{(A)}\right] & \text{if } \left(\boldsymbol{u}^{(M)},\boldsymbol{u}^{(A)}\right)\in\mathcal{X}_\lambda\\ \infty & \text{else}\end{cases}
\end{aligned} \tag{68}$$

where $\boldsymbol{u}:=\boldsymbol{u}_\lambda$. A pair $\left(\boldsymbol{u}_\lambda^{(M)},\boldsymbol{u}_\lambda^{(A)}\right)$ is admissible for level λ, i.e., $\left(\boldsymbol{u}_\lambda^{(M)},\boldsymbol{u}_\lambda^{(A)}\right)\in\mathcal{X}_\lambda^{c_L}$ if the following conditions hold:

1. $\left(\boldsymbol{u}_\lambda^{(M)},\boldsymbol{u}_\lambda^{(A)}\right)\in H^1\left((-l,0)\times(0,1);\mathbb{R}^3\right)\times H^1\left((0,L)\times(0,1);\mathbb{R}^3\right)$.

2. There are Lipschitz functions $F_\lambda^\pm : (-l, 0) \to \mathbb{R}$ with Lipschitz constants c_L satisfying $0 \leq F_\lambda^+(t_1) - F_\lambda^-(t_1) \leq \frac{\epsilon}{2}$ point-wise for all $-l < t_1 < 0$, and numbers $\eta_\lambda \in \mathbb{R}$ such that $\boldsymbol{u}_\lambda^{(M)}$ satisfies the boundary conditions (63), and $\boldsymbol{u}_\lambda^{(A)}$ satisfies (65). The gluing condition Eq. (66) holds.

In the following, we skip the upper index c_L which corresponds to the uniform Lipschitz bound on the twin boundaries. The limit problem for $\lambda \to 0$ will turn out to be independent of this parameter.

Remark 6.1 *Fix an admissible quadruple of parameters* $(\mathbf{a}_\lambda, \mathbf{n}_\lambda, \mathbf{b}_\lambda, \mathbf{m}_\lambda)$. *Then there is an energy-preserving one-to-one correspondence between the set of admissible functions* $\mathcal{X}_\lambda$ *defined by these parameters and the sets of admissible functions* $\tilde{\mathcal{X}}_\lambda$ *defined by one set of parameters obtained by changing signs as in Eq.* (39).

Proof: We denote by $\tilde{\mathcal{X}}_\lambda$ the set of admissible functions for the equivalent parameters $\left(\tilde{\boldsymbol{a}}_\lambda, \tilde{\boldsymbol{n}}_\lambda, \tilde{\boldsymbol{b}}_\lambda, \tilde{\boldsymbol{m}}_\lambda\right) := (-\boldsymbol{a}_\lambda, -\boldsymbol{n}_\lambda, \boldsymbol{b}_\lambda, \boldsymbol{m}_\lambda)$ we define the map

$$\mathcal{F} : \mathcal{X}_\lambda \to \tilde{\mathcal{X}}_\lambda \quad , \quad \left(\boldsymbol{u}_\lambda^{(M)}, \boldsymbol{u}_\lambda^{(A)}\right) \mapsto \left(\tilde{\boldsymbol{u}}_\lambda^{(M)}, \tilde{\boldsymbol{u}}_\lambda^{(A)}\right) \quad \text{with} \quad \tilde{\boldsymbol{u}}_\lambda^{(M/A)}(t_1, t_2) = \boldsymbol{u}_\lambda^{(M/A)}(t_1, 1 - t_2) \ .$$

Then $\tilde{\boldsymbol{u}}_\lambda^{(M)}$ and $\tilde{\boldsymbol{u}}_\lambda^{(A)}$ satisfy the Dirichlet boundary conditions (63) and (65) with $\tilde{F}_\lambda^\pm = -F_\lambda^\mp$ and $\tilde{\eta}_\lambda = -\lambda - \eta_\lambda$, the periodicity condition, and the gluing condition (66). For the coefficient functions we find

$$\begin{aligned}
\tilde{g}_\lambda(t_1, t_2) &= \frac{t_2 \tilde{F}_\lambda^{-\prime}(t_1) + (1 - t_2)\, \tilde{F}_\lambda^{+\prime}(t_1)}{\xi - \left(\tilde{F}_\lambda^+(t_1) - \tilde{F}_\lambda^-(t_1)\right)} = -g_\lambda(t_1, 1 - t_2) \ , \\
\tilde{h}_\lambda(t_1, t_2) &= \frac{1}{\xi - \left(\tilde{F}_\lambda^+(t_1) - \tilde{F}_\lambda^-(t_1)\right)} = h_\lambda(t_1, t_2) = h_\lambda(t_1, 1 - t_2) \ .
\end{aligned}$$

Further, for the determinant of the Jacobian, $\tilde{J}_\lambda(t_1, t_2) = J_\lambda(t_1, t_2) = J_\lambda(t_1, 1 - t_2)$, and hence the energy of $\tilde{\boldsymbol{u}}$ is given by

$$\tilde{I}_\lambda\left(\tilde{\boldsymbol{u}}^{(M)}, \tilde{\boldsymbol{u}}^{(A)}\right) = I_\lambda\left(\boldsymbol{u}^{(M)}, \boldsymbol{u}^{(A)}\right) \ .$$

Similarly for $\left(\tilde{\boldsymbol{a}}_\lambda, \tilde{\boldsymbol{n}}_\lambda, \tilde{\boldsymbol{b}}_\lambda, \tilde{\boldsymbol{m}}_\lambda\right) = (\mathbf{a}_\lambda, \mathbf{n}_\lambda, -\mathbf{b}_\lambda, -\mathbf{m}_\lambda)$ we define the map $\mathcal{X}_\lambda \to \tilde{\mathcal{X}}_\lambda$ by

$$\tilde{\boldsymbol{u}}_\lambda^{(M/A)}(t_1, t_2) = -\boldsymbol{u}_\lambda^{(M/A)}(t_1, 1 - t_2) \ .$$

Composing the two one-to-one maps yields an energy-preserving one-to-one map for the quadruple of parameters $(-\mathbf{a}_\lambda, -\mathbf{n}_\lambda, -\mathbf{b}_\lambda, -\mathbf{m}_\lambda)$. □

6.1 Computation of the Γ-limit for $\lambda \to 0$

We now turn to the computation of the limit functional for $\lambda \to 0$ of the sequence of energy functionals defined in Eq. (68) in the sense of Γ-convergence [13, 24, 23, 2]. We start with a compactness result, which characterizes weak limits of low energy deformations. We characterize the limits in the martensite and the austenite part separately and show then that the two parts are connected at the interface.

Lemma 6.2 *Suppose* $\left\{\boldsymbol{u}_\lambda^{(M)}, \boldsymbol{u}_\lambda^{(A)}\right\}$ *is a low energy sequence, that is,* $I_\lambda\left(\boldsymbol{u}_\lambda^{(M)}, \boldsymbol{u}_\lambda^{(A)}\right) \leq C$ *with a uniform constant* C *independent of* λ*. Then for a subsequence (not relabeled) we have in the martensite part* $\boldsymbol{v}_\lambda^{(M)} := \frac{1}{\lambda}\boldsymbol{u}_\lambda^{(M)} \rightharpoonup \boldsymbol{v}_0^{(M)}$ *weakly in* $H^1\left((-l,\, 0) \times (0,1)\,; \mathbb{R}^3\right)$*. The limit function satisfies*

$$\begin{aligned}
&\boldsymbol{v}_0^{(M)}(-l, t_2) = \xi\,(1+\eta-t_2)\,\boldsymbol{a}_0 \quad \textit{for} \quad 0 < t_2 < 1 \quad \textit{with some} \quad \eta \in \mathbb{R}\,,\\
&\boldsymbol{v}_0^{(M)}(t_1, 0)\,\|\boldsymbol{a}_0\|\boldsymbol{v}_0^{(M)}(t_1, 1) \quad \textit{and} \quad \left(\boldsymbol{v}_0^{(M)}(t_1, 0) - \boldsymbol{v}_0^{(M)}(t_1, 1)\right)\cdot \boldsymbol{a}_0 \geq 0 \quad \textit{for} \quad -l < t_1 < 0\,.
\end{aligned}$$

Similarly for the austenite part $\boldsymbol{v}_\lambda^{(A)} := \frac{1}{\lambda}\boldsymbol{u}_\lambda^{(A)} \rightharpoonup \boldsymbol{v}_0^{(A)}$ *weakly in* $\left(H^1\left((0, \mathcal{L}) \times (0,1)\right); \mathbb{R}^3\right)$*. For the limit function,*

$$\boldsymbol{v}_0^{(A)}(t_1, 0) = \boldsymbol{v}_0^{(A)}(t_1, 1) \quad \textit{for} \quad 0 < t_1 < \mathcal{L}\,, \quad \textit{and} \quad \boldsymbol{v}_0^{(A)}(\mathcal{L}, t_2) = \boldsymbol{0} \quad \textit{for} \quad 0 < t_2 < 1\,.$$

Finally, $\boldsymbol{v} \in H^1\left((-l, \mathcal{L}) \times (0,1)\,; \mathbb{R}^3\right)$*, where*

$$\boldsymbol{v}(t_1, t_2) = \begin{cases} \boldsymbol{v}_0^{(M)}(t_1, t_2) & \textit{if} \quad t_1 < 0 \\ \boldsymbol{v}_0^{(A)}(t_1, t_2) & \textit{if} \quad t_1 > 0 \end{cases}. \tag{69}$$

Proof: We follow closely the paths of [56, Sec. 8.4.2] and recall the arguments for completeness, pointing out the modifications necessary due to relaxation of the austenite. By the assumptions on ϕ_λ, $F_\lambda^{\pm}$, $\boldsymbol{A}_\lambda$ and $\boldsymbol{y}_\lambda$, there is a constant $C > 0$ such that for all λ,

$$C\lambda^2 \;\geq\; \int_{\mathcal{M}_\lambda} \operatorname{dist}^2\left(\nabla \boldsymbol{y}_\lambda^{(M)}, SO(3)\,\boldsymbol{A}_\lambda\right) d\boldsymbol{x}\,, \text{ and } \quad C\lambda^2 \geq \int_{\mathcal{A}_\lambda} \operatorname{dist}^2\left(\nabla \boldsymbol{y}_\lambda^{(A)}, SO(3)\right) d\boldsymbol{x}\,.$$

By the rigidity lemma [37, Theorem 3.1], there exist rotations $\boldsymbol{R}_\lambda^{(M)}$, $\boldsymbol{R}_\lambda^{(A)} \in SO(3)$ and a constant $C > 0$, which depends only on the uniform Lipschitz bounds of the domains, such that

$$\int_{\mathcal{M}_\lambda} \left|\nabla \boldsymbol{y}_\lambda^{(M)} - \boldsymbol{R}_\lambda^{(M)}\boldsymbol{A}_\lambda\right|^2 dx_2 dx_1 \leq C\lambda^2\,, \text{ and } \int_{\mathcal{A}_\lambda} \left|\nabla \boldsymbol{y}_\lambda^{(A)} - \boldsymbol{R}_\lambda^{(A)}\right|^2 d\boldsymbol{x} \leq C\lambda^2\,.$$

We consider the austenite part first and apply the arguments from [56, Sec. 8.4.2]. By assumption (59), we may without loss of generality assume $x_3 = 0$. Then for $S^{(A)} := \{\boldsymbol{x} \in \mathcal{A}_\lambda \;:\; x_1 = \mathcal{L}\,,\; x_3 = 0\}$, by trace theorem there is a constant $\boldsymbol{c}_\lambda^{(1)}$ such that

$$\int_{S^{(A)}} \left|\boldsymbol{y}_\lambda^{(A)}(\mathbf{x}) - \boldsymbol{R}_\lambda^{(A)}\boldsymbol{x} - \boldsymbol{c}_\lambda^{(1)}\right|^2 dA \leq C\lambda^2\,. \tag{70}$$

We define $\boldsymbol{x}_0 \in S^{(A)}$ by $\boldsymbol{x}_0 \cdot \boldsymbol{m}_\lambda = \left(\boldsymbol{n}_\lambda^{\perp} \cdot \boldsymbol{m}_\lambda\right)\mathcal{L} = L$ and $\boldsymbol{x}_0 \cdot \boldsymbol{n}_\lambda = \frac{\epsilon}{2}$, and we denote the ball with center $\boldsymbol{x}_0$ and radius r by $B(\boldsymbol{x}_0, r)$. By the boundary condition (55), Eq. (70) turns into

$$\int_{\{\boldsymbol{x}\cdot\boldsymbol{m}_\lambda = L\} \cap B(\boldsymbol{x}_0, r)} \left|\left(\boldsymbol{I} - \boldsymbol{R}_\lambda^{(A)}\right)\boldsymbol{x} - \eta_\lambda \epsilon \boldsymbol{B}_\lambda \boldsymbol{n}_\lambda - \boldsymbol{c}_\lambda^{(1)}\right|^2 dA \leq C\lambda^2\,.$$

If we put $\boldsymbol{F}_\lambda := \boldsymbol{I} - \boldsymbol{R}_\lambda^{(A)}$ and choose $r \ll 1$, by the symmetry of $\{\boldsymbol{x}\cdot\boldsymbol{m}_\lambda = L\}\cap B(\boldsymbol{x}_0, r)$ with respect to $\boldsymbol{x}_0$,

$$C\lambda^2 \;\geq\; \left(\boldsymbol{F}_\lambda^T\boldsymbol{F}_\lambda\right)\cdot\int_{\{\boldsymbol{x}\cdot\boldsymbol{m}_\lambda=L\}\cap B(\boldsymbol{x}_0,r)} (\boldsymbol{x}-\boldsymbol{x}_0)\otimes(\boldsymbol{x}-\boldsymbol{x}_0)\,d\boldsymbol{x} + 2r\left|\boldsymbol{F}_\lambda\boldsymbol{x}_0 - \eta_\lambda\epsilon\boldsymbol{B}_\lambda\boldsymbol{n}_\lambda - \boldsymbol{c}_\lambda^{(1)}\right|^2 .$$

Hence the two non-negative terms satisfy $\left|\boldsymbol{F}_\lambda\boldsymbol{x}_0 - \eta_\lambda\epsilon\boldsymbol{B}_\lambda\boldsymbol{n}_\lambda - \boldsymbol{c}_\lambda^{(1)}\right|^2 \leq C\lambda^2$ and $\left(\boldsymbol{F}_\lambda^T\boldsymbol{F}_\lambda\right)\cdot(\boldsymbol{I}-\boldsymbol{m}_\lambda\otimes\boldsymbol{m}_\lambda) \leq C\lambda^2$, which implies

$$\left|\boldsymbol{I}-\boldsymbol{R}_\lambda^{(A)}\right|^2 \leq 2\left(\boldsymbol{I}-\boldsymbol{R}_\lambda^{(A)}\right)^T\left(\boldsymbol{I}-\boldsymbol{R}_\lambda^{(A)}\right)\cdot(\boldsymbol{I}-\boldsymbol{m}_\lambda\otimes\boldsymbol{m}_\lambda) \leq C\lambda^2 .$$

Putting things together, we finally have by triangle inequality

$$\left\|\nabla\boldsymbol{y}_\lambda^{(A)} - \boldsymbol{I}\right\|_{L^2((0,L)\times(0,\xi);\mathbb{R}^3)} \leq \left\|\nabla\boldsymbol{y}_\lambda^{(A)} - \boldsymbol{R}_\lambda^{(A)}\right\|_{L^2((0,L)\times(0,\xi);\mathbb{R}^3)} + \left\|\boldsymbol{R}_\lambda^{(A)} - \boldsymbol{I}\right\|_{L^2((0,L)\times(0,\xi);\mathbb{R}^3)} \leq C\lambda . \tag{71}$$

To derive estimates for the martensite part, we observe that by the uniform Lipschitz bounds on $F_\lambda^\pm$, for any $\delta > 0$ there is for all $\lambda \leq \lambda_\delta > 0$,

$$\Omega_{\boldsymbol{A}_\lambda}^\delta := \left\{\boldsymbol{x}\in\mathbb{R}^3 \;:\; -l < x_1 < 0\;,\; F_\lambda^+(x_1)+\delta < x_2 < F_\lambda^-(x_1)+\xi-\delta\;,\; 0<x_3<1\right\} \subset \mathcal{M}_\lambda .$$

We make again use of assumption (59) and consider a part of the sliced interface, that is the subboundary

$$S^{(A/M)} := \left\{\boldsymbol{x}\in\mathbb{R}^3 \;:\; x_1 = 0,\; F^+(0)+\delta < x_2 < F^-(0)+\xi-\delta\;,\; x_3 = 0\right\} .$$

By the trace theorem and the bound (71) there is a constant $\boldsymbol{c}_\lambda^{(2)}$ such that

$$\int_{S^{(A/M)}}\left|\boldsymbol{y}_\lambda^{(A)}(\boldsymbol{x}) - \boldsymbol{I}(\boldsymbol{x}) + \boldsymbol{c}_\lambda^{(2)}\right|^2 dA \leq C\lambda^2 , \quad \text{i.e.,} \quad \left\|\boldsymbol{y}_\lambda^{(A)} - \boldsymbol{I} + \boldsymbol{c}_\lambda^{(2)}\right\|_{L^2\left(S^{(A/M)};\mathbb{R}^3\right)} \leq C\lambda .$$

On the other hand, the trace theorem implies that there is a constant $\boldsymbol{c}_\lambda^{(3)}$ such that

$$\left\|\boldsymbol{y}_\lambda^{(M)}(\boldsymbol{x}) - \boldsymbol{R}_\lambda^{(M)}\boldsymbol{A}_\lambda\boldsymbol{x} + \boldsymbol{c}_\lambda^{(3)}\right\|_{L^2\left(S^{(A/M)};\mathbb{R}^3\right)} \leq C\lambda .$$

By the triangle inequality,

$$\begin{aligned} &\left\|\boldsymbol{I} - \boldsymbol{R}_\lambda^{(M)}\boldsymbol{A}_\lambda - \boldsymbol{c}_\lambda^{(2)} + \boldsymbol{c}_\lambda^{(3)}\right\|_{L^2\left(S^{(A/M)};\mathbb{R}^3\right)} \\ \leq\;& \left\|\boldsymbol{y}_\lambda - \boldsymbol{I} + \boldsymbol{c}_\lambda^{(2)}\right\|_{L^2\left(S^{(A/M)};\mathbb{R}^3\right)} + \left\|\boldsymbol{y}_\lambda - \boldsymbol{R}_\lambda^{(M)}\boldsymbol{A}_\lambda + \boldsymbol{c}_\lambda^{(3)}\right\|_{L^2\left(S^{(A/M)};\mathbb{R}^3\right)} \leq C\lambda . \end{aligned}$$

Following [56, Eqs. (71)-(79)], an analogous calculation as spelled out above for the austenite part shows

$$\int_{\mathcal{M}_\lambda}|\nabla\boldsymbol{y}_\lambda - \boldsymbol{A}_\lambda|^2\,dx_2dx_1 \leq C\lambda^2 , \quad \text{and} \quad \int_{\mathcal{M}_\lambda}|\nabla\boldsymbol{y}_\lambda - \boldsymbol{A}_0|^2\,dx_2dx_1 \leq C\lambda^2 .$$

The H^1-bounds on the deformations $\boldsymbol{y}_\lambda$ imply bounds for the functions $\boldsymbol{v}_\lambda^{(A/M)}$. By the Dirichlet boundary condition at $t_1 = \mathcal{L}$, the gluing condition at $t_1 = 0$, and the assumption that $\boldsymbol{m}_\lambda \cdot \boldsymbol{n}_\lambda^\perp$ is uniformly bounded away from zero, there is a constant $C > 0$ independent of λ such that

$$\left\|\boldsymbol{v}_\lambda^{(M)}\right\|_{H^1((-l,0)\times(0,1))} \leq C \quad \text{and} \quad \left\|\boldsymbol{v}_\lambda^{(A)}\right\|_{H^1((0,\mathcal{L})\times(0,1))} \leq C \tag{72}$$

By trace theorem $\frac{\eta_\lambda}{\lambda}$ is bounded and hence has a convergent subsequence such that $\boldsymbol{v}_0^{(M)}(-l, t_2) = \xi(1+\eta-t_2)\,\boldsymbol{a}_0$ for $0 < t_2 < 1$ with some limit $\eta \in \mathbb{R}$. The remaining boundary conditions follow similarly. By the boundary conditions (63), the bounds from Eq. (72) imply that $\left\|F_\lambda^\pm\right\|_{L^2(-\ell,0)} \leq C\lambda$. Hence by the uniform Lipschitz assumption $\left\|F_\lambda^\pm\right\|_{L^\infty(-\ell,0)} \to 0$ for $\lambda \to 0$ (cf. [56, Sec. 8.4.3 and 8.4.4]). It remains to show that $\boldsymbol{v} \in H^1((-l,\mathcal{L}) \times (0,1))$, where $\boldsymbol{v}$ is defined by Eq. (69). By Rellich's lemma, the trace functions $\boldsymbol{v}_\lambda^{(M)}(0,\cdot) \to \boldsymbol{v}_0^{(M)}(0,\cdot)$ and $\boldsymbol{v}_\lambda^{(A)}(0,\cdot) \to \boldsymbol{v}_0^{(A)}(0,\cdot)$ converge strongly in $L^2\left((0,1);\mathbb{R}^3\right)$, and it suffices to show $\boldsymbol{v}_0^{(M)}(0,t_2) = \boldsymbol{v}_0^{(A)}(0,t_2)$ in $L^2(0,1)$. We use the notation

$$\tilde{\boldsymbol{v}}_\lambda^{(M)}(0,t_2) = \begin{cases} \boldsymbol{v}_\lambda^{(M)}(0,t_2) & \text{if } t_2 \in (0,1) \\ 0 & \text{else} \end{cases},$$

and the abbreviations

$$a_\lambda := \frac{\xi}{\xi + F_\lambda^-(0) - F_\lambda^+(0)}, \quad b_\lambda := -\frac{F_\lambda^+(0)}{\xi + F_\lambda^-(0) - F_\lambda^+(0)}, \text{ and } \quad I_\lambda := \left(0, \frac{F_\lambda^+(0)}{\xi}\right) \cup \left(\frac{F_\lambda^-(0)+\xi}{\xi}, 1\right).$$

In particular $a_\lambda \to 1$, $b_\lambda \to 0$, and $|I_\lambda| \to 0$ for $\lambda \to 0$. Hence

$$\begin{aligned} &\lim_{\lambda\to 0} \left\|\boldsymbol{v}_\lambda^{(M)}(0,\cdot) - \boldsymbol{v}_\lambda^{(A)}(0,\cdot)\right\|_{L^2(0,1)} \\ \leq\ &\lim_{\lambda\to 0} \left\|\boldsymbol{v}_\lambda^{(M)}(0,\cdot) - \boldsymbol{v}_\lambda^{(M)}(0, a_\lambda \cdot + b_\lambda)\right\|_{L^2(\mathbb{R})} + \lim_{\lambda\to 0} \left\|\boldsymbol{v}_\lambda^{(M)}(0,\cdot) - \boldsymbol{v}_\lambda^{(A)}(0,\cdot)\right\|_{L^2(I_\lambda)} = 0\,. \end{aligned}$$

□

The Γ-limiting energy functional is characterized by the following theorem.

Theorem 6.3 *Suppose $\left\{\boldsymbol{u}_\lambda^{(M)}, \boldsymbol{u}_\lambda^{(A)}\right\}$ is a low energy sequence, that is, $I_\lambda\left(\boldsymbol{u}_\lambda^{(M)}, \boldsymbol{u}_\lambda^{(A)}\right) \leq C$ with a uniform constant C independent of λ.*

1. **Lower bound.**

$$\begin{aligned} &\liminf_{\lambda\to 0} \frac{1}{\lambda^2} I_\lambda\left(\boldsymbol{u}_\lambda^{(M)}, \boldsymbol{u}_\lambda^{(A)}\right) \geq \\ \geq\ &\frac{\epsilon}{2}\left\{\int_{-l}^0 \int_0^1 \frac{\partial^2\phi(\boldsymbol{I})}{\partial F^2}\left(\boldsymbol{G}^{(M)}, \boldsymbol{G}^{(M)}\right) d\boldsymbol{x} + \int_0^L \int_0^1 \frac{\partial^2\phi(\boldsymbol{I})}{\partial F^2}\left(\boldsymbol{G}^{(A)}, \boldsymbol{G}^{(A)}\right) d\boldsymbol{x}\right\} =: I(\boldsymbol{v}) \end{aligned} \tag{73}$$

where

$$\boldsymbol{G}^{(M)} := \boldsymbol{v}_{,1} \otimes \boldsymbol{A}_0^{-T}\boldsymbol{m}_0 + \left(\boldsymbol{a}_0 + \frac{1}{\xi}\boldsymbol{v}_{,2}\right) \otimes \boldsymbol{A}_0^{-T}\boldsymbol{n}_0 \quad , \quad \boldsymbol{G}^{(A)} = \boldsymbol{v}_{,1} \otimes \boldsymbol{m}_0 + \frac{1}{\xi}\boldsymbol{v}_{,2} \otimes \boldsymbol{n}_0\,.$$

The function $\boldsymbol{v} = \boldsymbol{v}_0$ is defined piecewise by the weak limits of subsequences of $\boldsymbol{v}_\lambda^{(M)}$, and $\boldsymbol{v}_\lambda^{(A)}$.

2. **Upper bound.** *Suppose that* $\boldsymbol{v} \in H^1\left((-l, L)\times(0,1);\mathbb{R}^3\right)$ *satisfies the boundary conditions* $\boldsymbol{v}(-l,t_2) = \xi(1+\eta-t_2)\,\boldsymbol{a}_0$ *for* $0<t_2<1$ *with some* $\eta\in\mathbb{R}$, $\boldsymbol{v}(t_1,0)\,\|\boldsymbol{a}_0\|\boldsymbol{v}(t_1,1)$ *and* $(\boldsymbol{v}(t_1,0)-\boldsymbol{v}(t_1,1))\cdot\boldsymbol{a}_0\geq 0$ *for* $-l<t_1<0$; $\boldsymbol{v}(t_1,0)=\boldsymbol{v}(t_1,1)$ *for* $0<t_1<L$, *and* $\boldsymbol{v}(\mathcal{L},t_2)=\boldsymbol{0}$. *Then there exists a sequence* $\left(\boldsymbol{u}_\lambda^{(M)},\boldsymbol{u}_\lambda^{(A)}\right)\in\mathcal{X}_\lambda$ *such that* $\frac{1}{\lambda}\boldsymbol{u}_\lambda^{(M)}\rightharpoonup\boldsymbol{v}|_{(-l,0)\times(0,1)}$, $\frac{1}{\lambda}\boldsymbol{u}_\lambda^{(A)}\rightharpoonup\boldsymbol{v}|_{(0,L)\times(0,1)}$, *and* $I_\lambda\left(\boldsymbol{u}_\lambda^{(M)},\boldsymbol{u}_\lambda^{(A)}\right)\to I(\boldsymbol{v})$ *where the functional* I *is defined by Eq.* (73).

Proof: 1. **Lower Bound.** The limes inferior is superadditive, i.e., for arbitrary sequences a_λ, b_λ

$$\liminf_{\lambda\to0}(a_\lambda+b_\lambda)\geq\liminf_{\lambda\to0}a_\lambda+\liminf_{\lambda\to0}b_\lambda\,.$$

Hence, to derive the lower bound for the sum of the elastic energies of the martensite and the austenite part, the considerations from [56, Sec. 8.4.4], which are based on techniques from [37], can be applied to the martensite and the austenite part independently. For completeness, we recall them briefly. For simplicity of notation, we set $\Omega^{(M)}:=(-l,0)\times(0,1)$, and $\Omega^{(A)}:=(0,\mathcal{L})\times(0,1)$. As $\left(\boldsymbol{u}_\lambda^{(M)},\boldsymbol{u}_\lambda^{(A)}\right)$ is a low energy sequence,

$$C\;\geq\;\int_{\Omega^{(M)}}\phi\left(\boldsymbol{I}+\lambda\boldsymbol{G}_\lambda^{(M)}\right)J_\lambda^{(M)}d\boldsymbol{t}+\int_{\Omega^{(A)}}\phi\left(\boldsymbol{I}+\lambda\boldsymbol{G}_\lambda^{(A)}\right)J_\lambda^{(A)}d\boldsymbol{t}$$

where

$$\begin{aligned}\boldsymbol{G}_\lambda^{(M)}&=\left(\boldsymbol{v}_{\lambda,1}^{(M)}-g_\lambda\boldsymbol{v}_{\lambda,2}^{(M)}\right)\otimes\boldsymbol{A}_\lambda^{-T}\boldsymbol{m}_\lambda+\left(\boldsymbol{a}_\lambda+h_\lambda\boldsymbol{v}_{\lambda,2}^{(M)}\right)\otimes\boldsymbol{A}_\lambda^{-T}\boldsymbol{n}_\lambda\,,\\ J_\lambda^{(M)}\;&=\;\left(\xi-\left(F_\lambda^+-F_\lambda^-\right)\right)\boldsymbol{m}_\lambda\cdot\boldsymbol{n}^\perp\,,\quad\boldsymbol{G}_\lambda^{(A)}=\boldsymbol{v}_{\lambda,1}^{(A)}\otimes\boldsymbol{m}_\lambda+\frac{1}{\xi}\boldsymbol{v}_{\lambda,2}^{(A)}\otimes\boldsymbol{n}_\lambda\,,\quad J_\lambda^{(A)}=\epsilon\,,\end{aligned}$$

with $g_\lambda(t_1,t_2)=\frac{t_2F_\lambda^{-'}(t_1)+(1-t_2)F_\lambda^{+'}(t_1)}{\xi-\left(F_\lambda^+(t_1)-F_\lambda^-(t_1)\right)}$ and $h_\lambda(t_1,t_2)=\frac{1}{\xi-\left(F_\lambda^+(t_1)-F_\lambda^-(t_1)\right)}$. To do careful Taylor expansions of the integrands in the spirit of [37] we denote by $E_\lambda^{(M)}$ and $E_\lambda^{(A)}$ the sets where $\boldsymbol{G}_\lambda^{(M)}$ and $\boldsymbol{G}_\lambda^{(A)}$ are large, respectively, i.e.,

$$E_\lambda^{(M)}:=\left\{\boldsymbol{x}\in\Omega^{(M)}\;:\;\left|\boldsymbol{G}_\lambda^{(M)}(\boldsymbol{x})\right|\geq\lambda^{-1/2}\right\}\,,$$

and analogously for $E_\lambda^{(A)}$. We use the place-holder $j\in\{A,M\}$. The Taylor expansions on $\Omega^{(j)}\setminus E_\lambda^{(j)}$ read (recall that $\boldsymbol{I}$ is a critical point for $\phi\in\mathcal{C}^2$)

$$\phi\left(\boldsymbol{I}+\lambda\boldsymbol{G}_\lambda^{(j)}\right)=\frac{1}{2}\frac{\partial^2\phi(\boldsymbol{I})}{\partial\boldsymbol{F}^2}\left(\lambda\boldsymbol{G}_\lambda^{(j)},\lambda\boldsymbol{G}_\lambda^{(j)}\right)+\omega\left(\left|\lambda\boldsymbol{G}_\lambda^{(j)}\right|\right)\left|\lambda\boldsymbol{G}_\lambda^{(j)}\right|^2\,,\tag{74}$$

where $\omega(s)\to0$ as $s\to0$. Hence

$$\frac{1}{\lambda^2}\int_{\Omega^{(j)}}\phi\left(\boldsymbol{I}+\lambda\boldsymbol{G}_\lambda^{(j)}\right)J_\lambda^{(j)}d\boldsymbol{t}\;\geq\;\int_{\Omega^{(j)}\setminus E_\lambda^{(j)}}\left[\frac{1}{2}\frac{\partial^2\phi(\boldsymbol{I})}{\partial\boldsymbol{F}^2}\left(\boldsymbol{G}_\lambda^{(j)},\boldsymbol{G}_\lambda^{(j)}\right)+\omega\left(\left|\lambda\boldsymbol{G}_\lambda^{(j)}\right|\right)|\boldsymbol{G}_\lambda|^2\right]J_\lambda^{(j)}d\boldsymbol{t}\,.$$

By compactness, $\boldsymbol{G}_\lambda^{(j)}$ is bounded uniformly in $L^2\left(\Omega^{(j)}\right)$ and $\omega\left(\left|\lambda \boldsymbol{G}_\lambda^{(j)}\right|\right) \to 0$ uniformly. Therefore,

$$\begin{aligned} & \liminf_{\lambda\to 0} \frac{1}{\lambda^2}\int_{\Omega^{(j)}} \phi\left(\boldsymbol{I}+\lambda \boldsymbol{G}_\lambda^{(j)}\right) J_\lambda^{(j)} d\boldsymbol{t} \geq \liminf_{\lambda\to 0} \int_{\Omega^{(j)}\setminus E_\lambda^{(j)}} \frac{1}{2}\frac{\partial^2\phi\left(\boldsymbol{I}\right)}{\partial \boldsymbol{F}^2}\left(\boldsymbol{G}_\lambda^{(j)},\boldsymbol{G}_\lambda^{(j)}\right) J_\lambda^{(j)} d\boldsymbol{t} \\ = & \liminf_{\lambda\to 0} \int_{\Omega^{(j)}} \frac{1}{2}\frac{\partial^2\phi\left(\boldsymbol{I}\right)}{\partial \boldsymbol{F}^2}\left(\chi_{\Omega^{(j)}\setminus E_\lambda^{(j)}}\boldsymbol{G}_\lambda^{(j)},\chi_{\Omega^{(j)}\setminus E_\lambda^{(j)}}\boldsymbol{G}_\lambda^{(j)}\right) J_\lambda^{(j)} d\boldsymbol{t}\,. \end{aligned}$$

We have $J_\lambda^{(M)} \to \epsilon$ and $J_\lambda^{(A)} \to \epsilon$ uniformly on the respective $\Omega^{(j)}$. Since $\chi_{\Omega^{(j)}\setminus E_\lambda^{(j)}}$ converges boundedly almost everywhere to $\chi_{\Omega^{(j)}}$, we have $\chi_{\Omega^{(j)}\setminus E_\lambda^{(j)}}\boldsymbol{G}_\lambda^{(j)} \rightharpoonup \boldsymbol{G}^{(j)}$ in $L^2\left(\Omega^{(j)}\right)$. By the lower bound on ϕ,

$$\liminf_{\lambda\to 0} \frac{1}{\lambda^2}\sum_{j\in\{M,A\}}\int_{\Omega^{(j)}} \phi\left(\boldsymbol{I}+\lambda \boldsymbol{G}_\lambda^{(j)}\right) J_\lambda^{(j)} d\boldsymbol{t} \geq \frac{\epsilon}{2}\sum_{j\in\{M,A\}}^{2}\int_{\Omega^{(j)}} \frac{\partial^2\phi\left(\boldsymbol{I}\right)}{\partial \boldsymbol{F}^2}\left(\boldsymbol{G}^{(j)},\boldsymbol{G}^{(j)}\right) d\boldsymbol{t}\,.$$

Following [56, Eq. (95)-(98)], we can identify the weak limits

$$\boldsymbol{G}^{(M)} \;=\; \boldsymbol{v}_{,1}\otimes \boldsymbol{A}_0^{-T}\boldsymbol{m}_0 + \left(\boldsymbol{a}_0+\frac{1}{\xi}\boldsymbol{v}_{,2}\right)\otimes \boldsymbol{A}_0^{-T}\boldsymbol{n}\,, \quad \text{and} \quad \boldsymbol{G}^{(A)} = \boldsymbol{v}_{,1}\otimes \boldsymbol{m}_0 + \frac{1}{\xi}\boldsymbol{v}_{,2}\otimes \boldsymbol{n}\,.$$

2. **Upper bound.** To construct a recovery function we follow the paths of [56, Sec. 8.4.5] and extend the construction to the austenite part. Suppose first the function $\boldsymbol{v}_0 \in H^1\left((-l,0)\times(0,1);\mathbb{R}^3\right)$ is smooth in the sense of $\mathcal{C}^\infty$ and satisfies the limit boundary conditions given in the Theorem with some $\eta \in \mathbb{R}$. We define a sequence of linear transformations $\boldsymbol{L}_\lambda \in \mathbb{R}^{3\times 3}$ satisfying $\boldsymbol{L}_\lambda \boldsymbol{a}_0 = \boldsymbol{a}_\lambda$ and $\boldsymbol{L}_\lambda \to \boldsymbol{I}$ as $\lambda \to 0$. We define $\boldsymbol{u}_\lambda^{(M)} := \lambda \boldsymbol{L}_\lambda \boldsymbol{v}_0|_{\Omega^{(M)}}$ and $\boldsymbol{u}_\lambda^{(A)} := \lambda \boldsymbol{L}_\lambda \boldsymbol{v}_0|_{\Omega^{(A)}}$. By construction, $\boldsymbol{u}_\lambda^{(M)}$ and $\boldsymbol{u}_\lambda^{(A)}$ satisfy the required Dirichlet boundary conditions with $\eta_\lambda = \lambda\eta$, and the gluing condition Eq. (66). Further, the associated functions $F_\lambda^\pm$ are uniformly Lipschitz for small λ.
For general $\boldsymbol{v}_0 \in H^1\left((-l,0)\times(0,1);\mathbb{R}^3\right)$ we use density of $\mathcal{C}^\infty$ in H^1. There is a sequence $\boldsymbol{v}^{(\delta)} \in \mathcal{C}^\infty\left((-l,0)\times(0,1);\mathbb{R}^3\right)$ that satisfies the required boundary conditions and converges to $\boldsymbol{v}$ in H^1 as $\delta \to 0$. For $\boldsymbol{v}^{(\delta)}$ we find a recovery sequence $\boldsymbol{v}_\lambda^{(\delta)}$ as above. Then there is a diagonal sequence $\boldsymbol{v}_{\lambda_k(\delta)} \to \boldsymbol{v}_0$. In both cases, convergence of the energies follows by Taylor's formula (74) which now holds true on the whole domains, using strong convergence. □

6.2 The Γ-limit problem

We now turn to the discussion of the Γ-limit minimization problem for both, hard and for soft boundary conditions. In the hard boundary case one assumes pure austenite up to the interface. In particular, there is no elastic energy contribution from the austenite side. To be precise, we consider the hard boundary problem

$$\min_{\boldsymbol{v}\in\mathcal{A}_h}\int_{-l}^{0}\int_{0}^{1}\frac{1}{2}\frac{\partial^2\phi\left(\boldsymbol{I}\right)}{\partial \boldsymbol{F}^2}\left(\boldsymbol{G}^{(M)},\boldsymbol{G}^{(M)}\right)\epsilon d\boldsymbol{t}\,, \tag{75}$$

where

$$\boldsymbol{G}^{(M)} := \boldsymbol{G}^{(M)}\left(\boldsymbol{v}\right) = \boldsymbol{v}_{,1}\otimes \boldsymbol{A}^{-T}\boldsymbol{m} + \left(\boldsymbol{a}+\frac{1}{\xi}\boldsymbol{v}_{,2}\right)\otimes \boldsymbol{A}^{-T}\boldsymbol{n} \in \mathbb{R}^{3\times 3}\,. \tag{76}$$

The set of admissible functions is given by

$$\mathcal{A}_h := \left\{ \boldsymbol{v} \in H^1\left((-l,0)\times(0,1);\mathbb{R}^3\right) \,:\, \boldsymbol{v}(t_1,0)\,\|\boldsymbol{a}\|\boldsymbol{v}(t_1,1)\ ,(\boldsymbol{v}(t_1,0)-\boldsymbol{v}(t_1,1))\cdot\boldsymbol{a}\geq 0\ , \right.$$
$$\left. \boldsymbol{v}(0,t_2)=\boldsymbol{0}\ ,\ \boldsymbol{v}(-l,t_2)=\xi(1-t_2+\eta)\,\boldsymbol{a} \quad \text{for some } \eta\in\mathbb{R}\right\}\ . \tag{77}$$

We refer to the optimization problem given by Eqs. (75)-(77) as (HBC). This minimization problem is derived in [56] with ξ replaced by ϵ since there the volume factor $\boldsymbol{n}\cdot\boldsymbol{m}^{\perp}$ is missing after transformation to the reference domain. The soft boundary limit problem as derived in Section 6.1 reads

$$\min_{\boldsymbol{v}\in\mathcal{A}_s}\int_{-l}^{0}\int_0^1 \frac{1}{2}\frac{\partial^2\phi(\boldsymbol{I})}{\partial\boldsymbol{F}^2}\left(\boldsymbol{G}^{(M)},\boldsymbol{G}^{(M)}\right)\epsilon d\boldsymbol{t}+\int_0^{\mathcal{L}}\int_0^1\frac{1}{2}\frac{\partial^2\phi(\boldsymbol{I})}{\partial\boldsymbol{F}^2}\left(\boldsymbol{G}^{(A)},\boldsymbol{G}^{(A)}\right)\epsilon d\boldsymbol{t} \tag{78}$$

with

$$\begin{aligned}\boldsymbol{G}^{(M)} &= \boldsymbol{G}^{(M)}(\boldsymbol{v})=\boldsymbol{v}_{,1}\otimes\boldsymbol{A}^{-T}\boldsymbol{m}+\left(\boldsymbol{a}+\frac{1}{\xi}\boldsymbol{v}_{,2}\right)\otimes\boldsymbol{A}^{-T}\boldsymbol{n}\ ,\ \text{and}\\ \boldsymbol{G}^{(A)} &= \boldsymbol{G}^{(A)}(\boldsymbol{v})=\boldsymbol{v}_{,1}\otimes\boldsymbol{m}+\frac{1}{\xi}\boldsymbol{v}_{,2}\otimes\boldsymbol{n}\ .\end{aligned} \tag{79}$$

The set of admissible functions is

$$\mathcal{A}_s := \left\{\boldsymbol{v}\in H^1\left((-l,\mathcal{L})\times(0,1);\mathbb{R}^3\right)\,:\,\boldsymbol{v}(t_1,0)\,\|\boldsymbol{a}\|\boldsymbol{v}(t_1,1)\ ,(\boldsymbol{v}(t_1,0)-\boldsymbol{v}(t_1,1))\cdot\boldsymbol{a}\geq 0 \ \text{ for } t_1<0,\right.$$
$$\left.\boldsymbol{v}(-l,t_2)=\xi(1-t_2+\eta)\,\boldsymbol{a} \quad \text{for some } \eta\in\mathbb{R} \quad ,\ \boldsymbol{v}(t_1,0)=\boldsymbol{v}(t_1,1)\ \text{for } t_1>0\ ,\ \boldsymbol{v}(L,t_2)=\boldsymbol{0}\right\}\ . \tag{80}$$

We refer to the optimization problem given by Eqs. (78)-(80) as (SBC). From now on, for simplicity of notation, we refer to the coordinates (t_1,t_2) as (x,y).
The sets of admissible functions $\mathcal{A}_h$ and $\mathcal{A}_s$ as given in Eqs. (77) and (80), respectively, are both convex, closed and non-empty. For our examples we consider super-isotropic energy densities, i.e.,

$$\frac{1}{2}\frac{\partial^2\phi(\boldsymbol{I})}{\partial\boldsymbol{F}^2}(\boldsymbol{M},\boldsymbol{M})=\frac{1}{2}\frac{\partial^2\phi(\boldsymbol{I})}{\partial\boldsymbol{F}^2}(\boldsymbol{M},\boldsymbol{M})=\mu\left|\frac{\boldsymbol{M}+\boldsymbol{M}^T}{2}\right|^2 \quad \text{for all} \quad \boldsymbol{M}\in\mathbb{R}^{3\times 3} \tag{81}$$

with Lamé's second parameter μ. Then by Korn's inequality there are unique solutions to (HBC) and (SBC), respectively, see [31].

6.3 Needles are pinched

In this section we show that for any admissible function of the limit problem for hard, respectively soft boundary conditions, the associated rescaled needles are pinched at the martensite/austenite interface in a weak sense. More precisely, we show

$$\frac{f^+(\cdot)-f^-(\cdot)}{\sqrt{|\cdot|}}\in L^2(-l,0)\ , \tag{82}$$

where $f^+(t_1)=\boldsymbol{v}(t_1,0)\cdot\mathbf{a}$, and $f^-(t_1)=\boldsymbol{v}(t_1,1)\cdot\mathbf{a}$. Roughly speaking the condition (82) says that for small λ pinched needles are energetically more favorable than open laminates, see Fig. 6. Open laminates are admissible only for soft but not for hard boundary conditions. Hence we expect qualitatively the same

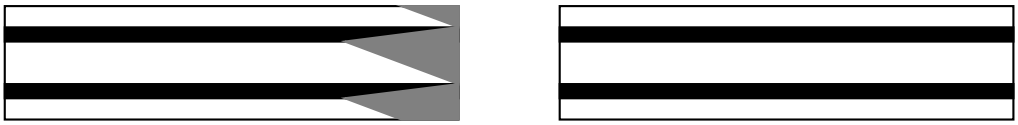

(a) Pinched needles (cf. Section 5) (b) Open laminates

Figure 6: For small λ pinched needles are energetically more favorable than open laminates.

needle structures for both types of boundary conditions, although in case of soft boundary conditions we allow for more general structures.
To prove the condition (82) we consider more generally extensions of functions in fractional order Sobolev spaces $W^{s,p}(\Omega)$ for $1 < p < \infty$ and $0 < s < 1$ on Lipschitz domains $\Omega \subset \mathbb{R}^N$, and prove a condition for extensions to be in $W^{s,p}(\mathbb{R}^N)$. The gluing condition characterizes possible extensions of fractional order Sobolev functions. For a Lipschitz domain $\Omega \subset \mathbb{R}^N$ the Sobolev space $W^{s,p}(\Omega)$ with $0 < s < 1$ and $1 < p < \infty$ is defined to consist of all functions $u \in L^p(\Omega)$ with finite semi-norm

$$[u]^p_{W^{s,p}(\Omega)} := \int_\Omega \int_\Omega \frac{|u(x) - u(y)|^p}{|x-y|^{N+sp}} dxdy \, .$$

6.3.1 Extensions of fractional order Sobolev functions

In this section, we prove and apply the following lemma.

Lemma 6.4 *Suppose $F : \mathbb{R}^{N-1} \to \mathbb{R}$ is a Lipschitz function. Naturally, F defines two Lipschitz domains*

$$\Omega_+ = \left\{x \in \mathbb{R}^N : x_N \geq F\left(\mathbf{x}'\right)\right\} \, , \quad \Omega_- = \left\{x \in \mathbb{R}^N : x_N \leq F\left(\mathbf{x}'\right)\right\} \, ,$$

where $\mathbf{x}' = (x_1, \ldots, x_{N-1}) \in \mathbb{R}^{N-1}$. Let $1 < p < \infty$ and $0 < s < 1$. For $f_\pm \in W^{s,p}(\Omega_\pm)$ we set

$$f(\mathbf{x}) = \begin{cases} f_+(\mathbf{x}) & \text{if } x \in \Omega_+ \\ f_-(\mathbf{x}) & \text{if } x \in \Omega_- \end{cases} \, .$$

Then $f \in W^{s,p}(\mathbb{R}^N)$ if and only if

$$\frac{|f_+(\mathbf{x}', x_N) - f_-(\mathbf{x}', 2F(\mathbf{x}') - x_N)|}{|x_N - F(\mathbf{x}')|^s} \in L^p(\Omega_+) \, .$$

Lemma 6.4 contains several well-studied results. For $H^{1/2}(\mathbb{R})$ with $\Omega_+ = [0, \infty)$ and $\Omega_- = (-\infty, 0]$, the implication

$$f \in H^{1/2}(\mathbb{R}) \Rightarrow \frac{|f(x) - f(-x)|}{\sqrt{|x|}} \in L^2(\mathbb{R})$$

has been derived to define a generalized notion of continuity that does not involve point evaluations (see [53, Lemma 33.1] and the references given there). Further in case of constant extension by zero, i.e., $f_-(\boldsymbol{x}) = 0$ for all $\boldsymbol{x} \in \Omega_- = \mathbb{R}^N \setminus \Omega_+$, Lemma 6.4 reduces to the well-known statement (see e.g. [53, Lemma 37.1])

$$f \in W^{s,p}\left(\mathbb{R}^N\right) \Leftrightarrow \frac{|f_+|}{\operatorname{dist}^s(\cdot, \partial\Omega_+)} \in L^p(\Omega_+) \ .$$

For Lipschitz domains Ω_+ as in Lemma 6.4, the denominator $|x_N - F(\boldsymbol{x}')|$ is comparable to $\operatorname{dist}(\cdot, \partial\Omega)$, see Lemma 6.7 for a quantitative statement. There is a close relation to fractional Hardy inequalities (see, e.g., [39, 43, 48, 33] and the references therein). These integral inequalities state that for $sp > 1$ for all $u \in C_0^\infty(\Omega)$ on nicely bounded domains $\Omega \subset \mathbb{R}^N$

$$\int_\Omega \frac{|u(x)|^p}{\operatorname{dist}(x, \partial\Omega)^{sp}} dx \leq c \int_\Omega \int_\Omega \frac{|u(x) - u(y)|^p}{|x-y|^{N+sp}} dxdy \ .$$

A recent focus of research lies on the search of the optimal constant for such inequalities on simple domains (see [35, 36, 10] and the references given there). The proof of Lemma 6.4 comes along with estimates. They are, however, far from being optimal.

For the critical case $sp = 1$, in particular for $s = \frac{1}{2}$ and $p = 2$, there are counter-examples to Hardy-type inequalities on Lipschitz domains [32]. Lemma 6.4, however, holds true even in the critical case because different spaces are considered. Hardy inequalities hold true for functions from $W_0^{s,p}$, that is the closure of the space of compactly supported smooth functions. The subspace of functions in $H^{1/2}$, however, whose constant extension by zero lies again in $H^{1/2}$ is not equal to $H_0^{1/2} = H^{1/2}$ (see [47, Theorem 11.7]). There are even functions $f \in H^{1/2} \cap C\left[0, \frac{1}{2}\right]$ with $f(0) = 0$ such that the extension to the negative axis by 0 is not contained in $H^{1/2}$. To have an example we consider $f \in C^\infty\left[0, \frac{1}{2}\right]$, with $f(0) = 0$ given by

$$f(x) = \frac{1}{\sqrt{-\log(x)}} \ .$$

We denote the radial-symmetric extension to the half unit ball in $\mathbb{R}^2$ by $F(\boldsymbol{x}) = f(|\boldsymbol{x}|)$. Then

$$[F]^2_{H^1\left(B\left(0,\frac{1}{2}\right)\right)} = \int_{B\left(0,\frac{1}{2}\right)} |\nabla F(\boldsymbol{x})|^2 \, d\boldsymbol{x} = c \int_0^{1/2} \frac{dr}{r\left(-\log(r)\right)^3} = c\left[\frac{1}{\log^2(r)}\right]_0^{1/2} < \infty \ ,$$

that is, $F \in H^1\left(B\left(0, \frac{1}{2}\right)\right)$ and hence by trace theorem $f \in H^{1/2}\left(0, \frac{1}{2}\right)$. The constant extension $f \equiv 0$ for $x < 0$, however, is not an $H^{1/2}$ function. The necessary condition from Lemma 6.4 is not satisfied,

$$\int_0^{1/2} \frac{f^2(x)}{x} dx = -\int_0^{1/2} \frac{dx}{x\log(x)} = \left[-\log|\log(x)|\right]_0^{1/2} = \infty \ .$$

Some properties of functions in $H^{1/2}$ on intervals can be read-off directly from Lemma 6.4. For $a < b$ and $0 < \alpha \leq 1$, we denote the space of Hölder-continuous functions by (see [1, (1.29)])

$$\mathcal{C}^\alpha([a,b]) := \{f : [a,b] \to \mathbb{R} \ : \exists 0 < K < \infty \text{ s.t. for all } \ x, y \in [a,b] \ : \ |f(x) - f(y)| \leq K|x-y|^\alpha\} \ .$$

Remark 6.5 *1. Assume $0 < \alpha \leq 1$, and $a < b < c$. For $f_1 \in \mathcal{C}^\alpha [a,b] \cap H^{1/2}([a,b])$ and $f_2 \in \mathcal{C}^\alpha [b,c] \cap H^{1/2}([b,c])$ let f be defined by*

$$f(x) = \begin{cases} f_1(x) & a < x < b \\ f_2(x) & b < x < c \end{cases} .$$

Then $f \in H^{1/2}(a,c)$ if and only if $f_1(b) = f_2(b)$.

2. The relation $R \subset H^{1/2}(a,b) \times H^{1/2}(a,b)$ defined by

$$(f,g) \in R :\Leftrightarrow h_{(f,g)} \in H^{1/2}(2a-b,b) \text{ , where } h_{(f,g)}(x) := \begin{cases} f(2a-x) \text{ ,} & 2a-b < x < a \\ g(x) \text{ ,} & a < x < b \end{cases}$$

is an equivalence relation on $H^{1/2}(a,b) \times H^{1/2}(a,b)$.

These properties imply that in the limit $\lambda = 0$, the rescaled needles are pinched at the interface. Recall that the needle boundaries are $f^+(t_1) = \boldsymbol{v}(t_1,0) \cdot \boldsymbol{a}$ and $f^-(t_1) = \boldsymbol{v}(t_1,1) \cdot \boldsymbol{a}$, for $-l \leq t_1 \leq 0$.

Lemma 6.6 *Let $\boldsymbol{v} \in \mathcal{A}_h$ (see* (77)*) or $\boldsymbol{v} \in \mathcal{A}_s$ (see* (80)*). Then*

$$\frac{f^+(t_1) - f^-(t_1)}{\sqrt{|t_1|}} \in L^2(-l,0) .$$

Proof: For hard boundary conditions, we have $\boldsymbol{v} \in H^1((-l,0) \times (0,1))$, and therefore by trace theorem on Lipschitz domains, $g^\pm \in H^{1/2}(-l,1)$, where

$$g^\pm(x) = \begin{cases} f^\pm(x) & x \leq 0 \\ 0 = \boldsymbol{v}(0,\cdot) \cdot \boldsymbol{a} & x \geq 0 \end{cases} .$$

By Remark 6.5, the pieced together function

$$f(x) = \begin{cases} f^+(x) & x < 0 \\ f^-(-x) & x > 0 \end{cases}$$

lies in $H^{1/2}$.The claim follows from Lemma 6.4.
In case of soft boundary conditions, the claim follows analogously using periodicity in the austenite, i.e., $\boldsymbol{v}(t_1,1) \cdot \boldsymbol{a} = \boldsymbol{v}(t_1,0) \cdot \boldsymbol{a}$ for $t_1 > 0$. □
To prove Lemma 6.4, we need two geometric estimates.

Lemma 6.7 *Let $F : \mathbb{R}^{N-1} \to \mathbb{R}$ be Lipschitz with Lipschitz constant L, and set*

$$\Omega_- := \left\{ \left(\boldsymbol{x}', x_N \right) \in \mathbb{R}^N \ : \ x_N \leq F\left(\boldsymbol{x}'\right) \right\} .$$

(i) For $\boldsymbol{x} \in \Omega_-$ we define the mirror point with respect to the graph of F by $\overline{\boldsymbol{x}} := (\boldsymbol{x}', 2F(\boldsymbol{x}') - x_N)$. Then for every $\boldsymbol{x}$, $\boldsymbol{y} \in \Omega_-$,

$$|\overline{\boldsymbol{x}} - \boldsymbol{y}| \geq \sqrt{\frac{1 + L^2 - L\sqrt{1+L^2}}{1 + L^2 + L\sqrt{1+L^2}}} \, |\boldsymbol{x} - \boldsymbol{y}| \ , \tag{83}$$

and the constant is optimal, i.e., there is a function F with Lipschitz constant L and points $\boldsymbol{x}$, $\boldsymbol{y} \in \Omega_-$ such that in Eq. (83) *equality holds.*

(ii) For all $\boldsymbol{x} \in \mathbb{R}^N \setminus \Omega_-$,

$$\operatorname{dist}(\boldsymbol{x}, \Omega_-) \geq \frac{1}{\sqrt{1+L^2}} \left| x_N - F\left(\boldsymbol{x}'\right) \right| .$$

Proof: (i) Without loss of generality, we may assume $\boldsymbol{x} = (\mathbf{0}, 0)$, and $F(\mathbf{0}) > 0$. For any $\boldsymbol{y} \in \Omega_-$, $\boldsymbol{y} \neq \boldsymbol{x}$, we have to bound the ratio $\frac{|\overline{\boldsymbol{x}}-\boldsymbol{y}|}{|\boldsymbol{x}-\boldsymbol{y}|}$ below. For that, it suffices to consider a plane containing the points $\boldsymbol{x}$, $\boldsymbol{y}$ and $\overline{\boldsymbol{x}}$. Hence we consider only the two-dimensional situation.
Let $\boldsymbol{y} \in \Omega_- \subset \mathbb{R}^2$. We may assume $y_1 > 0$ by symmetry and $y_2 > F(0)$ since otherwise $|\boldsymbol{y}| = |\boldsymbol{x} - \boldsymbol{y}| \leq |\overline{\boldsymbol{x}} - \boldsymbol{y}| = |(0, 2F(0)) - \boldsymbol{y}|$. Consider points $\boldsymbol{y}$ with fixed norm $|\boldsymbol{y}| = c$, and $y_1 \geq 0$. Then by the cosine theorem, the length $|\overline{\boldsymbol{x}} - \boldsymbol{y}|$ monotonically increases as $y_2 > 0$ decreases. As $\boldsymbol{y} \in \Omega_-$ and $\boldsymbol{x} = (0,0) \in \Omega_-$, the Lipschitz condition implies $y_2 \leq F(0) + Ly_1$. Therefore, for all $\boldsymbol{y} \in \Omega_-$ with $\boldsymbol{y} \neq \boldsymbol{x}$,

$$\frac{|\overline{\boldsymbol{x}} - \boldsymbol{y}|}{|\boldsymbol{x} - \boldsymbol{y}|} = \frac{|\overline{\boldsymbol{x}} - \boldsymbol{y}|}{|\boldsymbol{y}|} \geq \min_{y_1 \geq 0} \frac{|\overline{\boldsymbol{x}} - (y_1, F(0) + Ly_1)|}{|(y_1, F(0) + Ly_1)|} \geq \sqrt{\frac{1 + L^2 - L\sqrt{1+L^2}}{1 + L^2 + L\sqrt{1+L^2}}} ,$$

where the minimum is achieved for $y_1^{crit} := \frac{F(0)}{\sqrt{1+L^2}}$. Equality in Eq. (83) holds if $y_1^{crit} \in \Omega_-$, e.g., for affine functions $F(\boldsymbol{x}) = 1 + L\boldsymbol{x}$.
(ii) Without loss of generality, we may assume $(\boldsymbol{x}', F(\boldsymbol{x}')) = \mathbf{0}$, and $x_N > 0$. By the Lipschitz assumption, $\operatorname{dist}(\boldsymbol{x}, \Omega_-) \geq \operatorname{dist}(\boldsymbol{x}, K)$, where $K = \left\{ \boldsymbol{z} = (\boldsymbol{z}', z_N) \in \mathbb{R}^N \ : \ z_N = L|\boldsymbol{z}'| \right\}$. For $\boldsymbol{z} \in K$ we have

$$\left| \boldsymbol{x} - \left(\boldsymbol{z}', L|\boldsymbol{z}'|\right) \right|^2 = |\boldsymbol{z}'|^2 \left(1 + L^2\right) - 2x_N L |\boldsymbol{z}'| + x_N^2 ,$$

which is minimal for $|\boldsymbol{z}'| = \frac{Lx_N}{1+L^2}$. Hence,

$$\operatorname{dist}(\boldsymbol{x}, \Omega_-) \geq \frac{1}{\sqrt{1+L^2}} \left| x_N - F\left(\boldsymbol{x}'\right) \right| .$$

□

We now turn back to the gluing of functions from fractional Sobolev spaces on Lipschitz domains.

Proof: (Lemma 6.4) Suppose $f \in W^{s,p}\left(\mathbb{R}^N\right)$. We proceed along the lines of [53, Lemma 33.1], where the case $s = \frac{1}{2}$, $p = 2$ and $N = 1$ is studied. For a function $u \in W^{1,p}\left(\mathbb{R}^N\right)$, we denote the trace by $\gamma_0 u(\mathbf{x}) = u(\mathbf{x}', F(\mathbf{x}'))$. By Hardy's inequality [53, Lemma 13.5],

$$\begin{aligned}
\left\| \frac{u(\mathbf{x}', x_N) - \gamma_0 u(\mathbf{x})}{x_N - F(\mathbf{x}')} \right\|_{L^p(\Omega_+)} &\leq \frac{p}{p-1} \|u\|_{W^{1,p}(\Omega_+)} , \\
\left\| \frac{u(\mathbf{x}', x_N) - \gamma_0 u(\mathbf{x})}{x_N - F(\mathbf{x}')} \right\|_{L^p(\Omega_-)} &= \left\| \frac{u(\mathbf{x}', 2F(\mathbf{x}') - x_N) - \gamma_0 u(\mathbf{x})}{(2F(\mathbf{x}') - x_N) - F(\mathbf{x}')} \right\|_{L^p(\Omega_+)} \leq \frac{p}{p-1} \|u\|_{W^{1,p}(\Omega_-)} ,
\end{aligned}$$

which yields

$$\left\| \frac{u(\mathbf{x}', x_N) - u(\mathbf{x}', 2F(\mathbf{x}') - x_N)}{x_N - F(\mathbf{x}')} \right\|_{L^p(\Omega_+)} \leq \frac{2p}{p-1} \|u\|_{W^{1,p}(\mathbb{R}^N)} .$$

Therefore, there are bounded operators

$$T_1 : W^{1,p}\left(\mathbb{R}^N\right) \to \left(L^p(\Omega_+), \frac{d\boldsymbol{x}}{|x_N - F(\boldsymbol{x}')|^p} \right) \quad \text{and} \quad T_0 : L^p\left(\mathbb{R}^N\right) \to \left(L^p(\Omega_+), d\boldsymbol{x}\right)$$

given by

$$T_i : u \mapsto u\left(\boldsymbol{x}', x_N\right) - u\left(\boldsymbol{x}', 2F\left(\boldsymbol{x}'\right) - x_N\right) \ , \quad i = 0, 1 \ .$$

Hence by interpolation (see [43, Remark 5.31], [8, Cor. 4.13] and [53, Lemma 23.1]) there are for $0 < s < 1$ bounded operators

$$T_s : W^{s,p}\left(\mathbb{R}^N\right) \to \left(L^p\left(\Omega_+\right), \frac{d\boldsymbol{x}}{|x_N - F\left(\boldsymbol{x}'\right)|^{sp}}\right) \quad , \quad u \mapsto u\left(\boldsymbol{x}', x_N\right) - u\left(\boldsymbol{x}', 2F\left(\boldsymbol{x}'\right) - x_N\right) \ .$$

Reformulated, we have

$$\left\| \frac{|u\left(\mathbf{x}', x_N\right) - u\left(\mathbf{x}', 2F\left(\mathbf{x}'\right) - x_N\right)|}{|x_N - F\left(\mathbf{x}'\right)|^s} \right\|_{L^p(\Omega_+)} < \infty \ \text{ for all } u \in W^{s,p}\left(\mathbb{R}^N\right) \ .$$

To prove the other implication suppose $f_\pm \in W^{s,p}\left(\Omega_\pm\right)$, and $\frac{|f_+(\mathbf{x}', x_N) - f_-(\mathbf{x}', 2F(\mathbf{x}') - x_N)|}{|x_N - F(\mathbf{x}')|^s} \in L^p\left(\Omega_+\right)$. We have to bound the $W^{s,p}$-seminorm which we decompose into

$$[f]^p_{W^{s,p}(\mathbb{R}^N)} = [f_+]^p_{W^{s,p}(\Omega_+)} + [f_-]^p_{W^{s,p}(\Omega_-)} + 2\int_{\Omega_+}\int_{\Omega_-} \frac{|f_+\left(\boldsymbol{x}\right) - f_-\left(\boldsymbol{y}\right)|^p}{|\boldsymbol{x} - \boldsymbol{y}|^{N+sp}} d\boldsymbol{y}d\boldsymbol{x} \ .$$

The last term is estimated by

$$2 \cdot 2^p \left\{ \int_{\Omega_+}\int_{\Omega_-} \frac{|f_+\left(\boldsymbol{x}\right) - f_-\left(\overline{\boldsymbol{x}}\right)|^p}{|\boldsymbol{x} - \boldsymbol{y}|^{N+sp}} d\boldsymbol{y}d\boldsymbol{x} + \int_{\Omega_+}\int_{\Omega_-} \frac{|f_-\left(\overline{\boldsymbol{x}}\right) - f_-\left(\boldsymbol{y}\right)|^p}{|\boldsymbol{x} - \boldsymbol{y}|^{N+sp}} d\boldsymbol{y}d\boldsymbol{x} \right\} \ , \tag{84}$$

where $\overline{\boldsymbol{x}} := \left(\boldsymbol{x}', 2F\left(\boldsymbol{x}'\right) - x_N\right)$ denotes again the mirror point of $\boldsymbol{x}$. We consider the two terms of Eq. (84) separately. To see that the first term is bounded we adapt the computations done for constant extensions by zero [53, Lemma 37.1]. We find with generic constants depending only on the space dimension N and the Lipschitz constant L of F

$$\begin{aligned}
&\int_{\Omega_+}\int_{\Omega_-} \frac{|f_+\left(\boldsymbol{x}\right) - f_-\left(\overline{\boldsymbol{x}}\right)|^p}{|\boldsymbol{x} - \boldsymbol{y}|^{N+sp}} d\boldsymbol{y}d\boldsymbol{x} = \int_{\Omega_+} |f_+\left(\boldsymbol{x}\right) - f_-\left(\overline{\boldsymbol{x}}\right)|^p \int_{\Omega_-} \frac{1}{|\boldsymbol{x} - \boldsymbol{y}|^{N+sp}} d\boldsymbol{y}d\boldsymbol{x} \\
\leq\ & \int_{\Omega_+} |f_+\left(\boldsymbol{x}\right) - f_-\left(\overline{\boldsymbol{x}}\right)|^p \int_{\mathbb{R}^N \setminus B(\boldsymbol{x}, \operatorname{dist}(\boldsymbol{x}, \Omega_-))} \frac{1}{|\boldsymbol{z}|^{N+sp}} d\boldsymbol{z}d\boldsymbol{x} \\
\leq\ & c_N \int_{\Omega_+} |f_+\left(\boldsymbol{x}\right) - f_-\left(\overline{\boldsymbol{x}}\right)|^p \int_{\operatorname{dist}(\boldsymbol{x}, \Omega_-)}^{\infty} \frac{dr}{r^{1+sp}} d\boldsymbol{x} = c_N \int_{\Omega_+} \frac{|f_+\left(\boldsymbol{x}\right) - f_-\left(\overline{\boldsymbol{x}}\right)|^p}{\operatorname{dist}^{sp}\left(\boldsymbol{x}, \Omega_-\right)} d\boldsymbol{x} \\
\leq\ & c_{N,L} \int_{\Omega_+} \frac{|f_+\left(\boldsymbol{x}\right) - f_-\left(\overline{\boldsymbol{x}}\right)|^p}{|x_N - F\left(\boldsymbol{x}'\right)|^{sp}} d\boldsymbol{x} < \infty \ ,
\end{aligned} \tag{85}$$

where in the last step we used Lemma 6.7 (ii).
For the second term of Eq. (84) we have by Lemma 6.7 (i),

$$\int_{\Omega_+}\int_{\Omega_-} \frac{|f_-\left(\overline{\boldsymbol{x}}\right) - f_-\left(\boldsymbol{y}\right)|^p}{|\boldsymbol{x} - \boldsymbol{y}|^{N+sp}} d\boldsymbol{y}d\boldsymbol{x} = \int_{\Omega_-}\int_{\Omega_-} \frac{|f_-\left(\boldsymbol{x}\right) - f_-\left(\boldsymbol{y}\right)|^p}{|\overline{\boldsymbol{x}} - \boldsymbol{y}|^{N+sp}} d\boldsymbol{y}d\boldsymbol{x} \leq c_L \left[f_-\right]^p_{W^{s,p}(\Omega_-)} \ .$$

□

6.4 Approximate solution of the limit problem

We now turn to the actual (approximate) solution of the Γ-limit minimization problem. We employ two independent approaches to assess the validity of the results obtained. The techniques include a Fourier-type expansion and a numerical implementation via finite elements. The main difference is the way the boundary conditions and the inequality constraint are treated. The results for the various models studied in this and the previous sections are compared below in Sec. 6.5. We consider as model case the alloy $Ti_{50}Ni_{39}Pd_{11}$ introduced in Sec. 4, and implement the super-isotropic energy density given in Eq. (81). To compare the geometric factors of the energies to those of the simple test functions we set $\epsilon = 1$ and $\mu = 1$. The reduction by symmetry relations observed for the simplified model problems carry over to the Γ-limit problem, which is made precise in the following lemma.

Lemma 6.8 *Suppose two twin systems consisting of variants $\boldsymbol{U}_i/\boldsymbol{V}_i$ and variants $\boldsymbol{U}_\ell/\boldsymbol{V}_\ell$, respectively. Suppose further that variants are symmetry related in the sense of Section 4.1, i.e., there is a symmetric orthogonal transformation $\boldsymbol{Q}$ such that*

$$\boldsymbol{Q}\boldsymbol{V}_i = \boldsymbol{V}_\ell\boldsymbol{Q} \quad \textit{and} \quad \boldsymbol{Q}\boldsymbol{U}_i = \boldsymbol{U}_\ell\boldsymbol{Q} \; .$$

Then the minimal values of the super-isotropic and the isotropic energies as given in Eq.(81) *of the two systems coincide for both, hard and soft boundary conditions, and the minimizers are symmetry related via*

$$\boldsymbol{v}_\ell^{(\min)} = \boldsymbol{Q}\boldsymbol{v}_i^{(\min)} \; .$$

The analogous statement holds true for isotropic energy densities

$$\frac{1}{2}\frac{\partial^2\tilde{\phi}\left(\boldsymbol{I}\right)}{\partial\boldsymbol{F}^2}\left(\boldsymbol{M},\boldsymbol{M}\right) = \frac{1}{2}\frac{\partial^2\phi\left(\boldsymbol{I}\right)}{\partial\boldsymbol{F}^2}\left(\boldsymbol{M},\boldsymbol{M}\right) = \mu\left|\frac{\boldsymbol{M}+\boldsymbol{M}^T}{2}\right|^2 + \frac{\lambda}{2}\left(\mathrm{tr}\left(\frac{\boldsymbol{M}+\boldsymbol{M}^T}{2}\right)\right)^2$$

with Lamé's parameters λ and μ.

Proof: For corresponding sets of crystallographic parameters there is a one-to-one correspondence between the sets of admissible functions for the two twin systems induced by the orthogonal transformation $\boldsymbol{Q}$. Indeed, $\boldsymbol{v}_i\left(t_1,0\right)||\boldsymbol{a}_i$ holds if and only if $\boldsymbol{v}_\ell\left(t_1,0\right) = \boldsymbol{Q}\boldsymbol{v}_i\left(t_1,0\right)||\boldsymbol{Q}\boldsymbol{a}_i = \boldsymbol{a}_\ell$, and by orthogonality of $\boldsymbol{Q}$

$$\boldsymbol{Q}\boldsymbol{v}_i\left(t_1,0\right)\cdot\boldsymbol{Q}\boldsymbol{a}_i = \boldsymbol{v}_i\left(t_1,0\right)\cdot\boldsymbol{a}_i \geq \boldsymbol{v}_i\left(t_1,1\right)\cdot\boldsymbol{a}_i = \boldsymbol{Q}\boldsymbol{v}_i\left(t_1,1\right)\cdot\boldsymbol{Q}\boldsymbol{a}_i \; .$$

The remaining conditions follow similarly. Further, the energy is preserved under the orthogonal transformation, that is, $E_i\left(\boldsymbol{v}_i\right) = E_\ell\left(\boldsymbol{Q}\boldsymbol{v}_i\right)$, since for any vectors $\boldsymbol{x}$, $\boldsymbol{y}$, $\boldsymbol{a}$, $\boldsymbol{b} \in \mathbb{R}^3$ orthogonality of $\boldsymbol{Q}$ implies

$$\left|\left(\boldsymbol{Q}\boldsymbol{x}\right)\otimes\left(\boldsymbol{Q}\boldsymbol{y}\right)+\left(\boldsymbol{Q}\boldsymbol{a}\right)\otimes\left(\boldsymbol{Q}\boldsymbol{b}\right)\right|^2 = \left|\boldsymbol{Q}\left(\boldsymbol{x}\otimes\boldsymbol{y}+\boldsymbol{a}\otimes\boldsymbol{b}\right)\boldsymbol{Q}^T\right|^2 = \left|\boldsymbol{x}\otimes\boldsymbol{y}+\boldsymbol{a}\otimes\boldsymbol{b}\right|^2 \; ,$$

and

$$tr\left[\left(\boldsymbol{Q}\boldsymbol{x}\right)\otimes\left(\boldsymbol{Q}\boldsymbol{y}\right)+\left(\boldsymbol{Q}\boldsymbol{a}\right)\otimes\left(\boldsymbol{Q}\boldsymbol{b}\right)\right] = tr\left[\boldsymbol{Q}\left(\boldsymbol{Q}\boldsymbol{x}\right)\otimes\left(\boldsymbol{Q}\boldsymbol{y}\right)+\left(\boldsymbol{Q}\boldsymbol{a}\right)\otimes\left(\boldsymbol{Q}\boldsymbol{b}\right)\boldsymbol{Q}^T\right] = tr\left[\boldsymbol{x}\otimes\boldsymbol{y}+\boldsymbol{a}\otimes\boldsymbol{b}\right] \; .$$

□

6.4.1 Fourier-type ansatz

To get further insight into the interface-induced microstructures we semi-analytically compute approximate solutions for the limiting variational problems. The deformation $\boldsymbol{v}$ in the transition layer is decomposed into

$$\boldsymbol{v}(x,y) = \boldsymbol{w}(x,y) + \xi(1-y+\eta)\,\boldsymbol{a} \tag{86}$$

where $\boldsymbol{w}$ is the modification relative to the homogeneous infinitely extended martensite. Admissible functions $\boldsymbol{w} \in H^1\left((-l,L)\times(0,1);\mathbb{R}^3\right)$ satisfy the boundary conditions

$$\begin{aligned} &\boldsymbol{w}(x,0)\,||\boldsymbol{a}\,,\ \boldsymbol{w}(x,1)\,||\boldsymbol{a}\,, \quad \text{for } x<0\,;\ \boldsymbol{w}(-l,y)=\boldsymbol{0}\,,\ \boldsymbol{w}(L,y)=-\xi(1-y+\eta)\,\boldsymbol{a}\,,\\ &\boldsymbol{w}(x,0)=\boldsymbol{w}(x,1)-\xi\boldsymbol{a}\,, \quad \text{for } x>0\,. \end{aligned} \tag{87}$$

In this section we disregard the inequality constraint $(\boldsymbol{v}(x,0)-\boldsymbol{v}(x,1))\cdot\boldsymbol{a}\geq 0$ for admissible deformations. For the examples considered here, the inequality condition turns out to be satisfied by the solution of the unconstrained problem.
We proceed in three steps. We begin by discussing the martensite side describing the general ansatz for $\boldsymbol{w}$, deriving the resulting energy functional and the corresponding Euler-Lagrange equations for fixed values of $\boldsymbol{w}$ at the interface. Subsequently, the latter are solved adapting (HBC). Finally we allow for (SBC).

Martensite side: Ansatz for deformation, energy functional and Euler-Lagrange equations

To do some formal back-of-the-envelope calculations, we assume the functions to be sufficiently smooth. We interpolate the upper and lower boundary values with a linear polynomial. The linear interpolation can be replaced by any homotopy between the boundary curves, see [57] for a brief discussion. Admissible functions $\boldsymbol{w}:(-l,0)\times(0,1)\to\mathbb{R}^3$ can be represented as

$$\boldsymbol{w}(x,y) = \left((1-y)\,g^-(x)+y g^+(x)\right)\boldsymbol{a} + \sum_{n=1}^{\infty}\sin(n\pi y)\,\boldsymbol{w}_n(x)\ , \tag{88}$$

where we use the notation

$$\boldsymbol{w}(x,0)=:g^-(x)\boldsymbol{a}\,,\quad \boldsymbol{w}(x,1)=:g^+(x)\boldsymbol{a} \quad \text{and} \quad \boldsymbol{w}_n(x)=w_n^{(1)}(x)\,\boldsymbol{a}+w_n^{(2)}(x)\,\boldsymbol{b}+w_n^{(3)}(x)\,\boldsymbol{c} \tag{89}$$

with an orthogonal basis $\{\boldsymbol{a},\boldsymbol{b},\boldsymbol{c}\}$ of $\mathbb{R}^3$. Note that $f^-=g^++\eta\xi$, and $f^+=g^-+\xi(1+\eta)$. The ansatz (88) is inserted into the functional, and the integration with respect to the variable y is carried out. This yields a functional for the (generalized) coefficient functions $g^\pm$ and $w_n^{(\ell)}$, see [57] for the detailed computations. The variational problem is simplified by replacing the functions $g^\pm(x)$ with the linear combinations

$$\bar{g}(x) \;=\; \frac{1}{2}\left(g^+(x)+g^-(x)\right) \quad \text{and} \quad \delta g(x)=\frac{1}{2}\left(g^+(x)-g^-(x)\right) \tag{90}$$

which describe the evolution of the center and the width of the transformed needles , respectively. The functional does not depend on $\bar{g}$ but only on its derivative $\bar{g}'$, i.e., the coordinate $\bar{g}$ is cyclic and the corresponding canonically conjugated "momentum" is an integral of the system of stationary conditions. The functional to be considered is

$$\begin{aligned} &I\left((\bar{g})'(x),(\delta g)'(x),\left\{\left(w_n^{(\ell)}\right)'(x)\right\};(\bar{g})(x),(\delta g)(x),\left\{w_n^{(\ell)}(x)\right\}\right)=\\ &=\int_0^1\int_{-\ell}^0 \frac{1}{2}\frac{\partial^2\phi}{\partial \boldsymbol{M}^2}\left(\boldsymbol{w}_{,1}\otimes\boldsymbol{A}^{-T}\boldsymbol{m}+\boldsymbol{w}_{,2}\otimes\boldsymbol{A}^{-T}\boldsymbol{n},\boldsymbol{w}_{,1}\otimes\boldsymbol{A}^{-T}\boldsymbol{m}+\boldsymbol{w}_{,2}\otimes\boldsymbol{A}^{-T}\boldsymbol{n}\right)dy\,. \end{aligned} \tag{91}$$

There is a matrix $\boldsymbol{Q} = \left(q_{ij}^{(\ell,k)}\right)_{i,j=1,2;\ell,k=1,\ldots 3}$ such that

$$\frac{1}{2}\frac{\partial^2 \phi}{\partial \boldsymbol{M}^2}\left(\boldsymbol{w}_{,1}\otimes \boldsymbol{A}^{-T}\boldsymbol{m}+\boldsymbol{w}_{,2}\otimes \boldsymbol{A}^{-T}\boldsymbol{n}, \boldsymbol{w}_{,1}\otimes \boldsymbol{A}^{-T}\boldsymbol{m}+\boldsymbol{w}_{,2}\otimes \boldsymbol{A}^{-T}\boldsymbol{n}\right) = \sum_{i,j=1}^{2}\sum_{\ell,k=1}^{3} q_{ij}^{(\ell,k)} w_{,i}^{(\ell)} w_{,j}^{(k)} \ . \tag{92}$$

The Euler-Lagrange equations associated to the functional (91) are given by a set of ordinary differential equations with constant coefficients,

$$\begin{aligned}
&\frac{2q_{11}^{(1,1)}}{3}(\delta g)''(x) - \sum_{\ell=1}^{3}\left(q_{11}^{(1,\ell)}+q_{11}^{(\ell,1)}\right)\sum_{n=1}^{\infty}\frac{(1+(-1)^n)}{n\pi}\left(w_n^{(\ell)}\right)''(x) - \\
&-2\sum_{\ell=1}^{3}\left(q_{12}^{(1,\ell)}+q_{21}^{(\ell,1)}\right)\sum_{n=1}^{\infty}\frac{(1-(-1)^n)}{n\pi}\left(w_n^{(\ell)}\right)'(x) = \\
= \ & 2\left(4q_{22}^{(1,1)} - \frac{\left(q_{12}^{(1,1)}+q_{21}^{(1,1)}\right)^2}{q_{11}^{(1,1)}}\right)(\delta g)(x) + \\
&+2\sum_{\ell=1}^{3}\left(q_{21}^{(1,\ell)}+q_{12}^{(\ell,1)} - \frac{q_{12}^{(1,1)}+q_{21}^{(1,1)}}{2q_{11}^{(1,1)}}\left(q_{11}^{(1,\ell)}+q_{11}^{(\ell,1)}\right)\right)\sum_{n=1}^{\infty}\frac{(1-(-1)^n)}{n\pi}\left(w_n^{(\ell)}\right)'(x) \ ,
\end{aligned} \tag{93}$$

and for $\ell = 1,\ldots,3$ and $n = 1,2,\ldots$

$$\begin{aligned}
- \ & \left(q_{11}^{(1,\ell)}+q_{11}^{(\ell,1)}\right)\frac{(1+(-1)^n)}{n\pi}(\delta g)''(x) + \sum_{k=1}^{3} q_{11}^{(\ell,k)}(x)\left(w_n^{(k)}\right)''(x) \\
+ \ & 2\left(q_{21}^{(1,\ell)}+q_{12}^{(\ell,1)} - \frac{q_{12}^{(1,1)}+q_{21}^{(1,1)}}{2q_{11}^{(1,1)}}\left(q_{11}^{(1,\ell)}+q_{11}^{(\ell,1)}\right)\right)\frac{(1-(-1)^n)}{n\pi}(\delta g)'(x) - \\
- \ & \sum_{k=1}^{3}\left(q_{12}^{(\ell,k)}+q_{21}^{(k,\ell)}\right)\sum_{m=1}^{\infty}\left(1-(-1)^{n-m}\right)\frac{mn}{m^2-n^2}\left(w_m^{(k)}\right)'(x) + \\
- \ & 2\sum_{k=1}^{3}\frac{\left(q_{11}^{(1,\ell)}+q_{11}^{(\ell,1)}\right)\left(q_{11}^{(1,k)}+q_{11}^{(k,1)}\right)}{4q_{11}^{(1,1)}}\sum_{m=1}^{\infty}\frac{(1-(-1)^n)}{n\pi}\frac{(1-(-1)^m)}{m\pi}\left(w_m^{(k)}\right)''(x) \\
= \ & -2\sum_{\ell=1}^{3}\left(q_{12}^{(1,\ell)}+q_{21}^{(\ell,1)}\right)\sum_{n=1}^{\infty}\frac{(1-(-1)^n)}{n\pi}(\delta g)'(x) - \\
- \ & \sum_{k=1}^{3}\left(q_{12}^{(k,\ell)}+q_{21}^{(\ell,k)}\right)\sum_{m=1}^{\infty}\left(1-(-1)^{n-m}\right)\frac{mn}{n^2-m^2}\left(w_m^{(k)}\right)'(x) + \\
+ \ & \sum_{k=1}^{3}\left(q_{22}^{(\ell,k)}+q_{22}^{(k,\ell)}\right)\frac{\pi^2 n^2}{2}w_n^{(\ell)}(x) \ .
\end{aligned} \tag{94}$$

The needle tips are characterized in terms of the bending angles α and the opening angles θ. In the orthogonal reference coordinate system we use the standard basis $\boldsymbol{e}_1$, $\boldsymbol{e}_2$ and consider the boundary curves $\boldsymbol{\gamma}^{\pm}(x) = x\boldsymbol{e}_1 + f^{\pm}(x)\,\boldsymbol{e}_2$ with derivatives $(\boldsymbol{\gamma}^{\pm})'(x) = \boldsymbol{e}_1 + (f^{\pm})'(x)\,\boldsymbol{e}_2$. The opening angle θ is hence given by

$$\cos\theta = \frac{1 + (f^{+})'(0)\,(f^{-})'(0)}{\left|(\boldsymbol{\gamma}^{+})'(0)\right|\left|(\boldsymbol{\gamma}^{-})'(0)\right|}\,. \tag{95}$$

For the bending angle α in the orthogonal coordinate system, we parametrize the centerline of the needle as $\boldsymbol{\Gamma}(x) = x\boldsymbol{e}_1 + \frac{f^{+}(x)+f^{-}(x)}{2}\boldsymbol{e}_2$ with derivative $\boldsymbol{\Gamma}'(x) = \boldsymbol{e}_1 + \bar{g}'(x)\,\boldsymbol{e}_2$. The bending angle is then obtained from the scalar product of the tangent vector and the surface normal $\boldsymbol{e}_1$,

$$\cos\alpha = \frac{1}{\sqrt{1 + (\bar{g}'(0))^2}}\,. \tag{96}$$

Approximate solution for hard boundary conditions

As a first step, we disregard the Fourier coefficients and consider the linear interpolation of the boundary values only. This is a special case of the scalar-valued ansatz from Eq. (10) with the choice

$$s(x,y) = y\left(1 + f^{-}(x)\right) + (1-y)\,f^{+}(x)\,.$$

The homogeneous ODE (93) for δg is solved by

$$(\delta g)(x) = Ae^{\kappa x} + Be^{-\kappa x} \quad ; \quad \kappa = \frac{\sqrt{3}}{q_{11}^{(1,1)}}\sqrt{4q_{11}^{(1,1)}q_{22}^{(1,1)} - \left(q_{12}^{(1,1)} + q_{21}^{(1,1)}\right)^2} \tag{97}$$

where the constants A and B are determined by the boundary conditions. By direct integration one obtains

$$\bar{g}(x) = \frac{1}{2\,q_{11}^{(1,1)}}P(\bar{g})\,x - \frac{q_{12}^{(1,1)} + q_{21}^{(1,1)}}{q_{11}^{(1,1)}\,\kappa}\left\{Ae^{\kappa x} - Be^{-\kappa x}\right\} + C\,.$$

For large distance from the interface, i.e., for $x \to -\infty$ we assume the asymptotic behavior

$$g^{\pm}(x) = \bar{g}(x) \pm (\delta g)(x) \to 0\,,$$

from which we conclude $B = P(\bar{g}) = C = 0$. The boundary conditions $g^{+}(0) - g^{-}(0) = 2A = \xi$ imply

$$\eta = -\frac{1}{\xi}g^{+}(0) = -\frac{A}{\xi}\left(1 - \frac{q_{12}^{(1,1)} + q_{21}^{(1,1)}}{q_{11}^{(1,1)}\kappa}\right) = -\frac{1}{2}\left(1 - \frac{q_{12}^{(1,1)} + q_{21}^{(1,1)}}{q_{11}^{(1,1)}\kappa}\right)\,. \tag{98}$$

Within the simple approximation without Fourier coefficients the value of the energy is $E = \frac{q_{11}}{3}\left(\frac{\xi}{2}\right)^2\kappa$.

We next study the influence of the higher order Fourier coefficients and in particular account for the vector character of the solution by including the transversal components. Including more Fourier coefficients leads to a refinement of the needle shapes. We list the evolution of the energy, and the offset η for the various twin systems in the Tables 3 and 4 below. We conclude: Incorporating more Fourier coefficients does not change the offset η much. The refinement takes place only close to the interface.

Euler-Lagrange equations for soft boundary conditions

We next turn to the problem of soft boundary conditions. The calculation proceeds in close analogy to the one presented above. In the first step, we set up the variational expression. The main modification is now that the latter consists of two parts. For the martensite part $\boldsymbol{w}^{(M)}$ we stick to the ansatz given by Eq. (88) while for the austenite part, that is for $0 < x < L$ and $0 < y < 1$, we address the different boundary conditions by the ansatz

$$\boldsymbol{w}^{(A)}(x,y) = \boldsymbol{g}^{(A)}(x) + \xi(y-1-\eta)\,\boldsymbol{a} + \sum_{n=1}^{\infty} \sin(n\pi y)\,\boldsymbol{w}_n^{(A)}(x)\ . \tag{99}$$

The boundary conditions stated in Eq. (87) translate into boundary conditions for $\boldsymbol{g}^{(A)}$ and the Fourier coefficient functions $\left\{\boldsymbol{w}_n^{(A)}\right\}$. Note that $\boldsymbol{w}^{(A)}$ by construction satisfies the periodicity condition $\boldsymbol{w}^{(A)}(x,0) = \boldsymbol{w}^{(A)}(x,1) - \xi\boldsymbol{a}$. The matching condition at $x = 0$ requires compatibility between $\boldsymbol{w}^{(M)}$ and $\boldsymbol{w}^{(A)}$, i.e.,

$$(\bar{g}(0) - (\delta g)(0))\,\boldsymbol{a} = g^{-}(0)\,\boldsymbol{a} = \boldsymbol{g}^{(A)}(0) \quad \text{and} \quad \boldsymbol{w}_n^{(A)}(0) = \boldsymbol{w}_n^{(M)}(0) \quad \text{for all } n\ .$$

Further for $x \to \infty$ we assume $\boldsymbol{g}^{(A)}(x) \to \boldsymbol{0}$ and $\boldsymbol{w}_n^{(A)}(x) \to \boldsymbol{0}$ for all n. For simplicity of notation we suppress the super-indices (A) for the derivation of the stationary conditions. We proceed as for the martensite part. There is a matrix $\boldsymbol{P} = \left(p_{ij}^{(k,\ell)}\right)_{i,j=1,2;k,\ell=1,\ldots,3}$ such that

$$\begin{aligned}
&\frac{1}{2}\frac{\partial^2\phi(\boldsymbol{I})}{\partial \boldsymbol{M}^2}\left(\boldsymbol{w}_{,1}\otimes\boldsymbol{m} + \left(\frac{1}{\xi}\boldsymbol{w}_{,2} - \boldsymbol{a}\right)\otimes\boldsymbol{n}, \boldsymbol{w}_{,1}\otimes\boldsymbol{m} + \left(\frac{1}{\xi}\boldsymbol{w}_{,2} - \boldsymbol{a}\right)\otimes\boldsymbol{n}\right) \\
= &\sum_{k,\ell=1}^{3} p_{11}^{(k,\ell)}\left[\left(g^{(k)}\right)'(x) + \sum_{n=1}^{\infty}\sin(n\pi y)\left(w_n^{(k)}\right)'(x)\right]\left[\left(g^{(\ell)}\right)'(x) + \sum_{m=1}^{\infty}\sin(m\pi y)\left(w_m^{(\ell)}\right)'(x)\right] + \\
&+ \sum_{k,\ell=1}^{3} p_{22}^{(k,\ell)}\pi^2 \sum_{n,m=1}^{\infty} nm\cos(n\pi y)\cos(m\pi y)\,w_n^{(k)}(x)\,w_m^{(\ell)}(x) + \\
&+ \sum_{k,\ell=1}^{3}\left(p_{12}^{(k,\ell)} + p_{21}^{(\ell,k)}\right)\left[\left(g^{(k)}\right)'(x) + \sum_{n=1}^{\infty}\sin(n\pi y)\left(w_n^{(k)}\right)'(x)\right]\sum_{m=1}^{\infty} m\pi\cos(m\pi y)\,w_m^{(\ell)}(x)\ .
\end{aligned}$$

The stationary conditions again yield a system of ordinary differential equations with constant coefficients,

$$\sum_{\ell=1}^{3}\left\{\left(p_{11}^{(k,\ell)} + p_{11}^{(\ell,k)}\right)\left[\left(g^{(\ell)}\right)''(x) + \frac{1}{\pi}\sum_{m=1}^{\infty}\frac{1-(-1)^m}{m}\left(w_m^{(\ell)}\right)''(x)\right]\right\} = 0 \quad , \quad k = 1,2,3 \tag{100}$$

Variants	twin type	habit plane	$N=0$	$N=2$		$N=4$		$N=6$		$N=8$	
				HBC	SBC	HBC	SBC	HBC	SBC	HBC	SBC
1 and 2	compound	either one	3.0	2.7	2.4	2.7	2.3	2.6	2.3	2.6	2.2
1 and 3	type I	mpm	7.6	5.2	4.7	4.9	4.3	4.9	4.2	4.8	4.1
1 and 3	type II	mpm	10.6	9.6	8.8	9.5	8.3	9.5	8.1	9.5	8.0
1 and 3	type I	pmm	10.7	9.7	8.8	9.5	8.4	9.5	8.2	9.5	8.1
1 and 3	type II	pmm	10.6	4.3	3.8	3.8	3.4	3.7	3.2	3.6	3.1

Table 3: Variation of the energy $\times 10^3$ with the number N of Fourier coefficients.

and for $k = 1, 2, 3$ and $n = 1, 2, \ldots$

$$\begin{aligned} \sum_{\ell=1}^{3} & \left\{ \left(p_{11}^{(\ell,k)} + p_{11}^{(k,\ell)} \right) \left[\frac{1-(-1)^n}{n\pi} \left(g^{(\ell)} \right)'' (x) + \frac{1}{2} \left(w_n^{(\ell)} \right)'' (x) \right] \right. \\ & \left. - \left(p_{12}^{(k,\ell)} + p_{21}^{(\ell,k)} \right) \sum_{m=1}^{\infty} \frac{\left(1-(-1)^{n-m}\right) nm}{m^2-n^2} \left(w_m^{(\ell)} \right)' (x) \right\} \\ = \sum_{\ell=1}^{3} & \left\{ \left(p_{22}^{(k,\ell)} + p_{22}^{(\ell,k)} \right) \frac{\pi^2 n^2}{2} w_n^{(\ell)}(x) - \left(p_{12}^{(\ell,k)} + p_{21}^{(k,\ell)} \right) \sum_{m=1}^{\infty} \frac{\left(1-(-1)^{n-m}\right) nm}{n^2-m^2} \left(w_m^{(\ell)} \right)' (x) \right\} . \end{aligned} \tag{101}$$

Solution of the Euler-Lagrange equations for soft boundary conditions

As a first step, we again disregard the Fourier coefficients and consider the lowest order approximation given by $\mathbf{g}$. The Euler-Lagrange equations (100) reduce to

$$\sum_{\ell=1}^{3} \left(p_{11}^{(k,\ell)} + p_{11}^{(\ell,k)} \right) \left(g^{(\ell)} \right)'' (x) = 0 \quad , \quad k = 1, 2, 3 \, . \tag{102}$$

If the coefficient matrix $\left(p_{11}^{(k,\ell)} + p_{11}^{(\ell,k)} \right)_{k,\ell=1,2,3}$ is non-singular, the component functions of $\boldsymbol{g}$ are linear, i.e., $g^{(k)}(x) = a^{(k)} x + b^{(k)}$ with some $a^{(k)}, b^{(k)} \in \mathbb{R}$. By the asymptotic saturation condition, there is no energy contribution coming from the austenite part. The problem hence reduces to the hard boundary problem solved above.

The variation of the physical parameters with the number of Fourier coefficients is again illustrated in Tab.s 3 to 5.

Discussion of the results

Linear interpolation without Fourier coefficients provides a first insight into the qualitative shape of the transition layer. It allows for a first classification of twin systems with respect to the asymptotic offsets η

Variants	twin type	habit plane	$N=0$	$N=2$		$N=4$		$N=6$		$N=8$	
				HBC	SBC	HBC	SBC	HBC	SBC	HBC	SBC
1 and 2	comp.	either	-0.6	-0.60	-0.62	-0.60	-0.62	-0.60	-0.61	-0.60	-0.61
1 and 3	type I	mpm	-1.0	-0.82	-0.84	-0.81	-0.82	-0.80	-0.82	-0.80	-0.81
1 and 3	type II	mpm	-0.5	-0.51	-0.51	-0.51	-0.51	-0.51	-0.51	-0.51	-0.51
1 and 3	type I	pmm	-0.6	-0.54	-0.55	-0.54	-0.55	-0.54	-0.55	-0.54	-0.55
1 and 3	type II	pmm	-1.8	-1.02	-1.00	-0.96	-0.96	-0.94	-0.94	-0.93	-0.93

Table 4: Variation of the offset η with the number of Fourier coefficients.

Variants	twin type	habit plane	$N=0$	$N=2$		$N=4$		$N=6$		$N=8$	
				HBC	SBC	HBC	SBC	HBC	SBC	HBC	SBC
1 and 2	compound	either one	105°	121°	130°	125°	140°	126°	146°	126°	150°
1 and 3	type I	mpm	62°	101°	101°	105°	118°	103°	128°	100°	134°
1 and 3	type II	mpm	105°	119°	127°	125°	138°	128°	144°	130°	148°
1 and 3	type I	pmm	102°	116°	125°	122°	136°	125°	142°	127°	146°
1 and 3	type II	pmm	23°	43°	51°	60°	67°	70°	77°	76°	84°

Table 5: Variation of the opening angle θ with the number of Fourier coefficients.

Variants	twin type	habit plane	$N=0$	$N=2$		$N=4$		$N=6$		$N=8$	
				HBC	SBC	HBC	SBC	HBC	SBC	HBC	SBC
1 and 2	compound	either one	19°	55°	55°	48°	55°	42°	55°	38°	55°
1 and 3	type I	mpm	41°	57°	47°	50°	49°	42°	49°	36°	49°
1 and 3	type II	mpm	2°	57°	57°	57°	57°	57°	57°	57°	57°
1 and 3	type I	pmm	8°	57°	57°	56°	57°	54°	56°	53°	56°
1 and 3	type II	pmm	44°	49°	49°	55°	51°	57°	51°	57°	51°

Table 6: Variation of the bending angle α with the number of Fourier coefficients.

of the optimal needles. For the twin systems represented by compound twins consisting of variant 1 and 2, type II twins containing variants 1 and 3 with habit plane normal mpm, and type I twins containing variants 1 and 3 with habit plane normal pmm, we find an asymptotic offset $\eta \approx -0.5$. For the remaining twin systems represented by type I twinned variants 1 and 3 with habit plane normal mpm and type II twinned variants 1 and 3 with habit plane normal pmm, the simplest approximation within this Fourier ansatz predicts highly asymmetric needles with $|\eta + 0.5| \gg 0$. This observation qualitatively agrees with the results for the two-parameter optimization, see Tab. 2. This is in particular remarkable as the energy functional is minimized among different sets of deformations with different analytic properties. One can, however, not expect to capture the fine-scale behavior at the interfaces as reflected in the angles α and θ and the values of the energy. The latter is considerably improved by including Fourier coefficients which provides a refined description of the variation with y. The energy is found to converge rather fast for both, hard and soft boundary conditions. Allowing for relaxation of the austenite decreases the energy by roughly 15% while the overall shape of the needles is preserved.

The very local behavior at the interface, however, is not reliably captured as can be seen by the poor convergence behavior of the opening and bending angles. To better understand the difficulties in certain cases, we consider the eigenvalues for type II twin systems consisting of variants 1 and 3, see Fig. 7. Eigenvalues with imaginary parts give rise to oscillatory behavior of the solution. The amplitude, however, is damped by the real part. For the twin system with habit plane normal mpm, oscillatory solutions are strongly damped which can be seen from the fact that for the complex eigenvalues with non-zero imaginary part, the absolute values of the real parts are considerably larger than the smallest purely real eigenvalues. For the pathological case with habit plane normal pmm, there are only two real eigenvalues and the complex eigenvalues have very similar (even smaller) real parts. This could explain the overshooting observed in the figures of the needles, cf. Fig. 11. Such a behavior is inevitably connected to unreliable slopes at the interface from which the angles are deduced.

In conclusion, the Fourier-type ansatz as presented here is well-suited to get a quick back-of-the-envelope classification of the twin systems. As will be discussed below, in many cases the solution agrees remarkably well with the results obtained by a finite element approximation. The fine scale structure at the immediate vicinity of the interface, however, is not easily accessible.

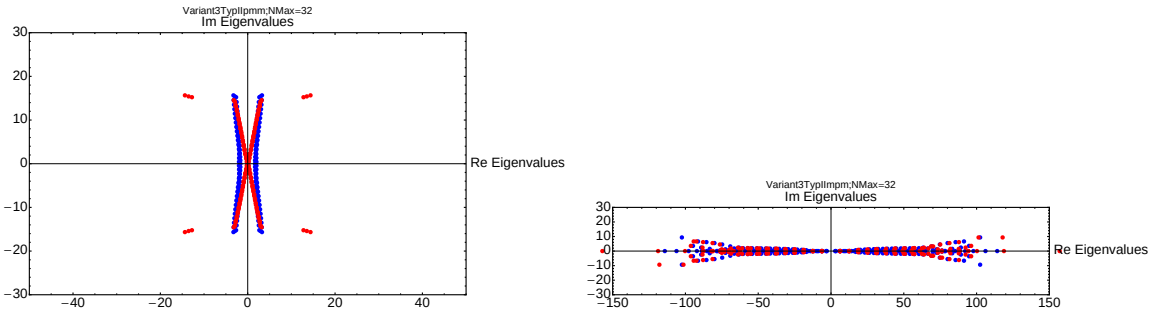

(a) Variants 1 and 3, type II, habit plane pmm

(b) Variants 1 and 3, type II, habit plane mpm

Figure 7: Eigenvalues for type II twins containing variants 1 and 3 for 32 Fourier coefficients. The blue points refer to the eigenvalues of the martensite side while the red ones refer to the eigenvalues of the austenite side.

6.4.2 Approximate solution via finite elements

A different approach to compute approximate solutions to the Γ-limiting variational problems is given by a standard finite element method (FEM). We implement a discretization of Rayleigh-Ritz type (see e.g. [12, 14]), i.e., we discretize the energy functional. Each component of the vector $\boldsymbol{v} = \boldsymbol{v}(x, y) \in \mathbb{R}^3$ is discretized separately, i.e., for $N \in \mathbb{N}$ we make an ansatz of the form

$$\boldsymbol{v}_N(x, y) := \begin{pmatrix} v_N^1(x, y) \\ v_N^2(x, y) \\ v_N^3(x, y) \end{pmatrix} = \begin{pmatrix} \sum_{n=1}^N v_n^1 \phi_n(x, y) \\ \sum_{n=1}^N v_n^2 \phi_n(x, y) \\ \sum_{n=1}^N v_n^1 \phi_n(x, y) \end{pmatrix},$$

where $\{\phi_n\}_{n=1}^N$ are piecewise linear C^0-finite elements This leads to a finite dimensional quadratic optimization problem which is solvable by standard methods. We explicitly incorporate the Dirichlet boundary conditions and the inequality constraint on the corners of the respective triangles. In contrast to the Fourier ansatz we do not assume an asymptotic boundary condition but implement the conditions as described in $\mathcal{A}_h$ and $\mathcal{A}_s$ at some finite $x_1 = \ell$ and $x_1 = L$, see Eqs. (77) and (80). Since the inequality constraint is affine, this is a conforming method. A detailed description of the implementation can be found in [57].
The computations are done on the domain $[-10, 1] \times [0, 1]$ (resp. $[-10, 0] \times [0, 1]$ in case of hard boundary conditions) with a stepsize $h = 0.05$. The values of the geometric factors of the energy and the asymptotic offset η for hard and soft boundary conditions are given in Tab. 7 and 8. Relaxation of austenite, that is allowing for soft rather than hard boundary conditions lowers the energy by roughly $10 - 20\%$. In both cases, the energies vary from twin system to twin system by about a factor of 3. To study the influence of the length of the domain of definition, we consider the type II twin system $1/3$ with habit plane pmm. In Fig. 8 the convergence of the energy with increasing length of martensite (Fig. 8(a)), resp. and austenite (Fig. 8(b)) is plotted. In both cases a rough step size 0.1 is used. In Fig. 8(b) the length of the martensite part is constant 10. Increasing the length of the martensite domain decreases the energy in particular for hard boundary conditions while for increasing length of austenite convergence seems to occur rapidly. This again indicates that relaxation of the austenite lowers the energy only moderately.

6.5 Model hierarchy

We now turn to a comparison of the various approximate solutions for the minimization problem of the elastic energy discussed in the previous sections. Tables 7 and 8 collect the results for the geometric factors of the energies and the asymptotic offsets, respectively. The values obtained by Fourier-ansatz and FEM agree in all cases very well within the numerical precision. Relaxation of austenite lowers the energy by $10 - 20\%$. The piecewise affine layer from [56] gives reasonable estimates for the highly asymmetric case. In particular, for the type II twin system $1/3$ with habit plane normal pmm even the less restrictive models yield a very similar shape for the optimal needle. As the model, however, intrinsically excludes symmetric needles, it is not surprising that the optimal solution from [56] has remarkably higher energies than the ones obtained by FEM and Fourier-ansatz for the compound twins, the type I twins $1/3$ with habit plane pmm and the type II twins $1/3$ with habit plane mpm. In these cases, both FEM and Fourier yield almost symmetric needles.
This shortcoming is overcome by the piecewise affine ansatz studied in Sec. 5.1. The latter leads to a two-parameter ansatz space which allows for a straight-forward explicit solution of the minimization problem. The optimal asymptotic offsets agree very well with the ones obtained by FEM and Fourier-ansatz and the

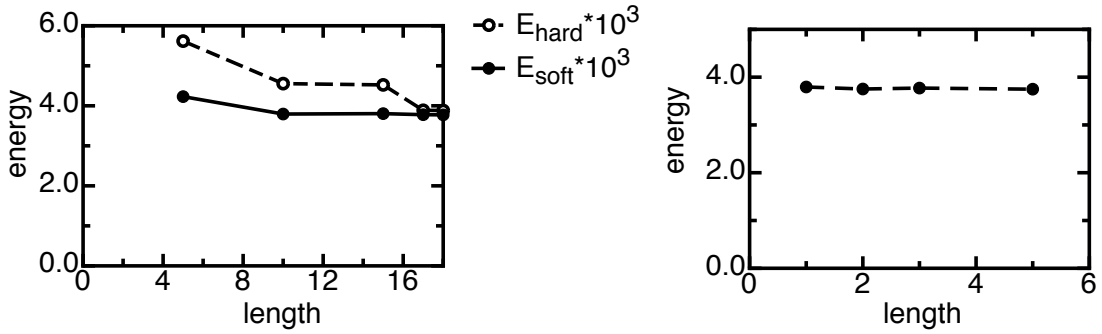

(a) Minimal energy as function of martensite length.

(b) Minimal energy as function of austenite length. Soft boundary conditions.

Figure 8: Geometric factor of the energy $\times 10^3$ for type II twin with variants 1 and 3, habit plane pmm as a function of the length of the martensite and austenite part.

Variants	Twin type	Habit plane	Piecewise affine		HBC		SBC	
			Sec. 5 [56]	Sec. 5.1	Fourier	FEM	Fourier	FEM
1 and 2	compound	either one	6.8	5.4	2.6	2.6	2.2	2.2
1 and 3	type I	mpm	7.3	6.8	4.8	5.0	4.1	4.5
1 and 3	type I	pmm	30.8	23.0	9.5	8.0	8.1	6.6
1 and 3	type II	mpm	35.2	25.2	9.5	9.6	8.0	6.8
1 and 3	type II	pmm	4.1	4.1	3.6	3.9	3.1	3.8

Table 7: Comparison geometric factors of the energy $\times 10^3$ for various approximations. Fourier-ansatz with $N_{\max} = 8$ coefficients. FEM on $[-10, 1] \times [0, 1]$ with step size 0.05.

overall shapes of the needles look very similar, see Figs. 9 - 11, where the rescaled boundary curves $f^{\pm}$ of the needles are plotted in the orthogonal reference coordinate system. In conclusion, all three models allowing for a variable asymptotic offset yield very similar results for the offsets and the overall shapes of the needles. Based on these considerations the simple two-parameter ansatz can be used to estimate the asymptotic offsets, while for the values of the energies the full problem has to be considered.

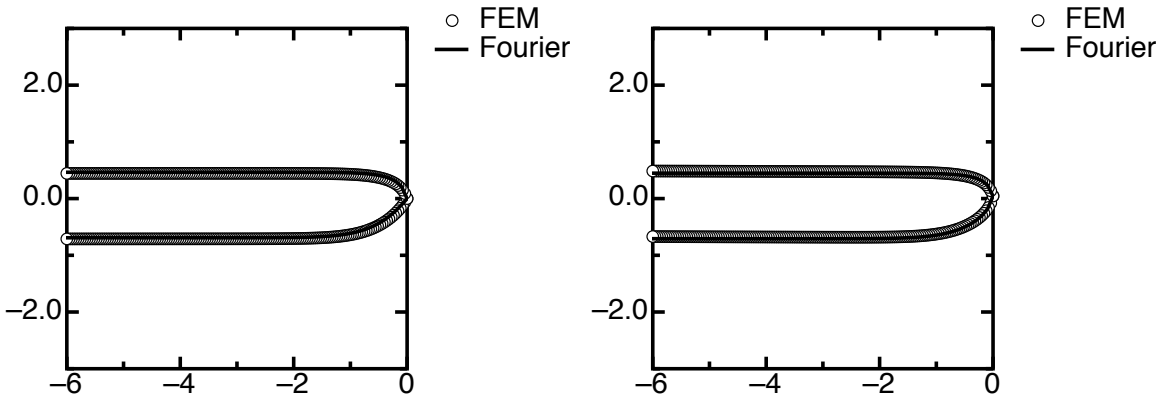

(a) Hard boundary conditions.

(b) Soft boundary conditions.

Figure 9: Comparison needles for FEM and Fourier. Compound twins with variants 1 and 2. Orthogonal coordinate system. FEM computed with discretization 0.05 and martensite length 6. Fourier-ansatz with $N_{\max} = 8$ vectorial coefficients.

Variants	Twin type	Habit plane	Piecewise affine		HBC		SBC	
			Sec. 5 [56]	Sec. 5.1	Fourier	FEM	Fourier	FEM
1 and 2	compound	either one	-1.0	-0.7	-0.6	-0.6	-0.6	-0.6
1 and 3	type I	mpm	-1.0	-0.9	-0.8	-0.8	-0.8	-0.7
1 and 3	type I	pmm	-1.0	-0.6	-0.5	-0.6	-0.6	-0.6
1 and 3	type II	mpm	-1.0	-0.5	-0.5	-0.5	-0.5	-0.5
1 and 3	type II	pmm	-1.0	-1.0	-0.9	-1.0	-0.9	-0.9

Table 8: Comparison of the asymptotic offsets η for various approximations. Fourier-ansatz with $N_{\max} = 8$ coefficients. FEM on $[-10, 1] \times [0, 1]$ with step size 0.05.

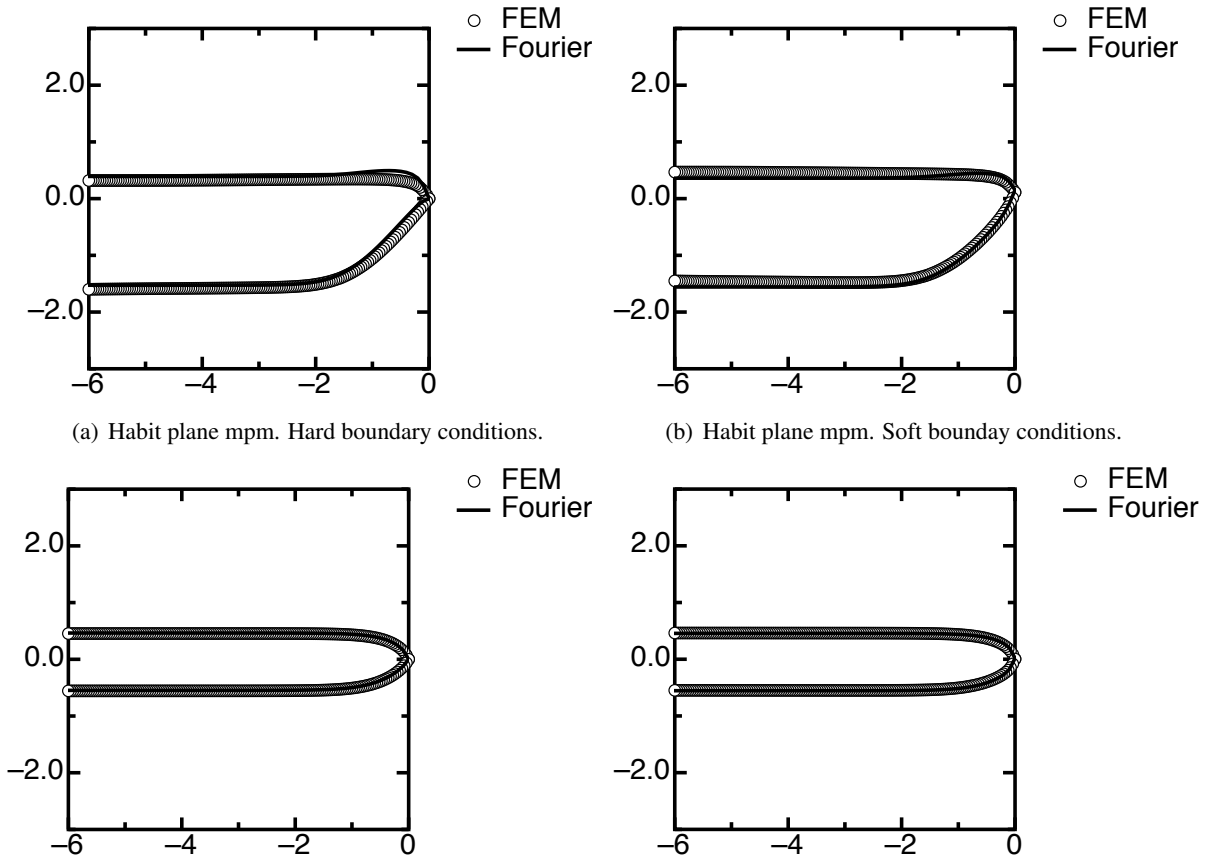

(a) Habit plane mpm. Hard boundary conditions.

(b) Habit plane mpm. Soft bounday conditions.

(c) Habit plane pmm. Hard boundary conditions.

(d) Habit plane pmm. Soft boundary conditions.

Figure 10: Comparison needles for FEM and Fourier. Type I twins with variants 1 and 3. Orthogonal coordinate system. FEM computed with discretization 0.05 and martensite length 6. Fourier-ansatz with $N_{\max} = 8$ vectorial coefficients.

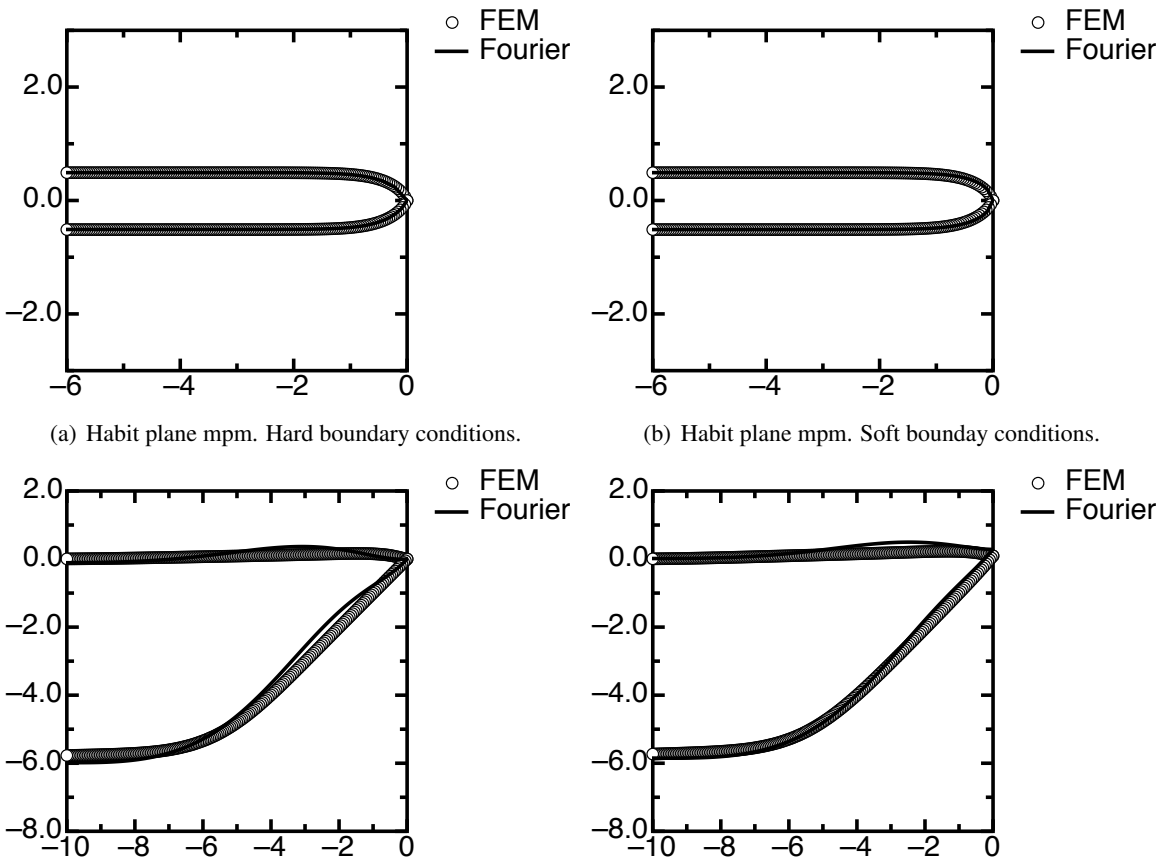

(a) Habit plane mpm. Hard boundary conditions.

(b) Habit plane mpm. Soft bounday conditions.

(c) Habit plane pmm. Hard boundary conditions.

(d) Habit plane pmm. Soft boundary conditions.

Figure 11: Comparison needles for FEM and Fourier. Type II twins with variants 1 and 3. Orthogonal coordinate system. FEM for habit plane mpm computed with discretization 0.05 and martensite length 6. Fourier-ansatz for habit plane mpm with $N_{\max} = 8$ vectorial coefficients. FEM for habit plane pmm computed with discretization 0.04 and martensite length 10. Fourier-ansatz for habit plane mpm with $N_{\max} = 12$ vectorial coefficients.

Acknowledgement

Most of the present results are part of my PhD thesis [57]. I would like to thank my advisor S. Müller for many fruitful discussions, and for his continuous support and encouragement. I greatly benefitted from discussions with S. Conti, R. D. James, and C. Rieger. The work has partly been funded by a postdoctoral fellowship of the NSF under Grant No. DMS-0905778.

References

[1] R.A. Adams and J.J.F. Fournier. *Sobolev Spaces*. Academic Press, Oxford (UK), 2003.

[2] G. Alberti. Variational models for phase transitions, and approach via Γ-convergence. In *Calculus of variations and partial differential equations*, pages 95–114. Springer, Berlin, 2000.

[3] L. Ambrosio, N. Fusco, and D. Pallara. *Functions of bounded variation and free discontinuity problems*. Oxford University Press, Oxford, 2000.

[4] X. Balandraud, D. Delpueyo, M. Grédiac, and G. Zanzotto. Almost compatible microstructures in shape memory alloys. *Acta Mat.*, 58(14):4559–4577, 2010.

[5] J.M. Ball. Mathematical models of martensitic microstructure. *Materials Science and Engineering A*, 378:61–69, 2004.

[6] J.M. Ball and R.D. James. Fine phase mixtures as minimizers of energy. *Arch. Rat. Mech. Anal.*, 100:13–52, 1987.

[7] J.M. Ball and R.D. James. Proposed experimental tests of a theory of fine microstructure, and the two-well problem. *Phil. Trans. Roy. Soc. London A*, 338:389–450, 1992.

[8] C. Bennett and R. Sharpley. *Interpolation of Operators*. Academic Press, 1988.

[9] K. Bhattacharya. *Microstructure of Martensite*. Oxford University Press, Oxford, 2004.

[10] K. Bogdan and B. Dyda. The best constant in a fractional Hardy inequality. *Math. Nachr.*, 5-6:629–638, 2008.

[11] Ph. Boullay, D. Schryvers, and R.V. Kohn. Bending martensite needles in $Ni_{65}Al_{35}$ investigated by two-dimensional elasticity and high-resolution transmission electron microscopy. *Phys. Rev. B*, 64:144105, 2001.

[12] D. Braess. *Finite Elements. Theory, Fast Solvers and Applications in Solid Mechanics*. Cambridge University Press, Cambridge, 2001.

[13] A. Braides. Γ-*convergence for beginners*. Oxford University press, Oxford, 2002.

[14] S. Brenner and L. Scott. *The Mathematical Theory of Finite Element Methods*. Springer, New York, 1994.

[15] A. Chan. Energieskalierung und Domänenverzweigung bei fest-fest phasenübergängen mit $so\,(2)$-Invarianz. Diploma thesis, Fachbereich Mathematik, Universität Duisburg-Essen, 2007.

[16] A. Chan and S. Conti. Domain branching in solid-solid phase transitions. in preparation, 2007.

[17] R. Choksi, S. Conti, R.V. Kohn, and F. Otto. Ground state energy scaling laws during the onset and destruction of the intermediate state in a type I superconductor. *Comm. Pure Appl. Math.*, 61(5):595–626, 2008.

[18] R. Choksi, R.V. Kohn, and F. Otto. Domain branching in uniaxial ferromagnets: a scaling law for the minimum energy. *Comm. Math. Phys.*, 201(1):61–79, 1998.

[19] C. Chu and R. James. Analysis of microstructures in Cu-14.0%Al-3.9%Ni by energy minimization. *Journal de Physique IV*, 05:143–149, 1995.

[20] S. Conti. A lower bound for a variational model for pattern formation in shape-memory alloys. *Cont. Mech. Thermodyn.*, 17 (6):469–476, 2006.

[21] S. Conti. Domain structures in solid-solid phase transitions. In H.W. Alt, S. Luckhaus, E. Presutti, and E.K.H. Salje, editors, *MFO report Phase transitions 2007*, pages 1586–1588. EMS Publishing House, 2007.

[22] J. Cui, Y.S. Chu, O.O. Famodu, Y. Furuya, J. Hattrick-Simpers, R.D. James, A. Ludwig, S. Thienhaus, M. Wuttig, Z. Zhang, and I. Takeuchi. Combinatorial search of thermoelastic shape-memory alloys with extremely small hysteresis width. *Nature materials*, 5:286–290, 2006.

[23] G. Dal Maso. *An Introduction to* Γ*-convergence*. Birkhäuser, Boston, 1993.

[24] E. DeGiorgi and T. Franzoni. Su un tipo di convergenza variazionale. *Atti Accad. Naz. Lincei Rend. Cl. Sci. Fis. Mat. Natur.*, 58:842–850, 1975.

[25] R. Delville. *From functional properties to micro/nano-structures: a TEM study of TiNi(X) shape memory alloys*. PhD thesis, Faculteit Wetenschappen, Universiteit Antwerpen, 2010.

[26] R. Delville, S. Kasinathan, Z. Zhang, J. Van Humbeeck, R.D. James, and D. Schryvers. Transmission electron microscopy study of phase compatibility in low hysteresis shape memory alloys. *Phil. Mag.*, 90:177–195, 2010.

[27] R. Delville, D. Schryvers, Z. Zhang, and R.D. James. Transmission electron microscopy investigation of microstructures in low-hysteresis alloys with special lattice parameters. *Scripta Materialia*, 60:293–296, 2009.

[28] R. Delville, D. Schryvers, Z. Zhang, S. Kasinathan, and R. D. James. TEM investigation of microstructures in low-hysteresis $Ti_{50}Ni_{50-x}Pd_x$ alloys with special lattice parameters. In S. Richter and A. Schwedt, editors, *EMC 2008 14th European Microscopy Congress, Aachen, Germany*, pages 413–414. Springer Berlin Heidelberg, 2008.

[29] R. Delville, H. Shi, R.D. James, and D. Schryvers. Special microstructures and twin features in $Ti_{50}Ni_{50-x}$(Pd,Au)$_x$. *Solid State Phenomena*, 172-174:105–110, 2011.

[30] G. Dolzmann. *Variational Methods for Crystalline Microstructure - Analysis and Computation*. Springer, Berlin Heidelberg, 2003.

[31] G. Duvant and J.L. Lions. *Inequalities in Mechanics and Physics*. Springer, Berlin Heidelberg, 1976.

[32] B. Dyda. The fractional Hardy inequality with a remainder term. *Colloq. Math.*, 122:59–67, 2011.

[33] N. Dyda. A fractional order Hardy inequality. *Illinois J. Math.*, 48 (2):575–588, 1996.

[34] J.L. Ericksen. Some phase transitions in crystals. *Arch. Rat. Mech. Anal.*, 73:99–124, 1980.

[35] R. L. Frank and R. Seiringer. Non-linear ground state representations and sharp Hardy inequalities. *J. Funct. Anal.*, 255(12):3407–3430, 2008.

[36] R. L. Frank and R. Seiringer. Sharp fractional Hardy inequalities in half-spaces. In Tamara Rozhkovskaya and Ari Laptev, editors, *Around the Research of Vladimir Maz'ya I*, volume 11 of *International Mathematical Series*, pages 161–167. Springer New York, 2010.

[37] G. Friesecke, R.D. James, and S. Müller. A theorem on geometric rigidity and the derivation of nonlinear plate theory from three-dimensional elasticity. *Comm. Pure Appl. Math.*, 55:1461–1506, 2002.

[38] C. Grossmann, J. Frenzel, V. Sampath, T. Depka, and G. Eggeler. Elementary transformation and deformation processes and the cyclic stability of niti and NiTiCu shape memory spring actuators. *Metallurgical and Materials Transactions A*, 40:2530–2544, 2009.

[39] H.P. Heinig, A. Kufner, and L.-E. Persson. On some fractional order Hardy inequalities. *J. Inequal. Appl.*, 1:25–46, 1997.

[40] R.D. James and Z. Zhang. A way to search for multiferroic materials with ¨unlikely¨ combinations of physical properties. In L. Manosa, A. Planes, and A.B. Saxena, editors, *The Interplay of Magnetism and Structure in Functional Materials*, volume 79. Springer, 2005.

[41] R.V. Kohn and S. Müller. Branching of twins near an austenite-twinned martensite interface. *Phil. Mag. A*, 66:697–715, 1992.

[42] R.V. Kohn and S. Müller. Surface energy and microstructure in coherent phase transitions. *Comm. Pure Appl. Math.*, XLVII:405–435, 1994.

[43] A. Kufner and L.-E. Persson. *Weighted inequalities of Hardy type*. World Scientific, Singapore, 2003.

[44] C.H. Lei, L.J. Li, Y.C. Shu, and J.Y. Li. Austenite-martensite interface in shape memory alloys. *Appl. Phys. Letters*, 96:141910, 2010.

[45] G. Leoni. *A first course in Sobolev spaces*, volume 105 of *Graduate Studies in Mathematics*. American Mathematical Society, Providence, RI, 2009.

[46] B. Li and M. Luskin. Theory and computation for the microstructure near the interface between twinned layers and a pure variant of martensite. *Materials Science and Engineering A*, 273:237–240, 1999.

[47] J.-L. Lions and E. Magenes. *Problemes aux limites non homogenes et applications*. Vol. 1, Dunod, Paris, 1968.

[48] M. Loss and C. Sloane. Hardy inequalities for fractional integrals on general domains. *J. Funct. Anal.*, 259(6):1369–1379, 2010.

[49] M.W. Louie, M. Kislitsyn, K. Bhattacharya, and S. Haile. Phase transformation and hysteresis behavior in $Cs_{1-x}Rb_xH_2PO_4$. *Solid state ionics*, 181:173–179, 2010.

[50] S. Müller. Variational methods for microstructure and phase transitions. In *Calculus of Variations and Geometric Evolution Problems (Cetraro, 1996)*, pages 85–210. Springer, Berlin, 1999.

[51] M. Pitteri and G. Zanzotto. *Continuum Models for Phase Transitions and Twinning in Crystals*. Chapman and Hall/CRC, London, 2002.

[52] C. Schreiber. Rapport de stage, d.e.a. Freiburg, 1994.

[53] L. Tartar. *An introduction to Sobolev spaces and interpolation spaces*. Springer, Berlin, 2007.

[54] M.S. Wechsler, D.S. Liebermann, and T.A. Reid. On the theory of the formation of martensite. *Journal of metals*, 197:1503–1515, 1953.

[55] Z. Zhang. *Special lattice parameters and the design of low hysteresis materials*. PhD thesis, University of Minnesota, 2007.

[56] Z. Zhang, R.D.James, and S. Müller. Energy barriers and hysteresis in martensitic phase transformations. *Acta Materialia*, 57(15):4332–4352, 2009.

[57] B. Zwicknagl. *Mathematical analysis of microstructures and low hysteresis shape memory alloys*. PhD thesis, University of Bonn, 2011.